Title
Studies of the structure and gating mechanism of the KAT1 voltage-gated potassium channel

Author
Lai, Helen C

Publication Date
2005

Peer reviewed|Thesis/dissertation

Studies of the Structure and Gating Mechanism
of the KAT1 Voltage-gated Potassium Channel

by

Helen C. Lai

DISSERTATION

Submitted in partial satisfaction of the requirements for the degree of

DOCTOR OF PHILOSOPHY

in

Biophysics

in the

GRADUATE DIVISION

of the

UNIVERSITY OF CALIFORNIA, SAN FRANCISCO

[redacted]

Date University Librarian

Degree Conferred:.....

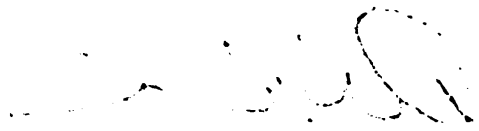

To Ben

and

my family

Acknowledgements

There are many people whom I would like to thank for helping me throughout my graduate career both scientifically and personally. First, I would like to thank my advisor, Lily Jan, from whom I have learned a great deal about the processes of scientific inquiry and mentorship. She has the uncanny ability to interpret data in new ways and fit it into the bigger picture. From her, I have learned there are always new ways to look at a problem and new ideas to pursue. Her patience and guidance have allowed me to develop and trust my own abilities, building the confidence necessary for all my life pursuits.

Next, I would like to thank Michael Grabe. Had he not joined the lab, this project would likely not exist. He convinced me early on that this project was worth pursuing and has been a constant source of support throughout its development. He contributed to the computational aspects of these projects and provided the text describing those details. I have benefited greatly from his expertise and enjoyed numerous intellectual discussions with him.

I thank my thesis committee members, Peter Walter and Dan Minor, who have always asked the tough questions and helped me think of how to proceed with this project. Their input and suggestions have been invaluable.

I would like to thank Yuh Nung Jan for his advice and scientific perspective and the entire Jan Lab for being the wonderfully big, semi-dysfunctional family that it is. Each person in the lab has contributed in some way to my scientific growth.

Monika Jain has been a great asset to this project executing many non-productive screens. Without her help, I would still be many months away from being finished. Delphine Bichet first taught me the yeast screens and has always encouraged and counseled me whenever I doubted my results or myself. Kim Raab-Graham has been a wonderful colleague to talk to about everything from running Westerns to running a lab.

Björn Schroeder, Ofer Wiser, Robin Shaw, and Xiang Qian have helped me learn electrophysiology. Björn has been especially patient and is a great resource for any kind of experiment one might want to do. Bruce Cohen has always offered his criticism which usually proves constructive in the end. Wei Zhou is very thorough and provides constant testing of my completeness of thought. Monika Avdeef, Sandy Barbel, Tong Chen, Lani Seto, Jacqueline Walters, and Sunny Yee are the backbone of the lab and have made sure that the lab keeps going.

Songhai Shi and Bing Ye in Yuh Nung's lab have provided me with inspiration and humor over the years. Their enthusiasm for science (and ping pong) is infectious and I hope to carry some of that spark with me as I continue in science.

I have thoroughly enjoyed the company of the graduate students in the lab. Cindy Huang was my backside and coffee companion and we commiserated during the gloomy years of graduate school. Patrick Haddick provided much needed entertainment and distraction when I needed to talk about anything, particularly the goings on outside our window. Alex Fay was the

person who first introduced me to Lily's research and he has provided deep insight into my science as well as discussions about life.

Horng Ou has been a good friend from the beginning. He is a novel thinker and I have enjoyed listening to all his next big ideas.

Friederike Haass and Toral Surti have been great friends and colleagues. Friederike is true to everything whether it is science or her friends. I admire her dedication to the principle of things even when the means does not provide the desired end. Toral has been a great source of comfort over the years. She is an incredibly giving person and has helped me understand myself as well as everyone else.

Annie Ditmars, Lisa Matus, Terri Sales, and Anand Rao are life-long friends and have supported me in this life-long endeavor.

Without my family, I would likely forget what the real world was like. They keep my life in perspective and are a relief from the hectic scientific life. My dad encouraged me to pursue a Ph.D. and my mom made sure I stayed healthy and safe. Jen and Connie are my sisters whom I have always looked up to and emulated. Bill and Eric provided a reprieve from my daily stresses when we were young.

Finally, I must thank Benjamin Tu. Without his love, kindness, respect, and devotion, I would not have made it through graduate school. He has constantly supported and helped me think through every major decision I have had to make. He is my pillar of strength and my most dear friend and love.

The text of Chapter II in this dissertation/thesis is a reprint of the material as it appears in Neuron. The co-author, Lily Yeh Jan, listed in this publication directed and supervised the research that forms the basis for the dissertation/thesis. The co-author, Michael Grabe, assisted in the modeling and alignment in this Chapter as well as the computational aspects of this thesis. The co-author, Yuh Nung Jan, advised this research. Chapter II is reprinted with permission from Cell Press as it appears in their journal, Neuron (Lai HC, Grabe M, Jan YN, and Jan LY (2005). The S4 voltage sensor packs against the pore domain in the KAT1 voltage-gated potassium channel. Neuron 47(3): 395-406). Helen C. Lai performed the experiments and analyses described in this thesis. This work is comparable to work for a standard thesis awarded by the University of California, San Francisco.

Lily Yeh Jan

Studies of the Structure and Gating Mechanism

of the KAT1 Voltage-gated Potassium Channel

Helen C. Lai

Abstract

Understanding how voltage-gated potassium (K_v) channels sense membrane potential and gate on a molecular level has been an area of intense research in recent years. The main voltage-sensing component, the S4 transmembrane segment, contains positively charged arginines that move in response to membrane potential changes. We set out to answer how S4 movement is coupled to pore opening and how the K_v channel transmembrane segments are oriented in a particular state and during the gating process using KAT1, a hyperpolarization-activated K_v channel from *Arabidopsis thaliana*.

KAT1 has the ability to rescue growth of a K^+ transporter-deficient yeast strain allowing for rapid screening of thousands of mutant KAT1 channels. Using this assay, we designed a conditional lethal/suppressor screen that could identify interactions between transmembrane segments. This screen identified two highly specific interactions between S4 and S5 of the pore region, indicating close apposition of these regions in the hyperpolarized state of KAT1.

We continued this screening process and identified six new interaction sets between S1 and S2, S1 and S4, and S4 and S5. Of the eight total interaction sets identified, six were simultaneously satisfied in one model of KAT1 in the down state of the voltage-sensor. This model suggests close apposition of all six transmembrane segments, most clearly demonstrated by the close

interaction network of residues in S1 (W75), S2 (I94 and N99), S4 (R165 and M169), and S5 (H210). The KAT1 model has the S4 segment positioned diagonally across the S5 of two adjacent subunits with S1 and S2 packed against S4.

Finally, we carried out a series of chimera and mutagenesis experiments examining the regions implicated in coupling (S4-S5 linker) and gating (S4-S5 linker and S6). In doing so, we attempted to reverse the voltage-dependence of KAT1 to a depolarization-activated channel without success. Preliminary results suggest that depolarization and hyperpolarization-activated channels have different ways to couple the voltage-sensor to the pore and that the open and closed states of these channels may be structurally similar.

Table of Contents

List of Figures and Tables

CHAPTER I

Introduction

Introduction

Voltage-gated ion channels are remarkable protein machines that gate the flow of ions across the cell membrane in response to changes in membrane potential. They are found in virtually all species and have a variety of physiological roles ranging from controlling guard cell movements in plants to precise control of the cardiac and neuronal action potentials in animals. Landmark work by Hodgkin and Huxley first described the time and voltage-dependent changes of sodium and potassium conductances in the giant squid axon for action potential generation (Hodgkin and Huxley, 1952a; Hodgkin and Huxley, 1952b), providing the first indication of the existence of selective voltage-dependent ion channels before their molecular identities were known. Cloning of the first voltage-gated sodium (Noda et al., 1984) and potassium channels (Tempel et al., 1987) confirmed the existence of these channels and ushered in a new era of investigations focused on understanding exactly how these channels gate (open and close) in response to membrane potential on a molecular level.

Voltage-gated potassium (K_v) channels are the most well-studied of voltage-gated ion channels and have been cloned from organisms ranging from archaebacteria to plants and animals (Anderson et al., 1992; Ruta et al., 2003; Tempel et al., 1987). They are tetrameric integral membrane proteins with six transmembrane (6-TM) segments per subunit labeled S1 through S6. S1-S4 comprise the voltage-sensor region responsible for sensing membrane potential and S5-S6 form the pore region through which potassium ions flow (Figure 1) (Bezanilla, 2000; Hille, 2001). Within the voltage-sensor region, the S4 segment

contains positively charged arginines that are primarily responsible for sensing voltage changes. Despite the seemingly straightforward and modular nature of these two regions (voltage-sensor and pore), how S4 moves in response to membrane potential changes, how the voltage-sensor movement is coupled to the pore region, and what interactions and conformational changes occur during the gating process to allow pore opening is not well understood.

Interestingly, different members of the K_v channel family are gated by either depolarization or hyperpolarization. Despite this difference, K_v channels have the same general topology (S1-S6); orientation in the membrane (The N- and C-termini are intracellular.); molecular contacts (There are salt bridges between S2 and S4, S3 and S4); and voltage-sensor movement (The gating current is positive when going toward more positive membrane potentials and negative when going toward more negative membrane potentials) (Aggarwal and MacKinnon, 1996; Anderson et al., 1992; Bezanilla, 2000; Hille, 2001; Latorre et al., 2003; Mannikko et al., 2002; Mura et al., 2004; Sato et al., 2003; Seoh et al., 1996; Tiwari-Woodruff et al., 1997). In addition, gating of many of these hyperpolarization-activated channels including the one discussed in this thesis is due to intrinsic voltage-sensing and not due to recovery from inactivation as seen in some K_v channels (i.e. HERG) (Hille, 2001; Hoshi, 1995; Spector et al., 1996). How do channels that retain such similarity on a molecular level respond in opposite ways to changes in membrane potential?

We set out to answer this question and realized the need for a structural model of a K_v channel. At the beginning of this thesis work, there were several models of transmembrane packing in depolarization-activated channels (Gandhi and Isacoff, 2002) based on functional data, but no crystal structure or structural restraints between segments. Structures of two-transmembrane potassium channels suggested that the pore regions of the voltage-gated channels would be structurally homologous, but how the voltage-sensor segments pack against one another as well as the pore has been of intense interest in recent years (Doyle et al., 1998; Gandhi and Isacoff, 2002; Jiang et al., 2002; Kuo et al., 2003). Spectroscopic studies provided some distance constraints for residues between subunits and mutagenesis scanning elucidated lipid-facing and protein-facing sides of all these segments (Cha et al., 1999; Glauner et al., 1999; Hong and Miller, 2000; Monks et al., 1999). In addition, cysteine accessibility studies correlated with the expected movement of S4 based on the direction of the gating current (Baker et al., 1998; Bezanilla, 2000; Larsson et al., 1996; Yusaf et al., 1996). Residues that should move toward the extracellular side upon depolarization were found to increase in accessibility from this side under those conditions and the same is true upon hyperpolarization, residues that move toward the intracellular side were found to increase in accessibility to this side. These data led to conceptual models of depolarization-activated channels where S4 was near the pore region and surrounded by the first three transmembrane segments, S1-S3. However, structural evidence for these models was still necessary.

To obtain a more definitive structural model and begin addressing the question of gating, we needed a model system from which we could obtain structural information and study questions of gating. KAT1, a K_v channel from *Arabidopsis thaliana* was chosen as the model system for three reasons. First, it was a hyperpolarization-activated K_v channel and we were interested in exploring the differences in the gating mechanism behind hyperpolarization and depolarization-activated channels. Any structural information or gating mechanism discovered for this channel could be compared to the vast body of work on depolarization-activated channels. Secondly, initial molecular characterization of its structure and function indicated its similarities to mammalian K_v channels. Chimeras of KAT1 with *Xenopus* Shaker channels are functional and negative charges in S2 and S3 make interactions with S4 as seen in Shaker channels (Sato et al., 2002; Sato et al., 2003; Seoh et al., 1996; Tiwari-Woodruff et al., 1997). In addition, its voltage-sensor was shown to have the same general movement as depolarization-activated channels (Latorre et al., 2003). Lastly, KAT1 and its family members were the only voltage-gated channels known to rescue K^+ transporter deficient yeast (Δ*trk1*, Δ*trk2*), conditions under which it was cloned, allowing for a quick and efficient assay in which to evaluate its function (Anderson et al., 1992). Of note, since that time, it was found that MVP, a hyperpolarization-activated K_v channel from archaebacteria, could also rescue this mutant yeast (Sesti et al., 2003). For reference, the amino acid sequence of the KAT1 transmembrane segments is shown in Figure 2 as determined by Anderson et al. (Anderson et al., 1992).

To construct a structural model of KAT1, we employed a novel approach using this yeast system to find structural restraints between transmembrane segments. We identified mutations in KAT1 S5 that were lethal on low K^+ media yeast plates and screened these against mutagenized regions of the voltage-sensor (S1-S4) looking for mutations that suppress the conditional lethal mutation. This approach proved successful and identified two specific conditional lethal/second-site suppressor pairs in S4 and S5 that suggested close apposition throughout their transmembrane segments. These experiments are the basis of Chapter II.

We believe that these interactions between S4 and S5 occur in the hyperpolarized state of the KAT1 S4 segment. Since we have started work on a hyperpolarization-activated channel while most of the field has worked on depolarization-activated channels, it is necessary to define new terms allowing a dialogue between these two channel types. We define here the "up state" as the ultimate state of the channel achievable with depolarization whereupon further depolarization does not move any more gating charge and the "down state" as the ultimate state of the channel achievable with hyperpolarization whereupon more hyperpolarization does not move any more gating charge. These correlate with the positively charged arginines in S4 being more toward the extracellular side in the up state and more toward the intracellular side in the down state. This was how these states were formerly defined in Chapter II. These states refer to all four S4 segments of a tetrameric K_v channel being in one state, either up or down, and for the purposes of this thesis we will not delve into the specifics of

how the S4 segments could be in different states in different subunits during channel gating. For hyperpolarization-activated channels, the down state of S4 corresponds to the open state of the channel and the up state corresponds to a closed channel. For depolarization-activated channels, the down state of S4 corresponds to the closed channel and the up state corresponds to an open channel and possibly a channel state following N-type inactivation (Bezanilla et al., 1991). This terminology allows us to talk specifically about the state of S4 independent of whether a channel is open or closed. For now, we will draw parallels between the up and down states of depolarization and hyperpolarization-activated channels. Whether the specific up state structure of a depolarization-activated channel will correspond to the up state structure of a hyperpolarization-actived channel will be the onus of future research in this area.

Since we found two highly specific interactions between S4 and S5 in the down state of KAT1, we continued this comprehensive screening and identified six additional conditional lethal/suppressor sets that were used to form a molecular model of KAT1 in the down state of the voltage-sensor. There are currently no molecular models of this state and this model of KAT1 gives a more atomistic view of this state. It suggests that S4 bridges the S5 of two adjacent subunits in the down state and helps address the extent of the voltage-sensor movement when compared to the structure of $K_v1.2$ in the up state (Chanda et al., 2005; Long et al., 2005; Phillips et al., 2005; Posson et al., 2005; Ruta et al., 2005; Tombola et al., 2005). These experiments form the work described in Chapter III.

The final question we set out to address is how K_v channels gate in response to membrane potential changes. We focused on the S4-S5 linker and S6 regions in KAT1, Shaker, a depolarization-activated K_v channel from *Drosophila melanogaster*, and SKOR, a depolarization-activated K_v channel from *Arabidopsis thaliana*. Through a series of mutation and chimera experiments, we analyzed these regions to assess different models of gating in Chapter IV. All the residues mutated for all the experiments in this thesis are in red on Figure 2.

The set of experiments described in this thesis aim to determine a structural model of KAT1 which provides a framework in which to understand gating mechanisms of hyperpolarization and depolarization-activated channels.

Figures

Figure 1. General topology of six transmembrane voltage-gated channels.

Two monomers of a tetrameric channel are shown with potassium ions flowing through the middle. Transmembrane segments are symbolized as cylinders and labeled S1 to S6 on the left monomer. The voltage-sensor region, S1-S4, and the pore region, S5-S6 with the P loop, are labeled. The positive charges in S4 are designated by red plus signs. The N- and C- termini are located on the intracellular side of the membrane.

Figure 1. General topology of six transmembrane voltage-gated channels.

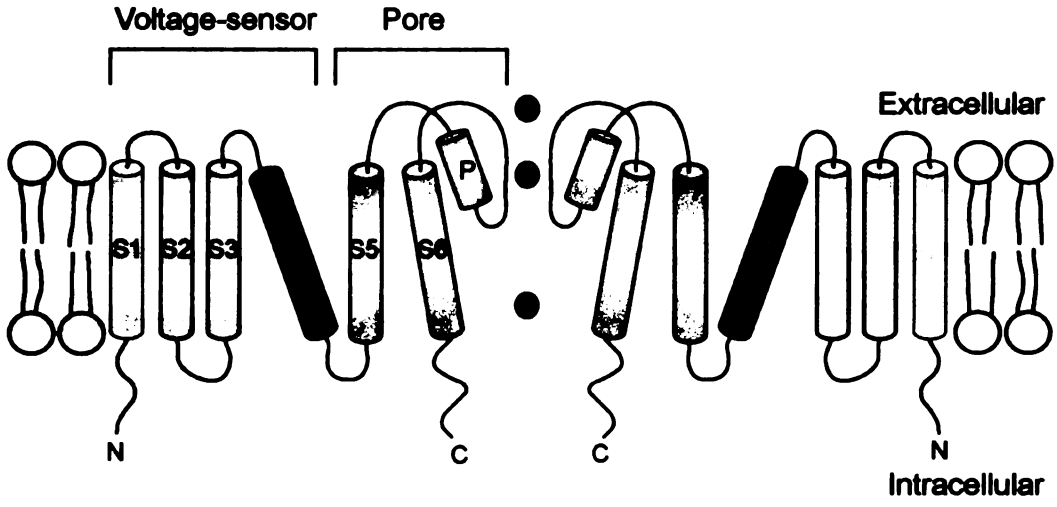

Figure 2. Sequence of the KAT1 transmembrane region.

The sequence of KAT1 around the predicted transmembrane segments is shown (Anderson et al., 1992). Transmembrane segments are underlined in black and labeled S1-S6. An alternate region of S5 is shown as an extended dashed line of S5 with the ends designated by Shealy et al. using the AKT sequence in this alignment and extending it to KAT1 (Shealy et al., 2003). Residues that were mutated in this thesis are in red.

Figure 2. Sequence of the KAT1 transmembrane region.

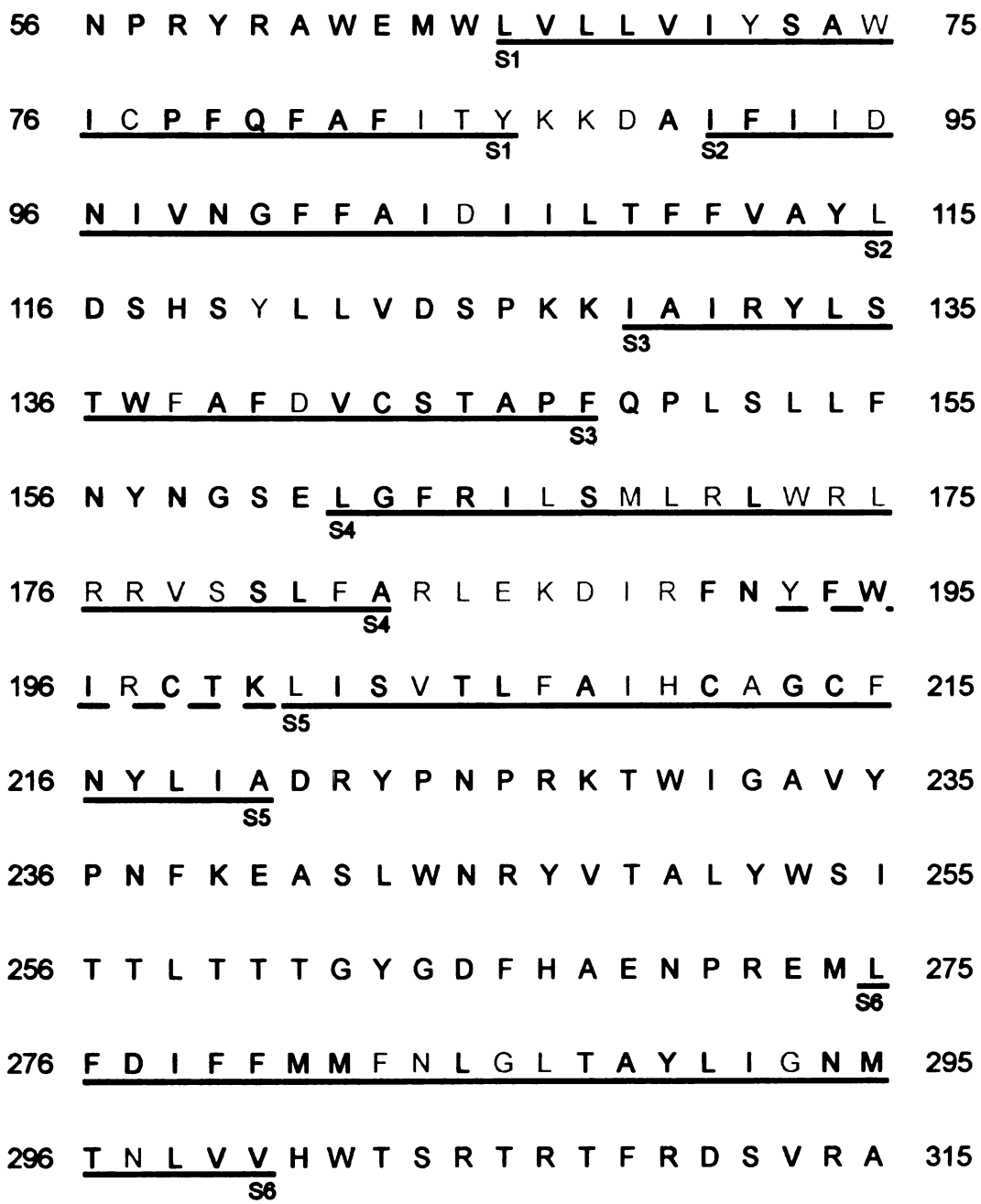

References

Aggarwal, S. K., and MacKinnon, R. (1996). Contribution of the S4 segment to gating charge in the Shaker K+ channel. Neuron *16*, 1169-1177.

Anderson, J. A., Huprikar, S. S., Kochian, L. V., Lucas, W. J., and Gaber, R. F. (1992). Functional expression of a probable Arabidopsis thaliana potassium channel in Saccharomyces cerevisiae. Proc Natl Acad Sci U S A *89*, 3736-3740.

Baker, O. S., Larsson, H. P., Mannuzzu, L. M., and Isacoff, E. Y. (1998). Three transmembrane conformations and sequence-dependent displacement of the S4 domain in shaker K+ channel gating. Neuron *20*, 1283-1294.

Bezanilla, F. (2000). The voltage sensor in voltage-dependent ion channels. Physiol Rev *80*, 555-592.

Bezanilla, F., Perozo, E., Papazian, D. M., and Stefani, E. (1991). Molecular basis of gating charge immobilization in Shaker potassium channels. Science *254*, 679-683.

Cha, A., Snyder, G. E., Selvin, P. R., and Bezanilla, F. (1999). Atomic scale movement of the voltage-sensing region in a potassium channel measured via spectroscopy. Nature *402*, 809-813.

Chanda, B., Asamoah, O. K., Blunck, R., Roux, B., and Bezanilla, F. (2005). Gating charge displacement in voltage-gated ion channels involves limited transmembrane movement. Nature *436*, 852-856.

Doyle, D. A., Morais Cabral, J., Pfuetzner, R. A., Kuo, A., Gulbis, J. M., Cohen, S. L., Chait, B. T., and MacKinnon, R. (1998). The structure of the potassium channel: molecular basis of K+ conduction and selectivity. Science *280*, 69-77.

Gandhi, C. S., and Isacoff, E. Y. (2002). Molecular models of voltage sensing. J Gen Physiol *120*, 455-463.

Glauner, K. S., Mannuzzu, L. M., Gandhi, C. S., and Isacoff, E. Y. (1999). Spectroscopic mapping of voltage sensor movement in the Shaker potassium channel. Nature *402*, 813-817.

Hille, B. (2001). Ion channels of excitable membranes, 3rd edn (Sunderland, Mass., Sinauer).

Hodgkin, A. L., and Huxley, A. F. (1952a). Currents carried by sodium and potassium ions through the membrane of the giant axon of Loligo. J Physiol *116*, 449-472.

Hodgkin, A. L., and Huxley, A. F. (1952b). A quantitative description of membrane current and its application to conduction and excitation in nerve. J Physiol *117*, 500-544.

Hong, K. H., and Miller, C. (2000). The lipid-protein interface of a Shaker K(+) channel. J Gen Physiol *115*, 51-58.

Hoshi, T. (1995). Regulation of voltage dependence of the KAT1 channel by intracellular factors. J Gen Physiol *105*, 309-328.

Jiang, Y., Lee, A., Chen, J., Cadene, M., Chait, B. T., and MacKinnon, R. (2002). The open pore conformation of potassium channels. Nature *417*, 523-526.

Kuo, A., Gulbis, J. M., Antcliff, J. F., Rahman, T., Lowe, E. D., Zimmer, J., Cuthbertson, J., Ashcroft, F. M., Ezaki, T., and Doyle, D. A. (2003). Crystal structure of the potassium channel KirBac1.1 in the closed state. Science *300*, 1922-1926.

Larsson, H. P., Baker, O. S., Dhillon, D. S., and Isacoff, E. Y. (1996). Transmembrane movement of the shaker K+ channel S4. Neuron *16*, 387-397.

Latorre, R., Olcese, R., Basso, C., Gonzalez, C., Munoz, F., Cosmelli, D., and Alvarez, O. (2003). Molecular coupling between voltage sensor and pore opening in the Arabidopsis inward rectifier K+ channel KAT1. J Gen Physiol *122*, 459-469.

Long, S. B., Campbell, E. B., and Mackinnon, R. (2005). Crystal structure of a mammalian voltage-dependent Shaker family K+ channel. Science *309*, 897-903.

Mannikko, R., Elinder, F., and Larsson, H. P. (2002). Voltage-sensing mechanism is conserved among ion channels gated by opposite voltages. Nature *419*, 837-841.

Monks, S. A., Needleman, D. J., and Miller, C. (1999). Helical structure and packing orientation of the S2 segment in the Shaker K+ channel. J Gen Physiol *113*, 415-423.

Mura, C. V., Cosmelli, D., Munoz, F., and Delgado, R. (2004). Orientation of Arabidopsis thaliana KAT1 channel in the plasma membrane. J Membr Biol *201*, 157-165.

Noda, M., Shimizu, S., Tanabe, T., Takai, T., Kayano, T., Ikeda, T., Takahashi, H., Nakayama, H., Kanaoka, Y., Minamino, N., and et al. (1984). Primary structure of Electrophorus electricus sodium channel deduced from cDNA sequence. Nature *312*, 121-127.

Phillips, L. R., Milescu, M., Li-Smerin, Y., Mindell, J. A., Kim, J. I., and Swartz, K. J. (2005). Voltage-sensor activation with a tarantula toxin as cargo. Nature *436*, 857-860.

Posson, D. J., Ge, P., Miller, C., Bezanilla, F., and Selvin, P. R. (2005). Small vertical movement of a K+ channel voltage sensor measured with luminescence energy transfer. Nature *436*, 848-851.

Ruta, V., Chen, J., and Mackinnon, R. (2005). Calibrated Measurement of Gating-Charge Arginine Displacement in the KvAP Voltage-Dependent K(+) Channel. Cell *123*, 463-475.

Ruta, V., Jiang, Y., Lee, A., Chen, J., and MacKinnon, R. (2003). Functional analysis of an archaebacterial voltage-dependent K+ channel. Nature *422*, 180-185.

Sato, Y., Sakaguchi, M., Goshima, S., Nakamura, T., and Uozumi, N. (2002). Integration of Shaker-type K+ channel, KAT1, into the endoplasmic reticulum membrane: synergistic insertion of voltage-sensing segments, S3-S4, and independent insertion of pore-forming segments, S5-P-S6. Proc Natl Acad Sci U S A *99*, 60-65.

Sato, Y., Sakaguchi, M., Goshima, S., Nakamura, T., and Uozumi, N. (2003). Molecular dissection of the contribution of negatively and positively charged residues in S2, S3, and S4 to the final membrane topology of the voltage sensor in the K+ channel, KAT1. J Biol Chem *278*, 13227-13234.

Seoh, S. A., Sigg, D., Papazian, D. M., and Bezanilla, F. (1996). Voltage-sensing residues in the S2 and S4 segments of the Shaker K+ channel. Neuron *16*, 1159-1167.

Sesti, F., Rajan, S., Gonzalez-Colaso, R., Nikolaeva, N., and Goldstein, S. A. (2003). Hyperpolarization moves S4 sensors inward to open MVP, a methanococcal voltage-gated potassium channel. Nat Neurosci *6*, 353-361.

Shealy, R. T., Murphy, A. D., Ramarathnam, R., Jakobsson, E., and Subramaniam, S. (2003). Sequence-function analysis of the K+-selective family of ion channels using a comprehensive alignment and the KcsA channel structure. Biophys J *84*, 2929-2942.

Spector, P. S., Curran, M. E., Zou, A., Keating, M. T., and Sanguinetti, M. C. (1996). Fast inactivation causes rectification of the IKr channel. J Gen Physiol *107*, 611-619.

Tempel, B. L., Papazian, D. M., Schwarz, T. L., Jan, Y. N., and Jan, L. Y. (1987). Sequence of a probable potassium channel component encoded at Shaker locus of Drosophila. Science *237*, 770-775.

Tiwari-Woodruff, S. K., Schulteis, C. T., Mock, A. F., and Papazian, D. M. (1997). Electrostatic interactions between transmembrane segments mediate folding of Shaker K+ channel subunits. Biophys J *72*, 1489-1500.

Tombola, F., Pathak, M., and Isacoff, E. (2005). How Far Will You Go to Sense Voltage? Neuron *48*, 719-725.

Yusaf, S. P., Wray, D., and Sivaprasadarao, A. (1996). Measurement of the movement of the S4 segment during the activation of a voltage-gated potassium channel. Pflugers Arch *433*, 91-97.

CHAPTER II

The S4 Voltage Sensor Packs Against the Pore Domain in the KAT1 Voltage-Gated Potassium Channel

Abstract

In voltage-gated ion channels, the S4 transmembrane segment responds to changes in membrane potential and controls channel opening. The local environment of S4 is still unknown, even regarding the basic question as to whether S4 is close to the pore domain. Relying on the ability of functional KAT1 channels to rescue potassium (K^+) transport-deficient yeast, we have performed an unbiased mutagenesis screen aimed at determining whether S4 packs against S5 of the pore domain. Starting with semilethal mutations of surface-exposed S5 residues of the KAT1 pore domain, we have screened randomly mutagenized libraries of S4 or S1-S3 for second-site suppressors. Our study identifies two S4 residues that interact in a highly specific manner with two S5 residues in the middle of the membrane spanning regions, supporting a model in which the S4 voltage sensor packs against the pore domain in the hyperpolarized or "down" state of S4.

Introduction

Voltage-gated potassium (K_v) channels are widely distributed and perform numerous physiological functions in the animal and plant kingdoms. Plant K_v channels play important roles in controlling the flow of salt and water (potassium uptake and translocation toward the shoots) and in regulating cell volume (stomatal movement and root hair growth) (Brownlee, 2002; Gaymard et al., 1998; Hosy et al., 2003; Rodriguez-Navarro, 2000; Very and Sentenac, 2003), whereas animal K_v channels control the excitability of neurons and muscles and have been linked to diseases of the brain (epilepsy and episodic ataxia), ear (deafness), muscle (myokymia) and heart (arrhythmia) (Ashcroft, 2000; Crunelli and Leresche, 2002; Hille, 2001; Shieh et al., 2000). The basic mechanism for voltage-gating —the ability of K_v channels to detect changes in membrane potential and respond with conformational changes that lead to channel opening or closing—is conserved in plant and animal K_v channels, though still not well understood at the molecular level.

There is a high degree of structural similarity between animal and plant K_v channels (Cao et al., 1995; Sato et al., 2002; Sato et al., 2003; Schroeder et al., 1994; Uozumi et al., 1998). Both are composed of four alpha subunits each containing six transmembrane (6-TM) segments labeled S1 through S6. The pore-forming region, S5-S6, makes up the ion conduction pathway and both channel types contain the potassium selective signature sequence, GYG. Both Shaker and KAT1, representatives from each family, require salt bridge interactions between conserved residues in S2 and S4 in order to fold and

function (Sato et al., 2003; Seoh et al., 1996; Tiwari-Woodruff et al., 1997) and the S3-S4 linkers of each are exposed to the extracellular side (Gandhi et al., 2003; Lee et al., 2003; Mura et al., 2004). Moreover, chimeric constructs of KAT1 and *Xenopus laevis* Shaker form functional channels (Cao et al., 1995). Most importantly, the S4 segments of both plant and animal K_v channels contain multiple positively charged residues. Biophysical studies of voltage-gated sodium and potassium channels have shown that these channels contain intrinsic voltage sensors, S1-S4 (Bezanilla, 2000; Hille, 2001; Hoshi, 1995; Swartz, 2004; Yellen, 2002). In particular, the highly charged S4 segment is the primary component of the voltage sensor (Aggarwal and MacKinnon, 1996; Latorre et al., 2003b; Marten and Hoshi, 1998; Seoh et al., 1996; Sigworth, 1994; Zei and Aldrich, 1998).

In voltage-gated ion channels, the S4 basic residues are closer to the cytoplasmic side of the membrane (the "down" state) during hyperpolarization but move toward the extracellular side of the membrane (the "up" state) upon depolarization. Membrane depolarization drives S4 from the down state to the up state causing depolarization-activated K_v channels to open (Bezanilla, 2002; Gandhi and Isacoff, 2002; Horn, 2002). In contrast, hyperpolarization-activated cation channels activate when S4 moves from the up state to the down state (Latorre et al., 2003b; Mannikko et al., 2002; Sesti et al., 2003). These differences in activation are likely due to different ways of coupling the voltage sensor to pore opening. Both depolarization and hyperpolarization-activated channels have been found in kingdoms and domains ranging from archea to

animals. For example, KvAP, SKOR, and Shaker are depolarization-activated channels from archea, plant, and animal, respectively (Gaymard et al., 1998; Ruta et al., 2003; Tempel et al., 1987). Hyperpolarization-activated channels of these same classifications are MVP, KAT1, and HCN (Anderson et al., 1992; Ludwig et al., 1999; Sesti et al., 2003). The high degree of gating and structural similarities of voltage-gated channels suggests that studying plant K_v channels will elucidate basic themes common to all K_v channels including animal K_v channels found in neurons, heart, and muscle cells.

Crucial to the mechanistic understanding of voltage-gating is the question of the location and surroundings of the S4 segment in the down state and the up state as well as along the gating transition pathway (Grabe et al., 2004). However, the existing models are rather divergent. Whereas several models suggest that S4 resides within the transmembrane domain in the down state and is at least partially surrounded by S1-S3 and S5-S6 (Broomand et al., 2003; Gandhi et al., 2003; Laine et al., 2003; Lee et al., 2003; Starace and Bezanilla, 2004), a different model, based upon the X-ray crystallographic data of the bacterial K_v channel, KvAP, bound to a Fab fragment (Jiang et al., 2003a), has S3b and S4 forming a paddle exposed at the periphery of the channel—far from S5 with S2 between the paddle and the pore domain—in the down state (Jiang et al., 2003a; Jiang et al., 2003b). As to the up state of KvAP, electron microscopic analysis suggests that S4 is positioned loosely at the channel periphery with its basic residues exposed to the membrane (Jiang et al., 2004; Sands et al., 2005). Another up state model of KvAP based on electron paramagnetic resonance

(EPR) spectroscopy has S4 on the periphery of the channel with most of the basic residues not exposed to the lipid (Cuello et al., 2004).

There has been much effort devoted to experimentally resolving the location of the S4 segment relative to the pore domain in K_v channels. Studies of the mammalian HERG and HCN2 channels, as well as chimeras between the 6-TM Shaker channel and the 2-TM KcsA channel, suggest close proximity of the cytoplasmic S4-S5 linker and the cytoplasmic end of S6 in the down state (Decher et al., 2004; Lu et al., 2002; Tristani-Firouzi et al., 2002). Moreover, cysteines introduced at the extracellular ends of S4 and S5 of the Shaker K_v channel can form disulfide bonds revealing close proximity between the ends of these segments in both the up and down states (Broomand et al., 2003; Gandhi et al., 2003; Laine et al., 2003; Neale et al., 2003). Attempts to induce disulfide bridge formation between cysteines within the S4 and S5 transmembrane segments have been unsuccessful (Gandhi et al., 2003; Laine et al., 2003), however, cysteines may not be as reactive in the hydrophobic environment of the protein/membrane core (Mordoch et al., 1999). Thus, whether S4 packs against S5 along their transmembrane segments remains an open question.

To circumvent these difficulties, we employed an alternative strategy involving random mutagenesis and a positive growth selection based on the ability of functional plant K_v channels to rescue the growth of the K^+ transport-deficient (D*trk1*D*trk2*) yeast strain SGY1528 in low K^+ media (Anderson et al., 1992; Ko and Gaber, 1991). To date, it has not been possible to rescue K^+ transport-deficient yeast with mutant or wildtype animal K_v channels. Therefore,

it is necessary to use hyperpolarization-activated plant K_v channels that are uniquely suited for this system due to their ability to selectively pass K^+ ions at the hyperpolarized membrane potential of yeast, estimated to be between –100 and –250 mV (Latorre et al., 2003a; Serrano and Rodriguez-Navarro, 2001). We have selected KAT1, a hyperpolarization-activated voltage-gated K^+ channel from *Arabidopsis thaliana* (Anderson et al., 1992; Schachtman et al., 1992), to carry out this study.

In this study, semilethal mutations are first introduced into the middle of the S5 segment so that the mutant KAT1 channel can rescue K^+ transport-deficient yeast for growth in 2 mM (selective), but not 0.4 mM K^+ (highly selective) media. If S4 packs against S5 within the transmembrane domain, a reduction of the channel function due to the semilethal mutation in the middle of S5 could conceivably be rescued by a second-site suppressor mutation in the middle of S4—such functional double mutant channels could in principle be selected from a library of KAT1 channels bearing the semilethal S5 mutation and a randomly mutagenized S4 segment. Likewise, similar screens of libraries of KAT1 channels bearing the same semilethal S5 mutation and randomly mutagenized S1-S3 segments would provide an opportunity of finding experimental support of S5 packing against the S1-S3 transmembrane segments. By constructing both types of libraries for mutant screens using yeast growth as a positive selection, we wished to search for evidence of specific interactions between the voltage sensing domain and S5 residues within the transmembrane domain of K_v channels.

Materials and Methods

Molecular Biology

KAT1 with its 5' and 3' UTRs was amplified by PCR and cloned into the HindIII-XhoI sites of a modified pYES2 vector containing a Met-25 promoter (Minor et al., 1999). Site-directed mutations were made using the QuikChange Site-Directed Mutagenesis Kit (Stratagene, LaJolla,CA). For the yeast libraries, the following silent mutations were made: AvrII-SacI cut sites (at residues 57 and 161) flanking the DNA region coding for S1-S3 and SacI-BamHI cut sites (at residues 161 and 195) flanking the DNA region coding for S4. A stuffer sequence containing the N- and C-terminus (residues 1-96 and 192-414 linked with a GGSGG sequence in between) of Kir 3.2 was inserted between either the AvrII-SacI sites or the SacI-BamHI sites to create the KAT1-S1-S3-stuffer and KAT1-S4-stuffer constructs, providing negative controls and also a non-functional background for library construction. All constructs were verified by fluorescence sequencing.

Library Construction

Libraries were created using primers containing the AvrII-SacI cut sites flanking S1-S3 and the SacI-BamHI cut sites flanking S4 of KAT1 to amplify S1-S3 (residues 66-154) or S4 (168-189, or 168-184 for the Y193E screen) by error-prone PCR: 1x Taq Buffer, 0.2 mM dATP, 1 mM dGTP, 1 mM dCTP, 1 mM dTTP, 0.5 μM forward primer, 0.5 μM reverse primer, 100 ng double stranded DNA template, 4 mM $MgCl_2$, 0.5 mM $MnCl_2$, and 5 units of Taq polymerase

(Promega, Madison, WI). This created a 2.1-3% base pair error rate corresponding to 4.6-5.3% amino acid changes per region in unselected clones.

Error-prone PCR products were gel purified and cut with the appropriate restriction enzymes and ligated into the KAT1-S1-S3-stuffer or KAT1-S4-stuffer constructs. Ligation mixtures were phenol/chloroform extracted, ethanol precipitated, and resuspended in 3 μL of autoclaved reagent grade water. 1 μL of the ligation mixture was used to transform DH10B competent cells (Invitrogen, Carlsbad, CA) via electroporation. The transformed cells were resuspended in 1 mL SOC and incubated at 37°C for 0.5-1 hour with shaking. One μL of these cells was plated onto LB + carbenicillin to determine library complexity and the rest was added to 100 mL LB + carbenicillin liquid culture for growth overnight. The plasmids from the library culture were extracted using the Qiagen maxiprep kit (Qiagen, Valencia, CA) for use in the yeast selection assay.

Randomized codons were created using the QuikChange site-directed mutagenesis kit (Stragene, LaJolla, CA) with primers containing NNN (25%A,C,G,T at each site) yielding 64 possible codons. A portion of the bacteria transformed with the QuikChange mixture was plated onto LB + carbenicillin plates, yielding colonies from which plasmids were extracted using the Qiagen miniprep kit (Qiagen, Valencia, CA) and sequenced by fluorescence sequencing to assess the mutation complexity. The number of colonies on the plate determines the library complexity. An equivalent portion was added to 100 mL LB + carbenicillin liquid culture for growth overnight. Plasmids from the library culture were extracted using the Qiagen maxiprep kit (Qiagen, Valencia, CA) for use in

the yeast selection assay. These libraries each contained more than 272 (500 in two cases) independent constructs (Table 1C) corresponding to greater than 40% (97% in those two cases) confidence level that all possible codons (64) are represented.

Yeast Selection

The yeast strain SGY1528 was transformed with mutant libraries via lithium acetate and plated onto nonselective conditions containing 100 mM K^+ (Minor et al., 1999). After growth for 3 days, yeast were either replica plated successively onto plates containing 2 mM K^+, 0.5 mM K^+, and finally 0.2 mM K^+ or directly plated onto 0.4 mM K^+ media plates with 1-3 days of growth in between replica plating. Plasmids were extracted from the colonies that grew on 0.2 mM or 0.4 mM K^+ plates, used to retransform yeast to verify the phenotype, and sequenced to identify mutations. Growth phenotypes were assessed by plating yeast transformed with wildtype or mutant KAT1 on 100 mM K^+ media and then streaking them onto 100 mM, 2 mM or 0.4 mM K^+ plates. After verifying the growth phenotype of a portion of surviving colonies on 0.2 mM or 0.4 mM K^+ media, the total number of true positives was estimated to determine the percent rescue (the estimated total number of surviving colonies divided by the total number of colonies screened).

Electrophysiology

Wildtype and mutant *KAT1* with a C-terminal HA tag linked via a BglII site, subcloned into the pLin vector (Yi et al., 2001) at the HindIII-XhoI restriction sites, were transcribed using the AmpliCap T7 High Yield Message Maker Kit (Epicentre Technologies, Madison, WI) to generate cRNA. 5 ng or 30 ng of KAT wildtype or 30 ng of mutant cRNAs in 50 nL were injected into Stage V-VI *Xenopus laevis* oocytes, which were recorded via two-electrode voltage-clamp (GeneClamp 500B, Axon Instruments, Foster City, CA) 4-6 days after injection (filter frequency, 500 Hz; sampling frequency, 2 kHz; pipet resistance, 0.4 – 1.5 MΩ), using the following recording solutions: High K^+ solution: 90 mM K(MES), 1 mM $Mg(MES)_2$, 1.8 mM $Ca(MES)_2$, 10 mM HEPES, pH to 7.4 with 10N KOH; Barium blocking solution: 90 mM K(MES), 1 mM $Mg(MES)_2$, 1.8 mM $Ca(MES)_2$, 10 mM HEPES, 1 mM $Ba(MES)_2$, pH to 7.4 with 10N KOH; Barium and TEA blocking solution: 90 mM K(MES), 1 mM $Mg(MES)_2$, 1.8 mM $Ca(MES)_2$, 10 mM HEPES, 1 mM $Ba(MES)_2$, 10 mM TEA(MES), pH to 7.4 with 10N KOH. Sorbitol was added to ensure the same osmolality for each solution. Exchange of solutions entailed perfusing 2 mL solutions into the oocyte chamber (300 mL volume). The pClamp software (Axon Instruments, Foster City, CA) was used for recording and analysis and Origin (Northampton, MA) or Microsoft Excel (Redmond, WA) for plotting graphs, traces, and data analysis. Statistical significance was determined using an unpaired two-tailed t-test.

Western Blotting

Homogenate of 5 oocytes, taken 6 days after cRNA injection of a particular cRNA (3 days for wildtype) and homogenized by pipeting up and down in 50 mL lysis buffer (20 mM Tris pH 7.5, 150 mM NaCl, 0.5% Triton, 1x Complete Protease Inhibitor Cocktail tablet (Roche, Indianapolis, IN)), was cleared by centrifugation at 20,800 xg for 10 min. at 4°C on a table top centrifuge. The supernatant (approximately 50 mL) was added to 12.5 mL 5x sample buffer (75 mM Tris pH 9.0, 12.5% glycerol, 10% SDS, 0.5 mM EDTA, 10 mM TCEP, bromophenol blue). After incubation at 75°C for 30 min, 15 mL of each sample were loaded onto a 10% SDS-PAGE gel with a 4% stacking gel. The gel was run for 1.5 hours at 100V and blotted onto nitrocellulose overnight at 30 V using the BioRad Ready-Gel mini gel system (Hercules, CA) in the following transfer buffer: 10 mM $NaHCO_3$, 3 mM Na_2CO_3, 0.025% SDS, 20% Methanol. The western blot was blocked with 5% milk/TBST (20 mM Tris pH 7.5, 150 mM NaCl, and 0.05% Tween) and probed with the 3F10 rat anti-HA antibody (Roche, Indianapolis, IN) for the primary antibody and a goat anti-rat F(ab')2 HRP antibody (Jackson ImmunoResearch Laboratories, West Grove, PA) as the secondary antibody. Bands were visualized by chemiluminescence, exposed on film for 15 seconds to 5 minutes and quantified using the AlphaImager 2200 system (Alpha Innotech Corporation, San Leandro, CA).

Wildtype and mutant KAT1 channels with a C-terminal HA tag expressed in yeast were grown to 0.7-0.9 O.D. in100 mM K^+ SD –URA/-MET media and 2 O.D.'s were harvested at 500 xg. The pellet was resuspended in 100 μL of 1x

sample buffer and 0.2 g of acid-washed glass beads (425-600 μm). Samples were vortexed for 90 sec., centrifuged at 14000 xg, and the supernatant sample retained. The samples were then denatured, separated, and blotted as described for the oocyte western blot.

Modeling and Sequence Alignments

Modeller6v2 was used to construct a three dimensional model of the KAT1 central pore (S5-S6) based upon the crystal structure of KvAP (Jiang et al., 2003a; Sali and Blundell, 1993). A truncated form of the KvAP central pore, consisting of K147-V240, was used as a template, and onto this was modeled Y193-S312 of KAT1. The sequence alignment was an extension of an earlier alignment (Shealy et al., 2003), from the AKT subfamily to the KAT1 subfamily determined from our alignment. 100 initial models were made. From these models, the one with the lowest objective energy function was used as a starting point for creating 100 additional models, which had four fold symmetry imposed upon each of the subunits and alpha-helical restraints placed upon the S5 and S6 segments. Again, the model with the lowest objective energy function was selected and is represented in Figure 2B.

Fluorescence Microscopy

KAT1 wildtype and mutants were C-terminally tagged with EGFP via an AgeI site and subcloned into the modified pYES2 vector (Minor et al., 1999; Yi et al., 2001) at the HindIII-XhoI restriction sites. Yeast expressing the KAT1-EGFP

wt and mutants were grown to an O.D. of 0.5-1 in 100 mM K^+ SD –URA/-MET media. Cells were fixed with 2% formaldehyde for 15 min. at room temperature, harvested at 1500 xg for 2 min., resuspended in 0.5 mL 100 mM potassium phosphate, pH 6.6 , incubated for 10 min. at room temperature, harvested at 1500 xg for 2 min., and resuspended in 25 μL of 100 mM potassium phosphate, pH 6.6. Five μL of the cell suspension was mixed with 5 μL of mounting media (Biomeda Corporation, Foster City, CA) on a glass slide and overlaid with a cover slip. Cells were visualized using a Nikon Eclipse E800 Epifluorescence Compound Microscope (Melville, NY) with a 100x objective and 1 second exposure time. Pixel intensity was determined using ImageJ (Rasband, 1997-2005).

Results

The 6-TM K_v channels contain two functionally distinct transmembrane domains: the voltage sensor domain of S1-S4 and the pore domain of S5-S6 (Figure 1A). Because the outer helix of the pore domain, S5, is positioned to interact with the voltage-sensor domain, our attempt to identify transmembrane segments that pack against the pore domain began with a search for mutations in the S5 segment that rendered the mutant KAT1 channel incapable of rescuing the K^+-transport-deficient (*Δtrk1Δtrk2*) yeast strain, SGY1528, for growth on 0.2 or 0.4 mM K^+ (highly selective-low K^+) media. These semilethal mutant channels were folded and expressed on the cell membrane, because they supported yeast growth on 2 mM K^+ (selective -see below) media. We then screened libraries of KAT1 channels carrying a semilethal S5 mutation and a randomized region of the voltage-sensing domain, either S1-S3 or S4, for functional rescue of the SGY1528 yeast strain. KAT1 channels carrying multiple mutations were isolated based on their ability to support yeast growth. In cases where specific suppressors emerged repeatedly from the screens, the specific mutation needed to suppress the original S5 semilethal mutation was identified and verified by constructing double mutants of the suppressor mutation together with the S5 semilethal mutation and showing that the suppressor complemented the S5 semilethal mutation not only in functional rescue of K^+-transport-deficient yeast, but also in functional expression of K^+ channels in *Xenopus* oocytes, as described below.

Identification of semilethal mutations in S5

A BLAST search was performed to the *Arabidopsis* KAT1 sequence (gi: 15237407) revealing 30 highly homologous, distinct channels, with a BLAST index of 500 and greater. A multiple alignment using ClustalW revealed five strictly conserved amino acids in S5 with a roughly helical periodicity (Thompson et al., 1994). All five S5 residues are on the surface of a structural model constructed of the KAT1 pore domain based upon the bacterial K_v channel KvAP using the program Modeller6v2 (Jiang et al., 2003a; Sali and Blundell, 1993); they project away from the central axis of the pore (Figure 1B). This finding agrees with the identification of outward-facing high impact residues based on tryptophan scanning of the Shaker S5 segment (Li-Smerin et al., 2000), and suggests that S5 of the pore domain is in contact with another part of the channel.

We mutated these strictly conserved residues in S5 to glutamate (E), aspartate (D), or glutamine (Q) and tested whether these mutant channels could support yeast growth on low K^+ media. Glutamate substitution of four of these S5 residues (highlighted in Figure 1B), Y193, R197, V204, and H210, as well as glutamine substitution of R197, and aspartate substitution of V204 or H210, prevented the mutant channel from rescuing yeast growth on 0.4 mM K^+ (highly selective) media, whereas these mutant channels were compatible with yeast growth in media containing 100 mM (unselective) or 2 mM K^+ (selective) (Figure 1C). The ability of these semilethal S5 mutants to support yeast growth in 2 mM K^+ media indicates that the mutant KAT1 channels are folded and functional to

some extent, since negative controls of KAT1 with insertion of unrelated protein (KAT1-S1-S3-stuffer and KAT1-S4-stuffer fusion proteins – see Materials and Methods) do not support growth on 2 mM K^+ (data not shown) media. The strong detrimental effect of the semilethal mutation is likely due to compromised interactions of the S5 segment with the rest of the channel protein surrounding the pore domain, since our model of the KAT1 pore domain predicts that these S5 residues are exposed on the surface of the pore domain (Figure 1B – red and yellow). In particular V204 and H210 are located well within the vertical extent of the membrane (red - Figure 1B), far from either end of the S5 segment with at least seven flanking residues (Figure 1D) (Shealy et al., 2003).

Screening for interactions between S5 and S1-S4

To test whether the voltage sensor packs against S5, we screened libraries of KAT1 channels carrying one of the following S5 semilethal mutations, Y193E, R197E or Q, V204E or H210E, along with randomly mutagenized S1-S3 segments or a randomly mutagenized S4 segment. Thus, each set of experiments involved one S5 semilethal mutation screened against a library of S1-S3 or S4. Channels that acquired compensatory mutations in S1-S3 or S4, thereby suppressing the semilethal S5 mutations and permitting yeast growth, were isolated (see Table 1A, B for screening data). Interestingly, the outcome of the screens fell into two distinct categories: constructs with highly specific mutations—recovered repeatedly—that supported more robust yeast growth

(Class I) and constructs with more diverse mutations that were recovered at much lower frequencies likely due to weaker yeast growth (Class II).

Screening several thousand constructs with mutagenized S1-S3 and a specific S5 semilethal mutation resulted in less than 0.5% rescued colonies on low K^+ media from each individual screen (Table 1A) with no clear pattern of second-site suppressor mutations (Class II). Despite different overall patterns, many constructs shared common mutations in S1-S3 irrespective of the initial S5 semilethal mutation (Figure 7). Therefore, some of these S1-S3 mutations have enhanced channel activity in a manner that is not specific to the S5 semilethal mutations that they suppressed.

Both classes of suppressor mutations were obtained from the S4 mutant library screens. For the S5 semilethals, Y193E and R197Q, the outcome was similar to what we observed with the S1-S3 mutant library screens with less than 0.15% rescued colonies on low K^+ media (Class II) (Table 1B). By contrast, a unique S4 suppressor was repeatedly isolated from all of the sampled colonies recovered on highly selective media in the S4 library screens against either V204E or H210E S5 semilethals (Table 1B) with greater than 1.1% rescued colonies on low K^+ media (Class I). The double mutants S179N+V204E and M169L+H210E rescued K^+ transport-deficient yeast (Figure 2A, B). Unlike the single S5 mutants V204E and H210E, the S179N and M169L single mutations did not impair the ability of KAT1 channels to rescue mutant yeast (Figure 2A, B), probably due to the more conservative nature of these S4 mutations. The suppression of the S5 semilethal mutations by these S4 mutations, well within

the transmembrane segment (Figure 2C), is specific, since the double mutants S179N+H210E and M169L+V204E failed to support yeast growth (Figure 2A, B).

The S4 mutations suppressed the S5 semilethals without increasing channel protein expression. HA-tagged double mutants containing the S4 suppressor and the S5 semilethal had comparable or less expression than the HA-tagged S5 semilethal alone (Figure 8). Moreover, epifluorescence microscopy revealed comparable levels of surface expression in yeast expressing EGFP-tagged S5 semilethal mutant channels or double mutant channels carrying the S5 mutation together with its S4 suppressor (Figure 9). All KAT1 constructs tagged with either HA or EGFP gave the same yeast growth phenotypes as the untagged versions. Taken together with the fact that the S5 semilethal mutant must have yielded functional channels on the cell membrane to rescue yeast grown on 2 mM K^+, these observations support the notion that the suppression takes place in functional channels on the cell membrane.

Functional expression of the double mutants in Xenopus *oocytes*

The double mutant of the S5 semilethal mutation together with its specific S4 suppressor yielded greater currents in *Xenopus* oocytes than the single S5 mutant did, as expected from the greater capacity of the double mutant to rescue yeast growth. Having eliminated the endogenous hyperpolarization-activated chloride currents and cation currents (Kuruma et al., 2000) by using chloride-free solutions for recording and by adding 1 mM Ba^{2+} as a channel blocker (Figure 3A), we found no detectable currents in oocytes expressing the H210E

semilethal mutant that failed to rescue yeast grown on 0.5 mM or lower K^+ media, whereas the single S5 mutant V204E—which supported yeast growth on 0.5 mM, but not 0.4 mM K^+ media—generated very low levels of currents compared to wild type KAT1 (Figure 3B, C). Inclusion of the specific S4 suppressor in the double mutant led to greater currents than those due to the respective S5 semilethal single mutants (Figure 3C) (S179N+V204E, V204E, $p<0.001$; M169L+H210E, H210E, $p<0.01$; Figure 3D). When the current amplitudes were normalized for total channel protein (Figure 3D), four pairwise comparisons revealed that the mutants that rescued yeast growth on 0.4 mM K^+ yielded more current than those that did not (S179N+V204E, V204E, $p<0.001$; M169L+H210E, H210E, $p<0.01$; M169L+H210E, V204E, $p<0.02$; S179N+V204E, S179N+V204D, $p<0.001$; Figure 3E).

The mutant channels displayed pharmacological properties characteristic of KAT1 channels, but required greater hyperpolarization for their activation. KAT1 was slightly reduced by 1 mM Ba^{2+} and further reduced by 10 mM TEA^+ (tetraethylammonium) (Schachtmann et al., 1991) (Figure 3B), while the endogenous hyperpolarization-activated currents were blocked only by 1 mM Ba^{2+} (data not shown). Like wildtype KAT1 channels, the single mutants and double mutants were TEA^+ sensitive (data not shown). Whereas the double mutants activated at more hyperpolarized potentials than wildtype KAT1 channels (note that all current traces in Figure 3C were induced by greater hyperpolarization pulses), their voltage-dependence appeared to be in between that of the S5 semilethal single mutants and the wildtype channel, because the

S5 single mutants yielded smaller or non-detectable currents even at the most hyperpolarized membrane potential tested. Thus, while the oocyte recordings may not have revealed the magnitude of the mutant channel activity at the yeast membrane potential, these electrophysiological experiments support the notion that the specific interaction between the S5 semilethal mutations and their respective S4 suppressors increased the ability of channels containing a S5 semilethal mutation to conduct K^+ currents at the yeast's hyperpolarized membrane potential, thereby allowing the double mutants to support yeast growth not only at 2 mM K^+ (selective), but also at 0.4 mM K^+ (highly selective).

For the rest of the study, we have focused on the specificity of the interaction between S179N and V204E and between M169L and H210E. These specific second-site suppressors of the semilethal S5 mutations, V204E and H210E, are located roughly in the middle of the S4 segment (Figure 2C), at least four residues from either end (Anderson et al., 1992), far from both the cytoplasmic S4-S5 loop and residues at the extracellular end of S4 that are in close proximity to the extracellular end of S5 (Broomand et al., 2003; Decher et al., 2004; Gandhi et al., 2003; Laine et al., 2003; Lu et al., 2002; Mannikko et al., 2002; Neale et al., 2003; Tristani-Firouzi et al., 2002). The locations of these specific S4 mutations are compatible with the expectation that the second-site suppressors are adjacent to the semilethal mutations of the S5 segment, lending support to the notion that S4 packs against S5 within the membrane spanning region.

Effects of shortening the S5 side chain length on the suppression of channel semilethality by the S4 mutation

We began our analysis of the specificity of suppression by first asking whether the same S4 mutation could suppress the semilethal mutation due to substitution of the S5 residue with aspartate rather than glutamate. Interestingly, the S179N mutation of S4 could not suppress the semilethality of V204D (Figure 4A) when comparably expressed (Figure 8). Thus the interaction between the polar asparagine substituting S179 on S4 and the glutamate semilethal mutation of V204 on S5 is highly sensitive to the side chain length.

In an analogous test, we found that the same S4 mutation, M169L, suppressed both H210E and H210D mutations, so that the double mutants, but not the single S5 mutants, supported yeast growth on 0.4 mM K^+ media (Figure 4B) when comparably expressed (Figure 8). The ability of the leucine substitution for the S4 methionine to enhance the function of mutant KAT1 channels with either glutamate or the smaller aspartate replacing the S5 histidine is likely due to hydrophobic interactions involving these side chains within the protein, since structural studies have shown that cavities created by shortening a side chain may be partially compensated for by small movements of surrounding atoms (Eriksson et al., 1992).

The S4-S5 interactions are specific

To further scrutinize the specificity of the interaction between the S5 semilethal mutations and their respective S4 suppressors, we randomized the

codon for the S4 residue at position 179 or 169 in channels carrying either aspartate or glutamate at the semilethal positions in S5, position 204 and 210, respectively (Figure 5). The randomized codon was created using a DNA primer containing NNN as the codon for the particular S4 residue, by mixing equal amounts of the four nucleotides at each of the three positions during primer synthesis. We then sequenced a number of mutant constructs from the library without subjecting them first to selection based on yeast growth to verify that all four nucleotides were represented at each of the three positions of that S4 codon.

After this extensive screen of libraries with a randomized S4 codon at position 179, we came to the surprising conclusion that only S179N can suppress the V204E semilethal S5 mutation. From a total of thirteen colonies recovered on highly selective media, both asparagine codons were represented, but no codons for any other amino acids emerged from the mutant screen (Figure 5A). Moreover, a similarly exhaustive screen of libraries of KAT1 bearing the V204D rather than V204E semilethal S5 mutation gave rise to no viable yeast colonies on highly selective media (Figure 5B). We further used site-directed mutagenesis to generate the double mutant S179Q + V204D and verified that this double mutant could not rescue yeast on low K^+ media (data not shown). Thus, evidently no amino acid at position 179 can accommodate the V204D mutation, further reinforcing the notion that the S179N suppression of V204E is highly specific.

The randomized screen of position 169 recovered only leucine as a viable suppressor of the H210D and H210E semilethal mutants. So, while M169L can rescue both H210D and H210E, the interaction between positions 169 and 210 is still highly specific. All possible codons for leucine were represented in ten suppressors of the S5 H210D mutant and 14 suppressors of the H210E mutant (Figure 5C, D), indicating that leucine at position 169 of the S4 segment is uniquely capable of packing against the S5 segment bearing the H210D or H210E mutation.

Discussion

To understand how the S4 segment of K_v channels could function as the voltage sensor by detecting changes in membrane potential and triggering conformational changes of the channel, it is important first to learn how the S4 segment is positioned relative to the rest of the channel protein. The use of yeast growth as a positive selection for the screening of randomly mutagenized K_v channels is crucial for identifying specific interactions between transmembrane segments in the absence of a structural guide, because thousands of mutants can be tested in an unbiased way to select for only folded and functional channels at the membrane surface. This approach has allowed us to uncover two highly specific interactions within the membrane-spanning regions of S4 and S5, likely occurring in the down state since channel opening is required for yeast growth at 2 mM and lower K^+ concentrations (Figure 6A,B). The fact that mutation of the "lower" (closer to the cytoplasmic side) S4 residue suppressed the "lower" S5 semilethal and mutation of the "higher" (closer to the extracellular side) S4 suppressed the "higher" S5 semilethal is suggestive that these highly specific interactions reflect physical proximity between the S5 semilethals and their respective S4 suppressors.

Previous studies support the assertion that suppressors for semilethal mutations usually reside on neighboring structural elements. For example, a variation of the method used here was applied successfully using mutagenesis coupled with yeast screens to determine the transmembrane helix packing of the two-transmembrane K^+ channel, Kir 2.1 (Minor et al., 1999), which turned out to

be in excellent agreement with the crystal structure of a homologous channel, KirBac1.1 (Kuo et al., 2003). This case highlights that semilethal-second-site suppressor pairs lie on interacting surfaces of neighboring transmembrane helices or that these segments are closely packed enough to transmit suppression through other well-packed residues. It also provides a concrete example of how such yeast screens of randomly mutagenized channels can reveal accurate structural information.

Substitution of V204 of the S5 segment with either acidic residue aspartate or glutamate reduced KAT1 channel function to such an extent that the mutant channel could facilitate the growth of K^+ transport-deficient mutant yeast on 2 mM but not 0.4 mM K^+ media. The semilethal mutation V204E, but not V204D, was suppressed only by the S179N mutation in the S4 segment suggesting a close interaction between these two residues. Similarly, both semilethal mutations H210D and H210E of the S5 segment were suppressed by exactly one mutation of the S4 segment, M169L. We have determined that these second-site suppressions are highly specific by carrying out multiple screens of different libraries of randomly mutagenized S4 residues; in no case were additional suppressors isolated (Table 1C, Figure 5). This complete specificity of the interactions between two residues in the middle of the S4 segment with two residues in the middle of the S5 segment is highly suggestive of close packing between the S4 and S5 segments. It is worth noting that other residues in the vicinity of the pair of S5 semilethal and S4 suppressor mutation likely participate in polar and hydrophobic interactions, as a side chain within a protein typically

interacts with parts of multiple side chains. Nonetheless, the highly specific interactions between S4 and S5 residues within these transmembrane segments lend strong support to the notion that the S4 voltage sensor packs against the pore domain.

Notably, the choice of semilethal S5 mutations that reduced, but did not abolish, KAT1 channel function in yeast (rescue of yeast growth at 2 mM and not 0.4 mM K^+) renders it highly unlikely that such mutations exert their impact by preventing folding of the channel. Whereas mutations that compromise protein folding could reduce protein levels, these S5 semilethal mutant channels gave similar levels of protein expression as those of the double mutants in *Xenopus* oocytes (Figure 3D) and in yeast (Figure 8 and 9). Not only did the combination of a semilethal S5 mutation with its specific S4 suppressor restore the ability to rescue yeast on 0.4 mM K^+ (Figure 2), the double mutant also yielded greater currents than the respective single S5 mutants in *Xenopus* oocytes (Figure 3C, D, E). Inclusion of the S4 suppressor mutation may have caused some right shift of the voltage dependence curve compared to that of the S5 single mutants, though it was difficult to quantify these shifts when even the largest hyperpolarization tested was insufficient to allow the mutant channels to reach maximal activation. Taken together, the interactions between V204E and S179N and between H210E and M169L in the double mutants likely increase the channel activity in the open state, or down conformation, of the channel relative to that of the single S5 mutants, which rescue yeast growth on 2 mM but not 0.4

mM K^+, since a greater ability of K^+ conduction is necessary to support yeast growth in lower K^+ concentrations.

The Class II mutations in S1-S3 or S4 provide evidence for close packing of the voltage-sensor and the pore domain, for a different reason. Screens of S5 semilethals against an S1-S3 library revealed that this class of mutations is nonspecific in that no common mutation existed across all of the sampled constructs that suppressed a particular S5 semilethal and several mutations suppressed more than one S5 semilethal (see Figure 7). This is in contrast to the highly specific, Class I, suppressors in S4 where each mutation uniquely compensates the detrimental effect of a particular S5 semilethal at position V204 or H210. Careful studies on globular proteins reinforce the notion that two regions of a protein in close apposition have stronger interactions than do two regions that are distant from each other (LiCata and Ackers, 1995; Schreiber and Fersht, 1995; Wells, 1990). This observation indicates that the Class I suppressors are in close contact with the semilethal mutation, while Class II mutations involve more distant allosteric interactions so that specific information about the chemistry of the substituted amino acid is lost as it is elastically transmitted through the protein to the initial semilethal site. It is also possible that Class II mutations enhance the channel activity in a manner completely independent of the original S5 semilethal mutation thus allowing channels bearing both the semilethal and the Class II mutations to be more active.

Our findings of second-site suppressors in the S4 segment interacting in very specific ways with two S5 residues located within the vertical extent of the membrane provide strong evidence that the voltage sensor packs against the pore domain. In the only high resolution structure of a K_v channel (Jiang et al., 2003a; Jiang et al., 2003b), the S4 segment packs only against S3b, and is separate from the pore domain. It is difficult to reconcile this structure, or the models based on this structure (Jiang et al., 2003a; Jiang et al., 2003b), with our findings of second-site suppressors in the S4 segment interacting in very specific ways with two S5 residues located within the membrane. It is conceivable that the Fab fragments in the co-crystal trapped the channel in a rarely visited conformation (Cohen et al., 2003), or the Fab fragments pulled the S4 segment down (Jiang et al., 2003a). Other confounding factors include the lack of a planar lipid membrane to support the correct juxtaposition of the pore domain and the voltage sensor domain and the possibility of these domains being incorporated into separate micelles (Gulbis and Doyle, 2004).

It is worth noting that the S4 residue M169 of KAT1 corresponds to the residue immediately following the first S4 basic residue of Shaker—R362 (Shealy et al., 2003). Furthermore, only when the Shaker channel is in the up state can the cysteine replacing R362 be cross-linked with a cysteine replacing either F416 or A419, at the extracellular end of S5 (Broomand et al., 2003; Gandhi et al., 2003; Laine et al., 2003) (Figure 6B). If the down state of KAT1 channel is indeed structurally analogous to the down state of Shaker channel, the highly specific interaction between M169 and a S5 residue within the confine of the membrane,

2-3 helical turns from the S5 residues corresponding to F416 and A419 of Shaker, would imply that the S4 segment moves outward—in the vicinity of the pore domain—as the channel transits from the down state to the up state (Figure 6A). This scenario for voltage gating of K_v channels is consistent with recent studies suggesting that S4 moves in a gating pore (Tombola et al., 2005), without concerted movement together with S3b as a paddle in the membrane (Ahern and Horn, 2004; Gonzalez et al., 2005).

The strategy of identifying specific second-site suppressors as reported in this study provides an unbiased paradigm to assess the proximity of transmembrane segments of K_v channels in a biological system. Using this approach, we have uncovered specific interactions over a large span of S4 and S5 suggesting that these two segments are in close proximity. Whether and how S1-S3 might pack against S4 is another question that could potentially be addressed in future studies employing yeast mutant screens. It is important to stress here the difference between S4 movement during voltage gating of K_v channels on the cell membrane and membrane insertion of S4 in the endoplasmic reticulum, a process that takes much longer and critically depends on the context—the hydrophobic segments that precede S4, the translocon and probably chaperones as well (Hessa et al., 2005; Sato et al., 2002). The finding that the S4 helix has intimate contact with other portions of the channel within the membrane span has profound implications on the energetics of voltage-gating (Grabe et al., 2004). Additionally, the close interactions between the voltage sensor S4 and the outer helix of the pore domain will be of critical importance in

considering how the motion of the S4 sensor might influence the conformation of the pore domain in channel gating (Doyle, 2004; Swartz, 2004; Yellen, 2002).

Figures

Figure 1. Identification of KAT1 semilethal mutations in S5.

Glu (E) semilethal mutations are in red. Asp (D) semilethal mutations are in brown. (A) General topology of a 6-TM subunit of the tetrameric K_v channel, with the voltage sensor S1-S4 and the pore region S5-S6 outlined. Transmembrane segments are shown as rods and loop regions as curved lines. The extracellular region is designated as "out" and the intracellular region is designated as "in." (B) The S5 residues Y193 (yellow), R197 (yellow), L201, V204 (red), and H210 (red) highlighted on a model of the KAT1 pore domain, S5-S6, reveal that all five residues are on the surface of the pore domain with V204 and H210 well within the predicted transmembrane segment of S5. S5 is shown in blue and S6 in grey, the subunit closest to the reader in darker shade than the remaining 3 subunits. Loop regions were not included in the figure for clarity. (C) All constructs, wt, V204E, V204D, H210E, and H210D grow on unselective 100 mM K^+ media and also on the selective 2 mM K^+ media. However, V204E, V204D, H210E, and H210D cannot rescue the K^+ transporter deficient yeast on the highly selective 0.4 mM K^+ media. (D) The KAT1 S5 sequence including V204 and H210 (red and underlined) and Y193 and R197 (black and underlined), based on a published alignment (Shealy et al., 2003).

Figure 1. Identification of KAT1 Semilethal Mutations in S5.

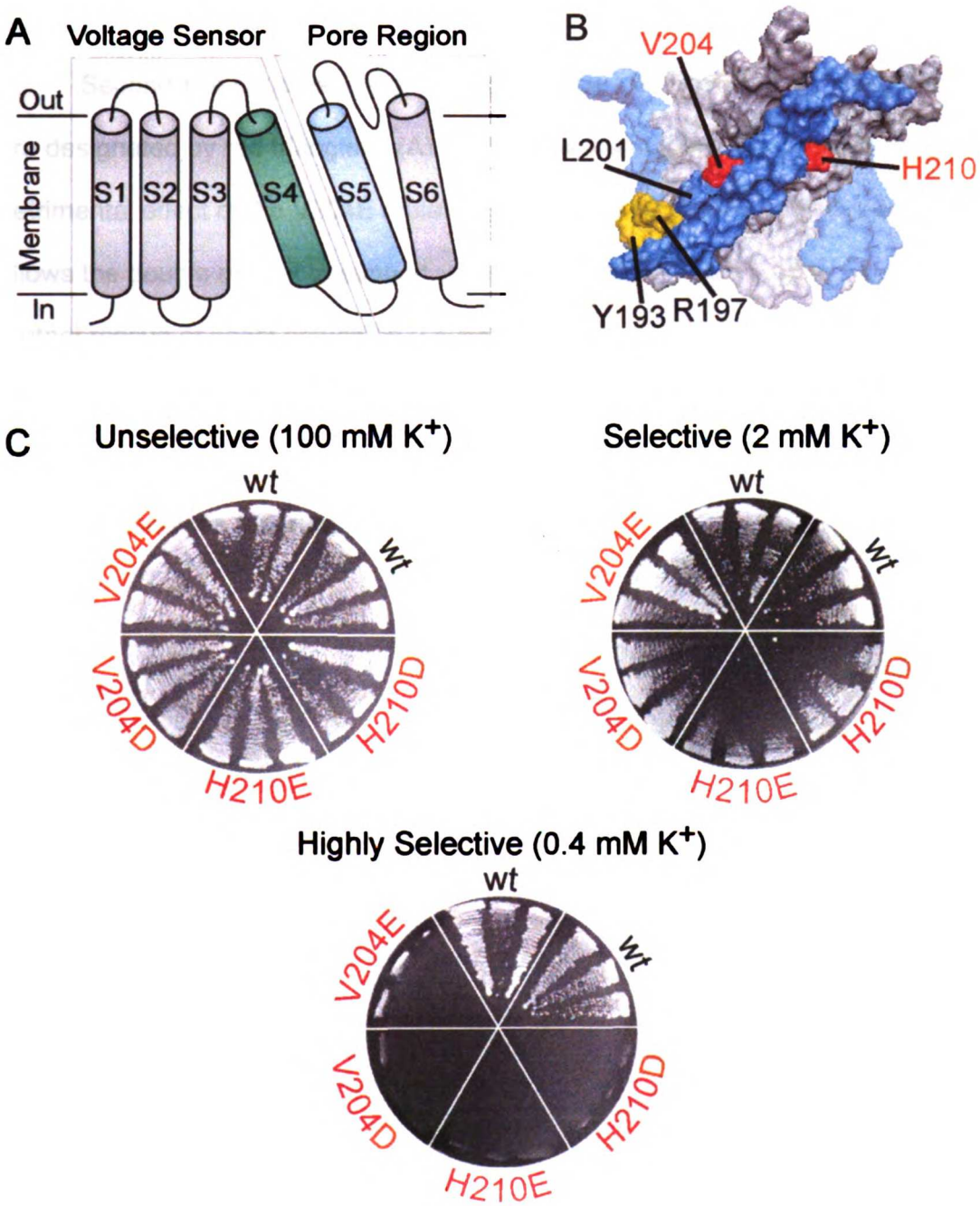

Figure 2. Specific second-site suppressors for two S5 semilethals within the transmembrane domain.

Second-site suppressors are designated by a purple pacman. Semilethals are designated by red triangles. (A) S179N (but not M169L) suppression of the detrimental effect of the V204E mutation, shown schematically on the right, allows the double mutant to support yeast growth on 0.4 mM K^+. (B) Double mutant rescue of yeast growth on 0.4 mM K^+ due to M169L (but not S179N) suppression of the detrimental effect of H210E, shown schematically on the right. (C) The KAT1 S4 sequence including M169 and S179 (purple and underlined) with boundaries as reported (Anderson et al., 1992).

Figure 2. S4 Second-Site Suppressors Are Specific for S5 Semilethal Mutations.

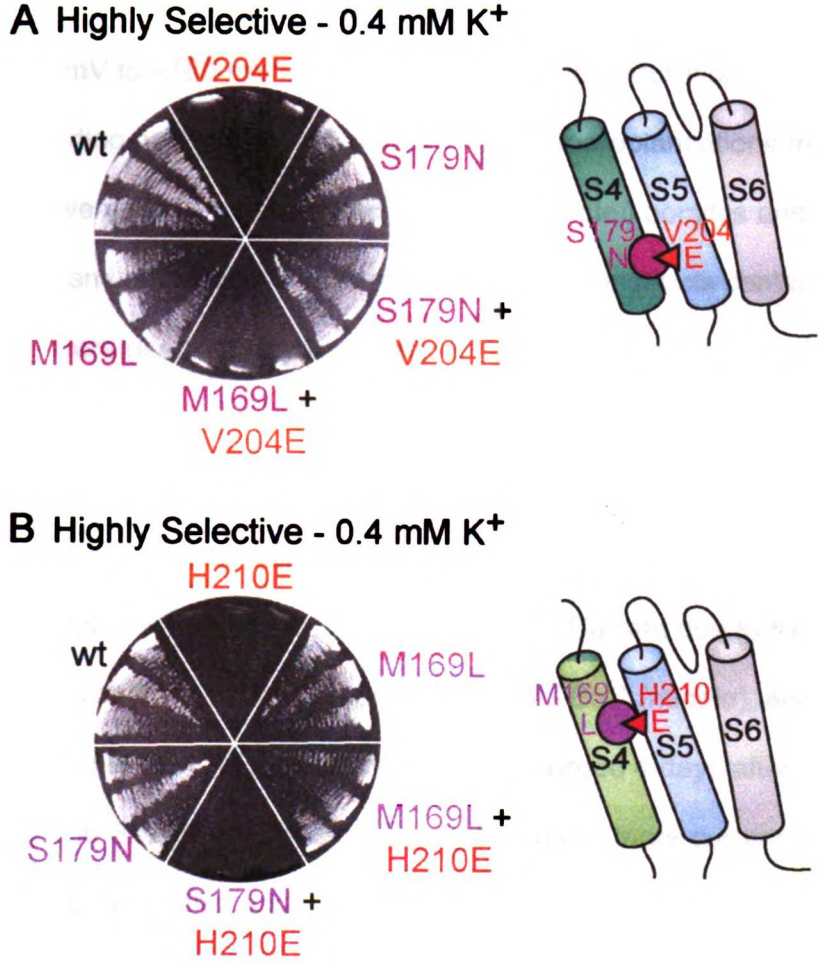

C KAT1 S4 162 LGFRILSMLRLWRLRRVSSLFA 183

Figure 3. Mutant KAT1 currents and protein expression.

Oocytes expressing KAT1 wildtype were subjected to voltage pulses from +20 mV to –180 mV in 10 mV increments for a duration of 5 seconds each, from a holding potential of –10 mV, whereas hyperpolarizations from –70 mV to –180 mV were given to uninjected and water injected oocytes and those expressing the semilethals and double mutants. KAT1 constructs containing a C-terminal HA tag were used in oocyte expression for both current recordings and protein expression measurements. (A) Endogenous hyperpolarization-activated currents, apparent at potentials more negative than –160 mV in uninjected oocytes (left), is blocked by 1 mM Ba^{2+} (middle) and undetectable after addition of 1 mM Ba^{2+} and 10 mM TEA^{+} (right). (B) Current due to KAT1 wildtype channels (left) is slightly reduced by 1 mM Ba^{2+} (middle), and is further blocked by 10 mM TEA^{+} (right). Oocytes were recorded 4 days after 5 ng cRNA injection. (C) The S179N + V204E double mutant gives more current compared to the V204E semilethal and the S179N + V204D double mutant, both of which cannot rescue yeast growth on 0.4 mM K^{+}. Likewise, the M169L + H210E double mutant gives more current than the H210E mutant. All traces are from the same batch of oocytes except for S179N+V204D.

Figure 3 (continued).

(D) Top: Steady-state current amplitudes of KAT1 double mutants and semilethals at −160 mV in barium blocking solution after subtraction of endogenous currents as measured in water injected oocytes in barium blocking solution (n=5 for each construct, mean and standard errors shown). Constructs are color coded as indicated in (E). Bottom: Western blot of KAT1 constructs from oocytes. All the double mutants and semilethals are for oocytes injected with 30 ng RNA and after 5.5-6 days expression. Oocytes from the 50 nL water injected control were taken 6 days after water injection while the 30 ng injected KAT1-HA wildtype control was taken after 3 days. All bands are from the same gel with the same exposure time in the linear range of the film. Lanes were rearranged to align with the graphs. (E) Single and double mutant KAT1 currents were normalized by the total channel protein expression in oocytes as determined from the western in (D) from the average pixel intensity of each band with background subtraction.

Figure 3. Mutant KAT1 Currents and Protein Expression.

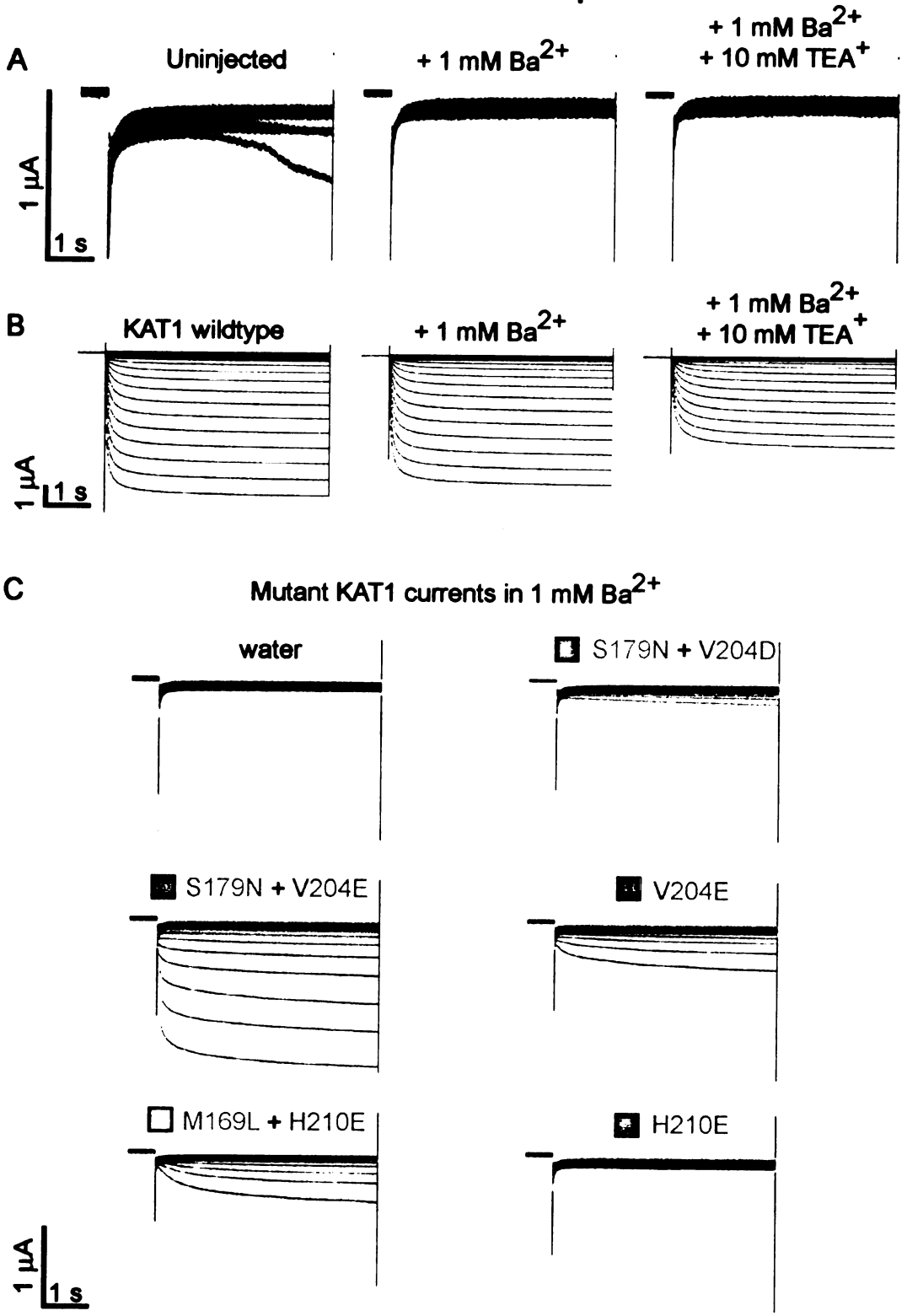

Figure 3 (continued). Mutant KAT1 Currents and Protein Expression.

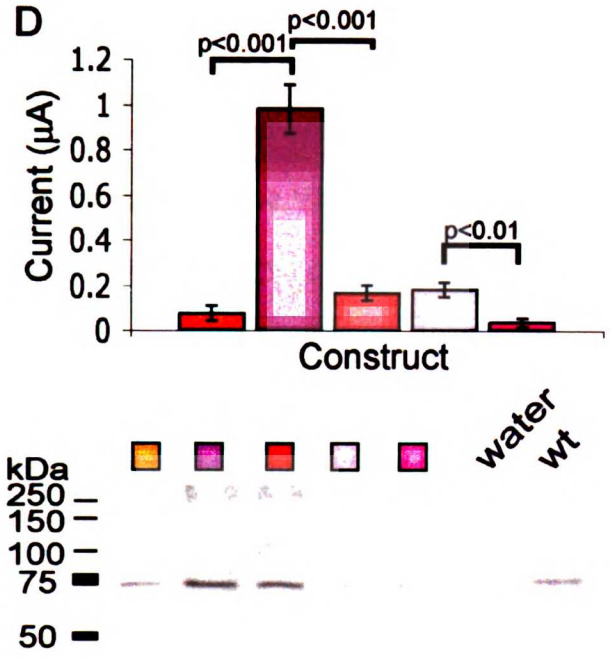

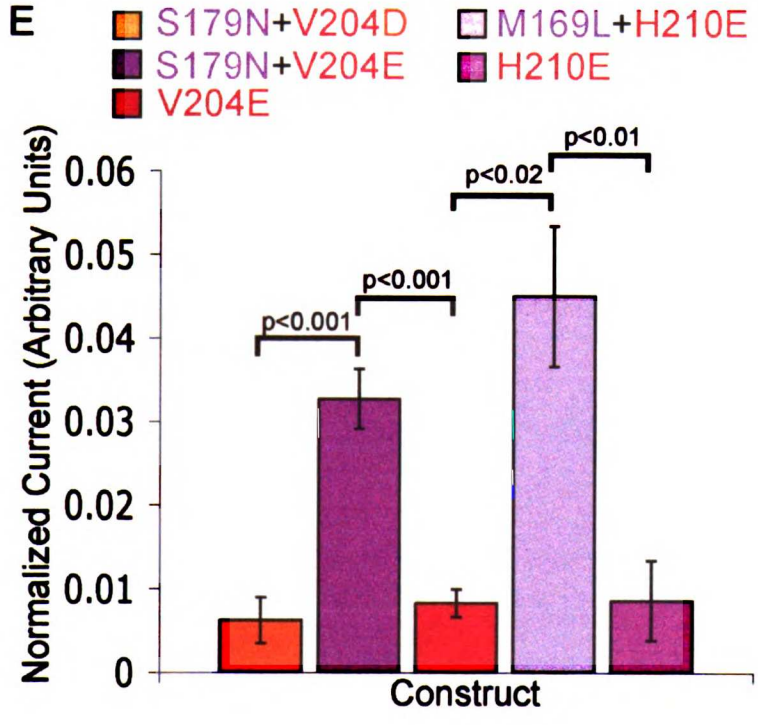

Figure 4. One of the S4 suppressors for S5 glutamate substitution cannot suppress the aspartate substitution of the same S5 residue.

Suppressors are in purple. Glutamate (E) substitutions are represented by red triangles and aspartate (D) substitutions by brown triangles. (A) S179N cannot suppress the V204D semilethal on 0.4 mM K^+. (B) M169L can suppress the H210D semilethal on 0.4 mM K^+.

Figure 4. Test of the Sensitivity of Second-Site Suppression on the Semilethal Mutation Side Chain Length

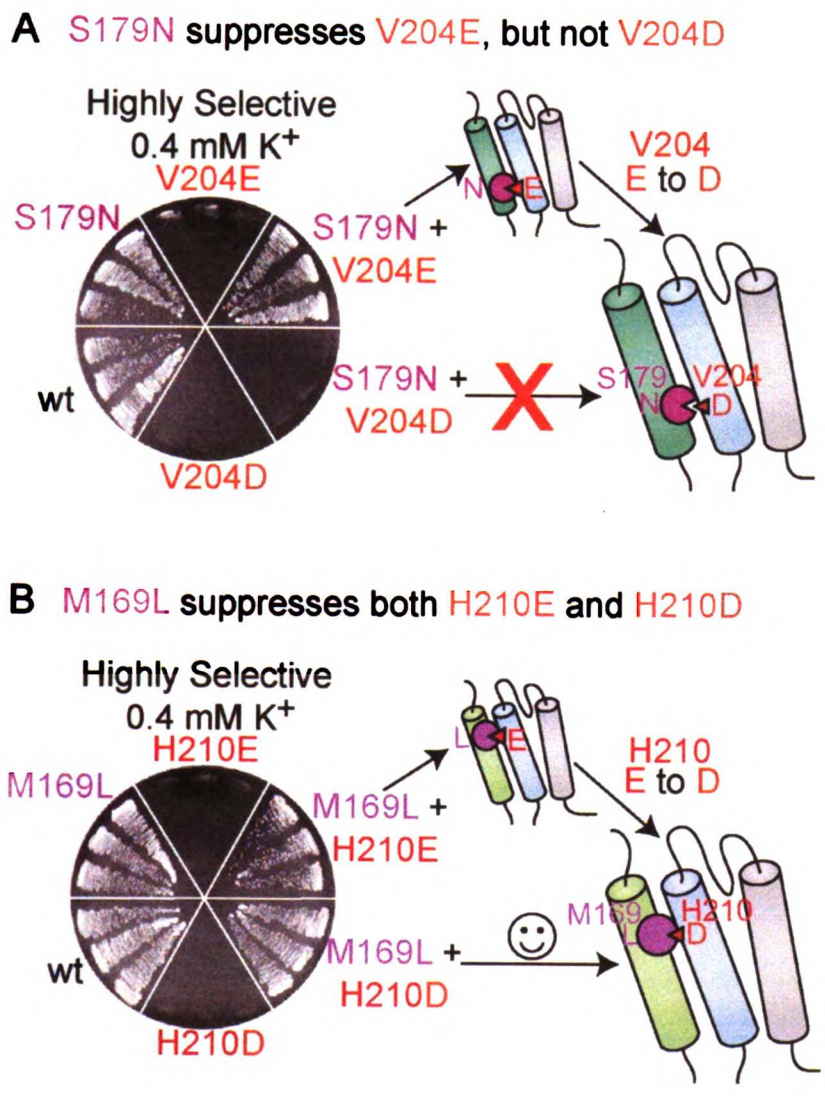

Figure 5. Second-site suppressors are highly specific for the S5 semilethal.

Suppressors are in purple and semilethals are in red for glutamate and brown for aspartate. The tables indicate the codons (left column) encoding the amino acid (right column) recovered from the suppressor screens. Those codons detected in the original S4 library screen against that particular S5 semilethal (Figure 3 and Table 1) are marked by an asterisk (*) and included in the number of times that codon was detected (middle column). (A) S179X + V204E screen recovered only codons for Asn (N), the original second-site suppressor. (B) S179X + V204D screen recovered no suppressors. (C) M169X + H210E screen recovered only codons for Leu (L). (D) M169X + H210D screen also recovered only codons for Leu (L).

Figure 5. Second-Site Suppressors Are Highly Specific for the S5 Semilethal.

A S179**X** + V204E **screen**

Codons recovered	# times	Amino Acid for S179X
AAC	13*	Asn (N)
AAT	1	Asn (N)

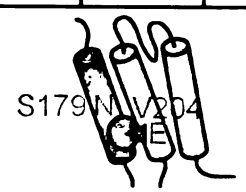

B S179**X** + V204D **screen**

No second-site suppressors recovered.

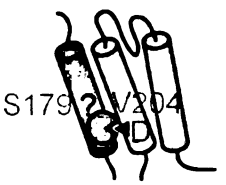

C M169**X** + H210E **screen**

Codons recovered	# times	Amino Acid for M169X
CTT	8	Leu (L)
CTC	2	Leu (L)
CTA	2	Leu (L)
CTG	3*	Leu (L)
TTG	1*	Leu (L)

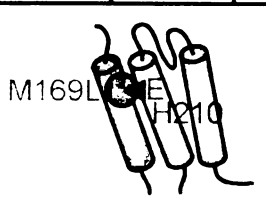

D M169**X** + H210D **screen**

Codons recovered	# times	Amino Acid for M169X
CTA	7	Leu (L)
CTG	2	Leu (L)
TTA	1	Leu (L)

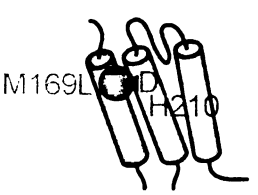

Figure 6. S4-S5 interactions for KAT1 and Shaker K_v channels.

(A) Schematic summary of likely S4 motion relative to the pore domain. (B) Arrows link S5 semilethals (red triangles) to second-site suppressors found from the yeast screens (purple pacmans), interactions that enhance KAT1 channel activity in the hyperpolarized state (left). Based on published alignment of S4 (Latorre et al., 2003b) and S5 (Shealy et al., 2003), a down state disulfide bridge interaction for Shaker found by Neale et al. is designated by a red line (Gandhi et al., 2003; Neale et al., 2003), disulfide bridges found for the depolarized or up state of Shaker (right) shown by dashed lines and marked with black triangles for R362C + F416C (Broomand et al., 2003; Gandhi et al., 2003; Laine et al., 2003), and disulfide bridges found in both the down and up states of Shaker by Gandhi et al. shown in grey (left and right) (Gandhi et al., 2003).

Figure 6. S4-S5 Interactions for KAT1 and Shaker K_V Channels.

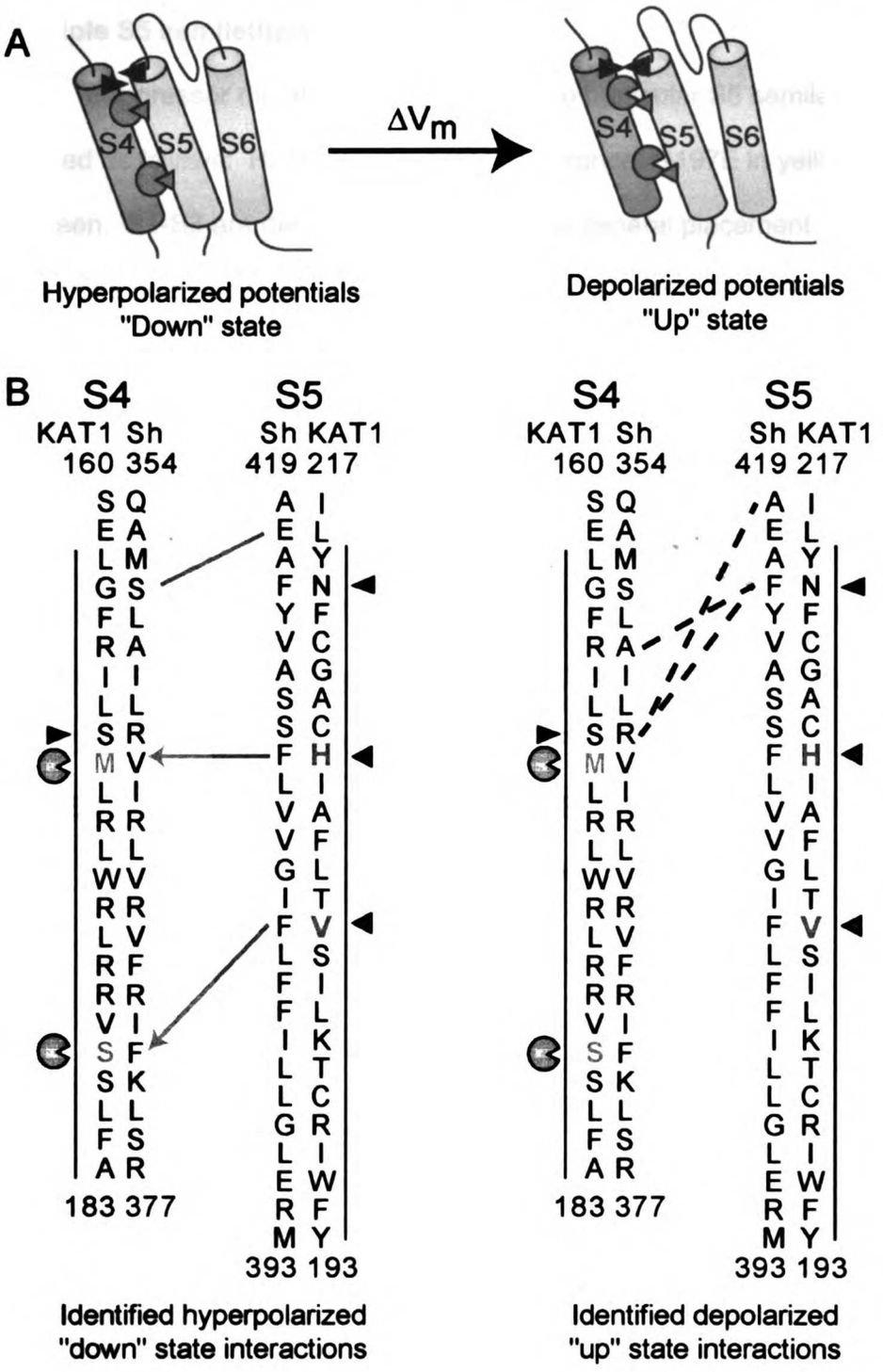

Figure 7. The S1-S3 mutant libraries yielded suppressor mutations of multiple S5 semilethals.

Suppressor mutations corresponding to particular S5 semilethals are colored as follows: H210E in red, V204E in orange, R197E in yellow, and Y193E in green. S1-S3 are depicted as rods to show general placement of the mutations on these segments; however, no tertiary structure is implied. Abutting circles indicate residue positions of common suppressor mutations for multiple S5 semilethals (triangles). The individual constructs that were recovered are as follows: For the H210E screen, F81I + I131V + H210E, H118R + F138L + A146V + S152G + H210E, K88N + H210E, and I76V + F79L + F92S + H210E; For the V204E screen, F92L + I94V + V204E, I71M + Q80R + V204E, and M64I + Q80H + V204E; For the R197E screen, I83V + R197E, F81S + I83V + S125C + I131T + R197E, Q80H + R197E, and I76V + F81S + F92S + I97V + R197E; For the Y193E screen, I131M + Y193E, I84D + Y193E, I94V + I97V + T109V + S125N + Y193E, K88N + H118R + Y193E, and K89G + Y193E.

Figure 7. The S1-S3 mutant libraries yielded suppressor mutations of multiple S5 semilethals.

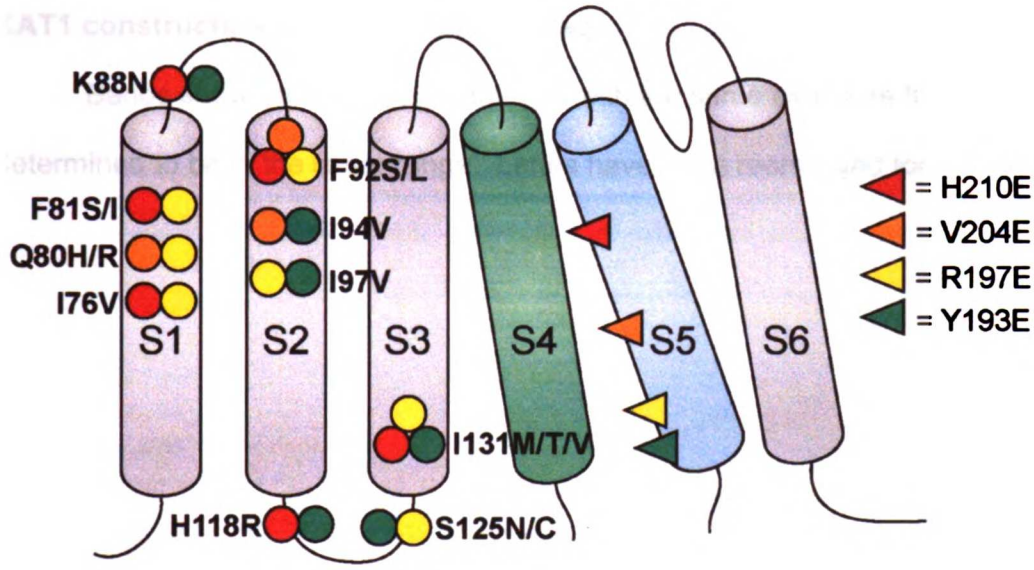

Figure 8. Comparable expression of yeast expressing KAT1 double mutants and the corresponding semilethal based on Western analyses of KAT1 constructs with a C-terminal HA tag.

Bands shown are from the same gel with the same exposure time and determined to be in the linear range. Lanes have been rearranged for clarity.

Figure 8. Comparable expression of yeast expressing KAT1 double mutants and the corresponding semilethal based on Western analyses of KAT1 constructs with a C-terminal HA tag.

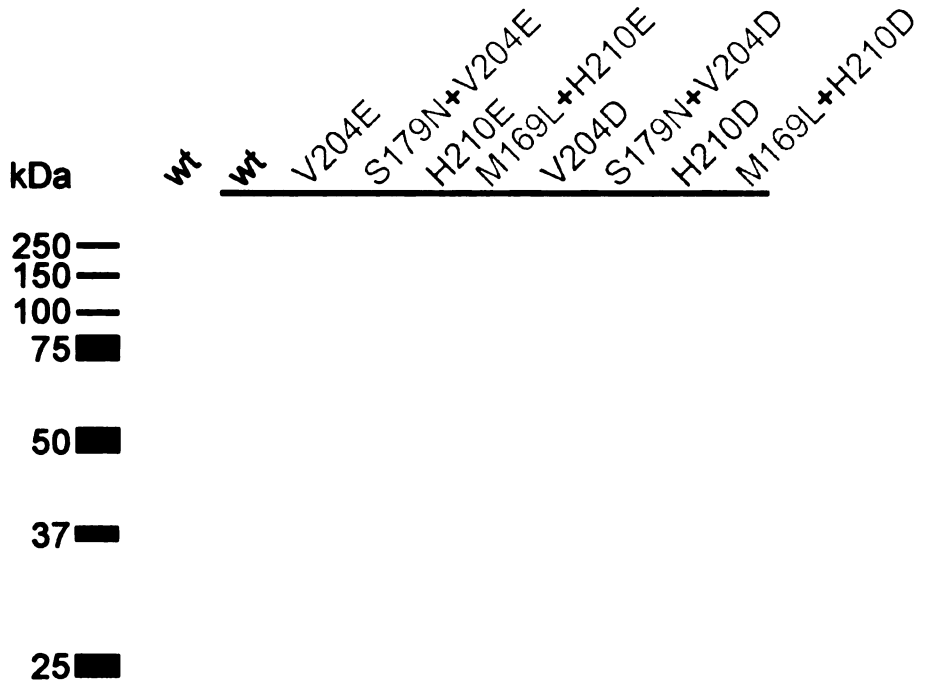

Figure 9. KAT1 wildtype and mutants fused with EGFP to the C-terminus show comparable fluorescence at the cell periphery.

(A) Sample images of EGFP fusion constructs of KAT1 wildtype and mutant are shown as well as the control of KAT1 wildtype channel without EGFP. Scale bar is 5 μm. (B) Cell periphery fluorescence was quantified for KAT1 wt-EGFP (45 cells) and EGFP tagged KAT1 mutants (60 cells). Median (top of colored bar), 25th percentile (lower border of box), and 75th percentile (upper border of box) are shown. Cell periphery fluorescence was not quantified in areas of the yeast that were budding, had saturated spots of fluorescence, or were out of focus.

Figure 9. KAT1 wildtype and mutants fused with EGFP to the C-terminus show comparable fluorescence at the cell periphery.

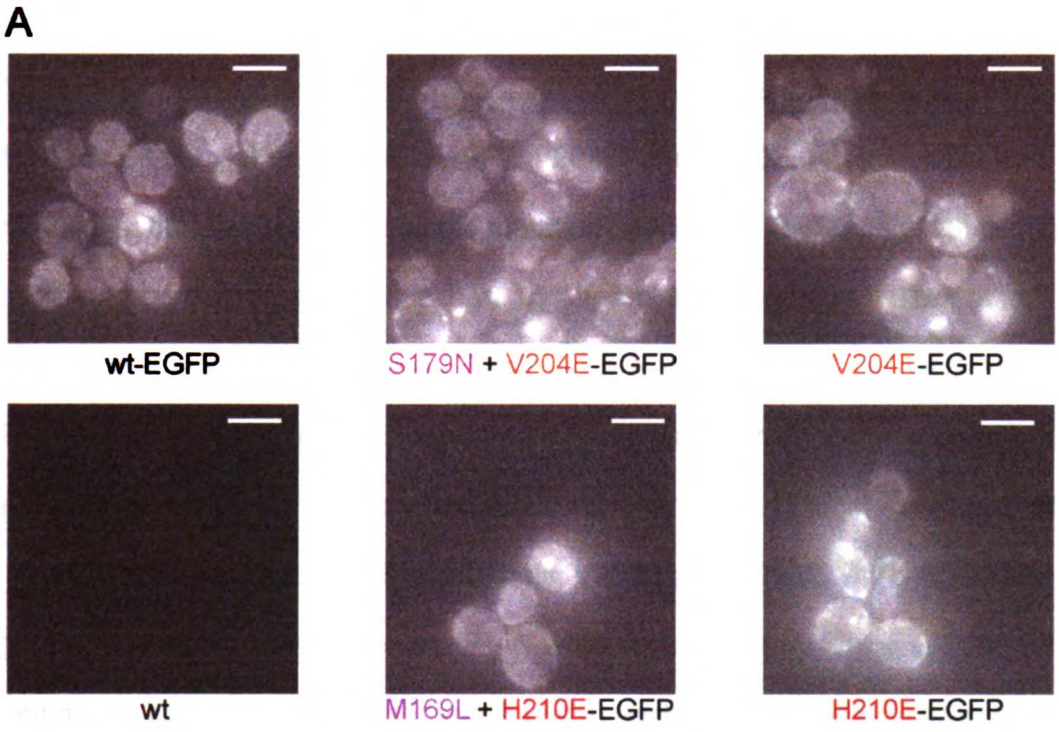

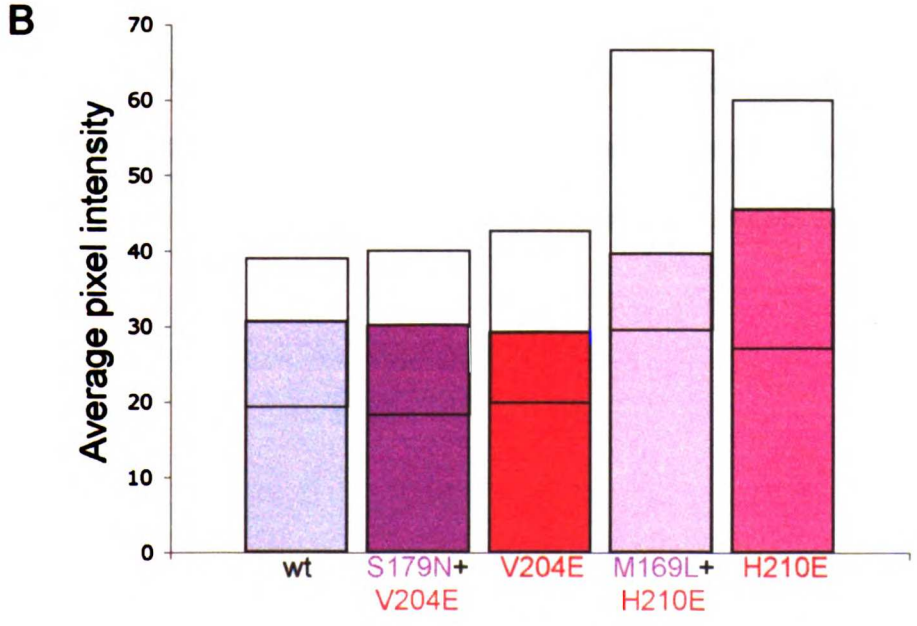

Tables

Table 1. Summary of yeast screens of mutant libraries.

N/A means not applicable. (A) Data for screening libraries containing an S5 semilethal and a randomly mutagenized S1-S3. The suppressors recovered for each S5 semilethal, Y193E, R197E, V204E, and H210E, have multiple mutations, but do not share a single mutation specific for the S5 semilethal. The estimated percent rescue is less than 0.5% for all these screens. (B) Data for screening libraries containing an S5 semilethal and a randomly mutagenized S4. For screens against the Y193E and R197Q semilethals, no specific suppressor emerged and the estimated percent rescue is less than 0.15%. By contrast, S4 library screens against the S5 semilethals, V204E and H210E, were rescued in greater than 1.1% of the colonies. They were suppressed by highly specific S4 mutations; the same suppressor was found in each colony growing on low K^+ media that was analyzed. Thus, S179N and M169L (purple) specifically suppressed V204E and H210E (red), respectively. (C) Data for screening libraries containing an S5 semilethal (red or brown) mutation and randomized codon of the S4 residue yielding the second-site suppressor (purple).

Table 1. Summary of Yeast Screens of Mutant Libraries.

A S5 semilethals screened against an S1-S3 library.

Semilethal Mutation	Library Complexity	# Screened	Estimated % Rescue	Specific Suppressor
Y193E	5.9×10^5	3144	0.25	N/A
R197E	6.0×10^4	8500	0.31	N/A
V204E	5.8×10^4	5796	0.50	N/A
H210E	1.2×10^5	6757	0.18	N/A

B S5 semilethals screened against an S4 library.

Semilethal Mutation	Library Complexity	# Screened	Estimated % Rescue	Specific Suppressor
Y193E	4.4×10^4	3083	0.13	N/A
R197Q	1.7×10^4	7748	0.15	N/A
V204E	1.0×10^4	8988	2.1	S179N
H210E	2.1×10^4	6840	1.1	M169L

C S5 semilethals screened against a randomized codon of the putative second-site suppressor.

Semilethal Mutation	Library Complexity	# Screened	Estimated % Rescue	Recovered Mutation
V204E	272	1040	5.7	S179N
V204D	2904	2361	0	None
H210E	288	958	14	M169L
H210D	609	2113	6.4	M169L

References

Aggarwal, S. K., and MacKinnon, R. (1996). Contribution of the S4 segment to gating charge in the Shaker K+ channel. Neuron *16*, 1169-1177.

Ahern, C. A., and Horn, R. (2004). Specificity of charge-carrying residues in the voltage sensor of potassium channels. J Gen Physiol *123*, 205-216.

Anderson, J. A., Huprikar, S. S., Kochian, L. V., Lucas, W. J., and Gaber, R. F. (1992). Functional expression of a probable Arabidopsis thaliana potassium channel in Saccharomyces cerevisiae. Proc Natl Acad Sci U S A *89*, 3736-3740.

Ashcroft, F. M. (2000). Ion channels and diseases (London, Academic Press).

Bezanilla, F. (2000). The voltage sensor in voltage-dependent ion channels. Physiol Rev *80*, 555-592.

Bezanilla, F. (2002). Voltage sensor movements. J Gen Physiol *120*, 465-473.

Broomand, A., Mannikko, R., Larsson, H. P., and Elinder, F. (2003). Molecular movement of the voltage sensor in a K channel. J Gen Physiol *122*, 741-748.

Brownlee, C. (2002). Plant K+ transport: not just an uphill struggle. Curr Biol *12*, R402-404.

Cao, Y., Crawford, N. M., and Schroeder, J. I. (1995). Amino terminus and the first four membrane-spanning segments of the Arabidopsis K+ channel KAT1 confer inward-rectification property of plant-animal chimeric channels. J Biol Chem *270*, 17697-17701.

Cohen, B. E., Grabe, M., and Jan, L. Y. (2003). Answers and questions from the KvAP structures. Neuron *39*, 395-400.

Crunelli, V., and Leresche, N. (2002). Childhood absence epilepsy: genes, channels, neurons and networks. Nat Rev Neurosci *3*, 371-382.

Cuello, L. G., Cortes, D. M., and Perozo, E. (2004). Molecular architecture of the KvAP voltage-dependent K+ channel in a lipid bilayer. Science *306*, 491-495.

Decher, N., Chen, J., and Sanguinetti, M. C. (2004). Voltage-dependent gating of hyperpolarization-activated, cyclic nucleotide-gated pacemaker channels: molecular coupling between the S4-S5 and C-linkers. J Biol Chem *279*, 13859-13865.

Doyle, D. A. (2004). Structural changes during ion channel gating. Trends Neurosci *27*, 298-302.

Eriksson, A. E., Baase, W. A., Zhang, X. J., Heinz, D. W., Blaber, M., Baldwin, E. P., and Matthews, B. W. (1992). Response of a protein structure to cavity-creating mutations and its relation to the hydrophobic effect. Science *255*, 178-183.

Gandhi, C. S., Clark, E., Loots, E., Pralle, A., and Isacoff, E. Y. (2003). The orientation and molecular movement of a k(+) channel voltage-sensing domain. Neuron *40*, 515-525.

Gandhi, C. S., and Isacoff, E. Y. (2002). Molecular models of voltage sensing. J Gen Physiol *120*, 455-463.

Gaymard, F., Pilot, G., Lacombe, B., Bouchez, D., Bruneau, D., Boucherez, J., Michaux-Ferriere, N., Thibaud, J. B., and Sentenac, H. (1998). Identification and disruption of a plant shaker-like outward channel involved in K+ release into the xylem sap. Cell *94*, 647-655.

Gonzalez, C., Morera, F. J., Rosenmann, E., Alvarez, O., and Latorre, R. (2005). S3b amino acid residues do not shuttle across the bilayer in voltage-dependent Shaker K+ channels. Proc Natl Acad Sci U S A *102*, 5020-5025.

Grabe, M., Lecar, H., Jan, Y. N., and Jan, L. Y. (2004). A quantitative assessment of models for voltage-dependent gating of ion channels. Proc Natl Acad Sci U S A *In press*.

Gulbis, J. M., and Doyle, D. A. (2004). Potassium channel structures: do they conform? Curr Opin Struct Biol *14*, 440-446.

Hessa, T., White, S. H., and von Heijne, G. (2005). Membrane insertion of a potassium-channel voltage sensor. Science *307*, 1427.

Hille, B. (2001). Ion channels of excitable membranes, 3rd edn (Sunderland, Mass., Sinauer).

Horn, R. (2002). Coupled movements in voltage-gated ion channels. J Gen Physiol *120*, 449-453.

Hoshi, T. (1995). Regulation of voltage dependence of the KAT1 channel by intracellular factors. J Gen Physiol *105*, 309-328.

Hosy, E., Vavasseur, A., Mouline, K., Dreyer, I., Gaymard, F., Poree, F., Boucherez, J., Lebaudy, A., Bouchez, D., Very, A. A., *et al.* (2003). The Arabidopsis outward K+ channel GORK is involved in regulation of stomatal movements and plant transpiration. Proc Natl Acad Sci U S A *100*, 5549-5554.

Jiang, Q. X., Wang, D. N., and MacKinnon, R. (2004). Electron microscopic analysis of KvAP voltage-dependent K+ channels in an open conformation. Nature *430*, 806-810.

Jiang, Y., Lee, A., Chen, J., Ruta, V., Cadene, M., Chait, B. T., and MacKinnon, R. (2003a). X-ray structure of a voltage-dependent K+ channel. Nature *423*, 33-41.

Jiang, Y., Ruta, V., Chen, J., Lee, A., and MacKinnon, R. (2003b). The principle of gating charge movement in a voltage-dependent K+ channel. Nature *423*, 42-48.

Ko, C. H., and Gaber, R. F. (1991). TRK1 and TRK2 encode structurally related K+ transporters in Saccharomyces cerevisiae. Mol Cell Biol *11*, 4266-4273.

Kuo, A., Gulbis, J. M., Antcliff, J. F., Rahman, T., Lowe, E. D., Zimmer, J., Cuthbertson, J., Ashcroft, F. M., Ezaki, T., and Doyle, D. A. (2003). Crystal structure of the potassium channel KirBac1.1 in the closed state. Science *300*, 1922-1926.

Kuruma, A., Hirayama, Y., and Hartzell, H. C. (2000). A hyperpolarization- and acid-activated nonselective cation current in Xenopus oocytes. Am J Physiol Cell Physiol *279*, C1401-1413.

Laine, M., Lin, M. C., Bannister, J. P., Silverman, W. R., Mock, A. F., Roux, B., and Papazian, D. M. (2003). Atomic proximity between S4 segment and pore domain in Shaker potassium channels. Neuron *39*, 467-481.

Latorre, R., Munoz, F., Gonzalez, C., and Cosmelli, D. (2003a). Structure and function of potassium channels in plants: some inferences about the molecular origin of inward rectification in KAT1 channels (Review). Mol Membr Biol *20*, 19-25.

Latorre, R., Olcese, R., Basso, C., Gonzalez, C., Munoz, F., Cosmelli, D., and Alvarez, O. (2003b). Molecular coupling between voltage sensor and pore opening in the Arabidopsis inward rectifier K+ channel KAT1. J Gen Physiol *122*, 459-469.

Lee, H. C., Wang, J. M., and Swartz, K. J. (2003). Interaction between extracellular Hanatoxin and the resting conformation of the voltage-sensor paddle in Kv channels. Neuron *40*, 527-536.

Li-Smerin, Y., Hackos, D. H., and Swartz, K. J. (2000). A localized interaction surface for voltage-sensing domains on the pore domain of a K+ channel. Neuron *25*, 411-423.

LiCata, V. J., and Ackers, G. K. (1995). Long-range, small magnitude nonadditivity of mutational effects in proteins. Biochemistry *34*, 3133-3139.

Lu, Z., Klem, A. M., and Ramu, Y. (2002). Coupling between voltage sensors and activation gate in voltage-gated K+ channels. J Gen Physiol *120*, 663-676.

Ludwig, A., Zong, X., Stieber, J., Hullin, R., Hofmann, F., and Biel, M. (1999). Two pacemaker channels from human heart with profoundly different activation kinetics. Embo J *18*, 2323-2329.

Mannikko, R., Elinder, F., and Larsson, H. P. (2002). Voltage-sensing mechanism is conserved among ion channels gated by opposite voltages. Nature *419*, 837-841.

Marten, I., and Hoshi, T. (1998). The N-terminus of the K channel KAT1 controls its voltage-dependent gating by altering the membrane electric field. Biophys J *74*, 2953-2962.

Minor, D. L., Jr., Masseling, S. J., Jan, Y. N., and Jan, L. Y. (1999). Transmembrane structure of an inwardly rectifying potassium channel. Cell *96*, 879-891.

Mordoch, S. S., Granot, D., Lebendiker, M., and Schuldiner, S. (1999). Scanning cysteine accessibility of EmrE, an H+-coupled multidrug transporter from Escherichia coli, reveals a hydrophobic pathway for solutes. J Biol Chem *274*, 19480-19486.

Mura, C. V., Cosmelli, D., Munoz, F., and Delgado, R. (2004). Orientation of Arabidopsis thaliana KAT1 channel in the plasma membrane. J Membr Biol *201*, 157-165.

Neale, E. J., Elliott, D. J., Hunter, M., and Sivaprasadarao, A. (2003). Evidence for intersubunit interactions between S4 and S5 transmembrane segments of the Shaker potassium channel. J Biol Chem *278*, 29079-29085.

Rasband, W. S. (1997-2005). ImageJ, U.S. National Institutes of Health.

Rodriguez-Navarro, A. (2000). Potassium transport in fungi and plants. Biochim Biophys Acta *1469*, 1-30.

Ruta, V., Jiang, Y., Lee, A., Chen, J., and MacKinnon, R. (2003). Functional analysis of an archaebacterial voltage-dependent K+ channel. Nature *422*, 180-185.

Sali, A., and Blundell, T. L. (1993). Comparative protein modelling by satisfaction of spatial restraints. J Mol Biol *234*, 779-815.

Sands, Z., Grottesi, A., and Sansom, M. S. (2005). Voltage-gated ion channels. Curr Biol *15*, R44-47.

Sato, Y., Sakaguchi, M., Goshima, S., Nakamura, T., and Uozumi, N. (2002). Integration of Shaker-type K+ channel, KAT1, into the endoplasmic reticulum membrane: synergistic insertion of voltage-sensing segments, S3-S4, and independent insertion of pore-forming segments, S5-P-S6. Proc Natl Acad Sci U S A *99*, 60-65.

Sato, Y., Sakaguchi, M., Goshima, S., Nakamura, T., and Uozumi, N. (2003). Molecular dissection of the contribution of negatively and positively charged residues in S2, S3, and S4 to the final membrane topology of the voltage sensor in the K+ channel, KAT1. J Biol Chem *278*, 13227-13234.

Schachtman, D. P., Schroeder, J. I., Lucas, W. J., Anderson, J. A., and Gaber, R. F. (1992). Expression of an inward-rectifying potassium channel by the Arabidopsis KAT1 cDNA. Science *258*, 1654-1658.

Schreiber, G., and Fersht, A. R. (1995). Energetics of protein-protein interactions: analysis of the barnase-barstar interface by single mutations and double mutant cycles. J Mol Biol *248*, 478-486.

Schroeder, J. I., Ward, J. M., and Gassmann, W. (1994). Perspectives on the physiology and structure of inward-rectifying K+ channels in higher plants: biophysical implications for K+ uptake. Annu Rev Biophys Biomol Struct *23*, 441-471.

Seoh, S. A., Sigg, D., Papazian, D. M., and Bezanilla, F. (1996). Voltage-sensing residues in the S2 and S4 segments of the Shaker K+ channel. Neuron *16*, 1159-1167.

Serrano, R., and Rodriguez-Navarro, A. (2001). Ion homeostasis during salt stress in plants. Curr Opin Cell Biol *13*, 399-404.

Sesti, F., Rajan, S., Gonzalez-Colaso, R., Nikolaeva, N., and Goldstein, S. A. (2003). Hyperpolarization moves S4 sensors inward to open MVP, a methanococcal voltage-gated potassium channel. Nat Neurosci *6*, 353-361.

Shealy, R. T., Murphy, A. D., Ramarathnam, R., Jakobsson, E., and Subramaniam, S. (2003). Sequence-function analysis of the K+-selective family of ion channels using a comprehensive alignment and the KcsA channel structure. Biophys J *84*, 2929-2942.

Shieh, C. C., Coghlan, M., Sullivan, J. P., and Gopalakrishnan, M. (2000). Potassium channels: molecular defects, diseases, and therapeutic opportunities. Pharmacol Rev *52*, 557-594.

Sigworth, F. J. (1994). Voltage gating of ion channels. Q Rev Biophys *27*, 1-40.

Starace, D. M., and Bezanilla, F. (2004). A proton pore in a potassium channel voltage sensor reveals a focused electric field. Nature *427*, 548-553.

Swartz, K. J. (2004). Towards a structural view of gating in potassium channels. Nat Rev Neurosci *5*, 905-916.

Tempel, B. L., Papazian, D. M., Schwarz, T. L., Jan, Y. N., and Jan, L. Y. (1987). Sequence of a probable potassium channel component encoded at Shaker locus of Drosophila. Science *237*, 770-775.

Thompson, J. D., Higgins, D. G., and Gibson, T. J. (1994). CLUSTAL W: improving the sensitivity of progressive multiple sequence alignment through

sequence weighting, position-specific gap penalties and weight matrix choice. Nucleic Acids Res *22*, 4673-4680.

Tiwari-Woodruff, S. K., Schulteis, C. T., Mock, A. F., and Papazian, D. M. (1997). Electrostatic interactions between transmembrane segments mediate folding of Shaker K+ channel subunits. Biophys J *72*, 1489-1500.

Tombola, F., Pathak, M. M., and Isacoff, E. Y. (2005). Voltage-sensing arginines in a potassium channel permeate and occlude cation-selective pores. Neuron *45*, 379-388.

Tristani-Firouzi, M., Chen, J., and Sanguinetti, M. C. (2002). Interactions between S4-S5 linker and S6 transmembrane domain modulate gating of HERG K+ channels. J Biol Chem *277*, 18994-19000.

Uozumi, N., Nakamura, T., Schroeder, J. I., and Muto, S. (1998). Determination of transmembrane topology of an inward-rectifying potassium channel from Arabidopsis thaliana based on functional expression in Escherichia coli. Proc Natl Acad Sci U S A *95*, 9773-9778.

Very, A. A., and Sentenac, H. (2003). Molecular mechanisms and regulation of K+ transport in higher plants. Annu Rev Plant Biol *54*, 575-603.

Wells, J. A. (1990). Additivity of mutational effects in proteins. Biochemistry *29*, 8509-8517.

Yellen, G. (2002). The voltage-gated potassium channels and their relatives. Nature *419*, 35-42.

Yi, B. A., Lin, Y. F., Jan, Y. N., and Jan, L. Y. (2001). Yeast screen for constitutively active mutant G protein-activated potassium channels. Neuron *29*, 657-667.

Zei, P. C., and Aldrich, R. W. (1998). Voltage-dependent gating of single wild-type and S4 mutant KAT1 inward rectifier potassium channels. J Gen Physiol *112*, 679-713.

CHAPTER III

Structural Model of KAT1 in the Down State of S4

Abstract

Structural models of voltage-gated channels in the up and down states of S4 are necessary to understand the principle of voltage-gating. Here we describe a structural model of KAT1 in the down state of S4 derived from six structural restraints obtained from yeast screens aimed at determining interacting transmembrane segments of this channel. Starting with conditional lethal mutations in S1, S4, S5, and S6 of KAT1 that are unable to rescue growth of a K^+ transporter deficient yeast strain on low K^+ media, we screened mutagenized libraries of various regions of the voltage-sensor, S1-S3, S2-S4, or S4, for suppressor mutations of these conditional lethals that rescue yeast growth. This screening identified six new sets of interactions between S1 and S4, S1 and S2, and S4 and S5, suggesting close apposition of these segments. An interaction network of residues between four transmembrane segments, S1 (W75), S2 (I94 and N99), S4 (R165 and M169), and S5 (H210), was discovered from four sets of suppressor and conditional lethal mutations. A preliminary KAT1 model that satisfied six of the eight total interaction sets has S4 packed against the pore domain and S1 and S2 packed against S4. The S4 segment is positioned diagonally across the S5 of two subunits with the N-terminal end of S4 making contacts with the S5 of one subunit (perhaps its own subunit) and the C-terminal end of S4 contacting S5 of the adjacent subunit. Comparing this model to the $K_v1.2$ structure suggests that the positively charged arginines in S4 that carry the gating charge might transit the outer leaflet of the membrane.

Introduction

Investigation of how the six transmembrane (6-TM) segments are arranged in the voltage-gated ion channel has been an area of intense research in recent years. The goal of these studies is to provide a physical description of how positively charged residues in the primary voltage-sensor, S4, transit the membrane electric field producing a gating current and couple this physical transition to pore opening (Broomand et al., 2003; Cuello et al., 2004; Gandhi et al., 2003; Jiang et al., 2003; Laine et al., 2003; Long et al., 2005a; Neale et al., 2003). The detection of the movement of positive charges in the main voltage-sensing segment, S4, as a gating current (Aggarwal and MacKinnon, 1996; Armstrong and Bezanilla, 1973; Bezanilla, 2002; Gandhi and Isacoff, 2002; Latorre et al., 2003), analysis of the movement of S4 by spectroscopic and cysteine accessibility techniques (Bezanilla, 2002; Cha et al., 1999; Glauner et al., 1999; Larsson et al., 1996; Latorre et al., 2003; Mannikko et al., 2002), and mutagenesis of each transmembrane segment identifying protein and lipid-facing regions (Hong and Miller, 2000; Li-Smerin et al., 2000a; Li-Smerin et al., 2000b; Monks et al., 1999) led to a general model of voltage-gated channel structure where the S4 segment is surrounded by the other proteinaceous transmembrane segments and possibly water (Hille, 2001; Starace and Bezanilla, 2004). The recent crystal structure of a mammalian channel, $K_v1.2$, confirmed the close apposition of these segments with respect to one another with S1 through S3 surrounding S4 and S4 perhaps contacting lipid in the space between S4 and S5 (Long et al., 2005a; Long et al., 2005b). Excellent reviews offer a more detailed

analysis of the differences between various structural models (Ahern and Horn, 2004; Cohen et al., 2003; Swartz, 2004; Tombola et al., 2005).

In order to understand voltage-gating from a structural perspective, one requires many different crystal structures and structural models of channels in various states (opened, closed, inactivated, and sub-states). Moreover, structures of different channel types, hyperpolarization and depolarization-activated, will be necessary to understand the various ways that these channels may gate with voltage (see Chapter IV). The crystal structure of a depolarization-activated K_v channel from rat, $K_v1.2$, likely in the up (open) state (see Introduction for the definition of this state), provides an entry point for building molecular models of other channels for which there are structural restraints. A model of the down state of the voltage-sensor is essential to understand how the voltage-sensor, mainly S4, moves between the down to up states and how much movement is involved in this process. Currently, there is much debate as to whether S4 undergoes a small movement (2-8 Å) across a focused electric field (Ahern and Horn, 2005; Chanda et al., 2005; Phillips et al., 2005; Posson et al., 2005) or a large movement (15-20 Å) (Ruta et al., 2005) to gate the pore. More structural studies will help address this question.

Previous work involving KAT1, a hyperpolarization-activated K_v channel from *Arabidopsis thaliana*, determined structural restraints of this channel using an activity-based yeast screen providing an ideal approach to obtain structural information about the down state of the S4 voltage-sensor of KAT1 (Lai et al., 2005). KAT1 complements a K^+ transporter deficient yeast strain on low K^+

media establishing an easy and efficient assay to screen for functional mutants of KAT1 in an *in vivo* system. Extending the conditional lethal/second-site suppressor approach described previously (Lai et al., 2005), conditional lethals were identified in S1, S4, S5, and S6 and screened against mutagenized regions of the voltage-sensor part of the channel, S2-S4, S1-S3, and S4, in a comprehensive manner to identify interactions between different transmembrane segments in KAT1.

Material and Methods

Molecular Biology and Library Construction

Yeast screens, selection, and library construction was carried out as in Chapter II (Lai et al., 2005). For yeast libraries of S2-S4, a SalI cut site was made at residue I94 thereby mutating this residue to valine, and a silent BamHI cut site was engineered in at residue W195. It was verified that this construct gave the same phenotype as wildtype in the yeast assay (Table 3 and 4).

Modeling

Modeller6v2 was used to construct an open state model of the KAT1 pore region based on the $K_v1.2$ crystal structure (Long et al., 2005a; Sali and Blundell, 1993). Separate models of the S1, S2, and S4 KAT1 transmembrane segments were also created from the homologous transmembrane regions of $K_v1.2$. A structural model of the packed voltage sensor was created from these segments as follows: S1, S2, and S4 were initially aligned with the central pore axis and centered on the pore. Each was then randomly translated away from the central pore, rotated about its own axis between 0 and 360 degrees, and then tilted off-axis between -45 and +45 degrees. Harmonic distance restraints with a force constant of 3 kcal/mol/Å^2 were applied between each of the lethal/suppressor pair residues identified from the yeast screen. Additional harmonic restraints with a force constant of 0.10 kcal/mol/Å^2 were applied to residues on S2 such that the highly conserved residues, based on an alignment of 30 homologous KAT1 channels, were attracted to other voltage sensor residues while the non-

conserved residues were repulsed.

Molecular dynamics simulations using NAMD 2.5 were performed at high temperature, 600K, for a total of 80 ps with a reduced 1.5 fs time step allowing the protein complex to pack together. This was followed by minimization of the entire system. This process was repeated 180 times.

A model of the up state of S4 (Figure 5B) based on the $K_v1.2$ crystal structure with the sequence of KAT1 according to the alignment by Shealy et al. was generated using Modeller6v2 (Sali and Blundell, 1993; Shealy et al., 2003).

Results

Screening for interactions between transmembrane segments

To find additional interactions between transmembrane segments, conditional lethal/second-site suppressor screens were carried out in a similar manner to the approach in Chapter II where two highly specific interacting pairs of residues between S4 and S5 were found. Conditional lethals were identified in S1, S4, S5, and S6 and were screened against mutagenized libraries of S1-S3, S2-S4, and S4. The region subjected to random mutagenesis was chosen depending on the location of the conditional lethal. Five interaction sets were identified from this screening as described below. A summary of these screens is in Table 1 A to C.

Additional screening was performed to test whether two residues believed to interact based on initial KAT1 models produced in the lab could indeed form a conditional lethal/suppressor pair. Conditional lethals in S4, S5, and S6 were tested for their suppression by screening mutant libraries with randomized S4 and S5 residue codons at these sites (Table 1 D). One interaction set was identified from this screening as described below.

Six new sets of interacting mutations were discovered

Intensive screening revealed six new sets of suppressor/conditional lethal mutations: one between S4 and S5, three between S1 and S4, and two between S1 and S2. The yeast phenotype for each conditional lethal and the suppressor(s) with the conditional lethal is shown in Figure 1. A summary of

these interactions, including ones from Chapter II (Lai et al., 2005), is shown in Table 2.

Three interaction sets were identified for conditional lethals in S4 and S5. Two sets of suppressors in S1 were isolated from screens of S1-S3 mutant libraries against a conditional lethal in S4. In one set, C77R in S1 suppressed the R171E conditional lethal. For the conditional lethal in S4, R174E, two mutations were needed for suppression, one near the C-terminal end of S1 and one in the S1-S2 loop, Y86H and D89G. The third set was between a conditional lethal in S5, H210E, and a suppressor in S4, R165K. This set was identified by screening H210E against a randomized codon at R165.

Three sets of suppressors with conditional lethal mutations in S1 were identified, two between S2 and S1 and one between S4 and S1. These were identified from a screen of conditional lethal mutations in S1, W75E + I94V and W75D + I94V, against a mutant library of S2-S4. The I94V mutation was created when introducing a SalI cut site to insert the S2-S4 mutant library into KAT1. The three interaction sets uncovered were W75E + I94V + N99D, W75E + I94V + L115P, and W75D + I94V + M169L.

Interestingly, the suppressor, M169L in S4 that suppresses the conditional lethal W75D in S1, also suppresses a conditional lethal in S5, H210E (Lai et al., 2005). This residue may be involved in a network of residues that interact between S1, S4, and S5. A further evaluation of these residues is described in the section "Four interaction sets elucidate an interaction network."

I94V is required sometimes for conditional lethality and sometimes for suppression

A detailed analysis of the necessity of the I94V mutation, which was mutated for the ease of generating S2-S4 libraries, was carried out by testing conditional lethals and identified suppressor/conditional lethal sets with and without I94V. These experiments revealed that I94V is necessary sometimes for the S1 substitutions to be conditional lethals and sometimes for other mutations to suppress a conditional lethal. For the conditional lethal phenotype, W75E + I94V and W75D + I94V were tested without the I94V mutation (Figure 2). In this case, it was found that W75D alone is still conditionally lethal, but W75E is not. Therefore, both W75E and I94V are necessary for the double mutant, W75E + I94V, to be conditionally lethal. As a shorthand expression, we will call these mutations, W75E + I94V, an S1 conditional lethal even though a mutation in S2, I94V, is required for the conditional lethal phenotype.

For the suppression phenotype, while I94V was not necessary for W75D to be conditionally lethal, it was found to be necessary in conjunction with M169L to suppress W75D. In other words, the suppressor M169L alone could not suppress the conditional lethal W75D, but the triple mutant, W75D + I94V + M169L, is able to rescue growth (Figure 2). Further evaluation of the necessity of I94V is in Table 3. The sensitivity of these interaction sets to a cavity creating mutation, isoleucine to valine, suggests that these interactions are involved in an interaction network of residues (see below).

Conditional lethals may affect channel biogenesis or function

Previously identified conditional lethals in S5, V204E and H210E, grow on 2 mM K^+ selective plates while nonfunctional channels (KAT1-stuffer) cannot grow indicating that some of these mutant channels must be at the surface to rescue growth (Figure 3). The same is true for the conditional lethals W75E + I94V and W75D. However, this is not the case for conditional lethal mutations in S4, R171E and R174E, which do not grow on 2 mM K^+ selective plates and thus, have the same phenotype as the nonfunctional channel negative control (stuffer). These results suggest that these mutations may affect channel biogenesis and prevent them from reaching the surface where they can allow K^+ influx required for yeast growth. Alternatively, these mutant channels may be on the cell membrane, but lack channel function.

Suppressors are specific for a particular conditional lethal

The suppressors of these six sets of mutations were tested for specificity by assessing the yeast phenotype of the suppressor mutation with a different conditional lethal in the same transmembrane segment as the original conditional lethal (Figure 4). For two sets where the suppressors were in S1 and the conditional lethal in S4, the yeast growth phenotype was not complemented by the suppressor of one with the conditional lethal of the other, C77R + R174E and Y86H + D89G + R171E, indicating that these S1 suppressor mutations specifically suppress one of the two S4 conditional lethal mutations tested. The

same is true of the S4 suppressor, R165K, which can suppress the S5 conditional lethal, H210E, but not the S5 conditional lethal, V204E (Figure 4).

A different type of analysis was performed for the suppressors of the S1 conditional lethal mutations. Because no other conditional lethals were found in S1 except those at residue W75, it was not possible to do a suppressor/conditional lethal swap as described above where at least two different conditional lethal amino acid sites were identified in the same transmembrane segment. We first tested the three suppressors in S2 and S4, N99D, L115P, and M169L, with a different conditional lethal at the W75 site, W75E + I94V + M169L, W75D + N99D, and W75D + L115P, and found that these suppressors could suppress another conditional lethal at the W75 site (Figure 4 and Table 3). A more extensive evaluation found that these three suppressors could suppress all known conditional lethal mutations at the W75 site except for mutation to arginine, W75R, and the one case described above where M169L requires I94V to suppress the conditional lethal W75D. A summary of these results is in Table 3.

Because these suppressor mutations were found originally for conditional lethals at the W75 site, it is not unexpected that these mutations could suppress other conditional lethal mutations at residue W75. To ensure that these suppressors were specific to the W75 site, we tested the S2 suppressors, N99D and L115P, against a conditional lethal in S4, R171E, and a conditional lethal in S5, H210E (Table 3). In this case, these suppressors could not suppress these conditional lethal mutations. In addition, the suppressor in S4, M169L, was

known to suppress the S5 conditional lethal, H210E, but not V204E (Lai et al., 2005), so we tested it against an additional S5 conditional lethal, F207K, and found that it could not suppress this conditional lethal in S5 either (Table 3).

A model of KAT1 in the down state of S4

A model of KAT1 in the down state of S4 was built using six of the eight interaction sets as restraints between transmembrane segments (Figure 5A). Two of the interaction sets, W75E + I94V + L115P and Y86H + D89G + R174E, could not be simultaneously satisfied with the other six sets during the model building. The requirement of two mutations for the suppression in one of these cases may be indicative of longer range interactions involving multiple residues. The KAT1 pore region was modeled onto the $K_v1.2$ structure and individual transmembrane segments of the KAT1, S1, S2, and S4, were created using Modeller6v2 (Long et al., 2005a; Sali and Blundell, 1993). The conservation of residues based on an alignment of 30 homologous KAT1 channels was used as an additional restraint to designate protein-packing faces of the helices.

S4 spans the S5 segments of two adjacent subunits

In this preliminary model of KAT1, the three interaction pairs found between S4 and S5 could be satisfied by having the S4 segment contact the S5 segments of two adjacent subunits (Figure 6A). The N-terminal end of S4 has contacts with S5, presumably of its own subunit when these models are compared to the $K_v1.2$ structure, through two interaction sets: the S4 suppressor

mutations, R165K and M169L, with the conditional lethal in S5, H210E. The C-terminal end of S4 contacts the S5 of the neighboring subunit through the S4 suppressor mutation, S179N, and the conditional lethal in S5, V204E. The shortest distance between side chains in this model is: 2 Å for the R165-H210 pair, 4 Å for the M169-H210 pair, and 8 Å for the S179-V204 pair. A shorter distance between this last pair, S179 and V204, has been seen in other models of KAT1 (personal communication, Michael Grabe) and future computational modeling will be performed to create better models.

Four interaction sets elucidate an interaction network

Four of the interaction sets had conditional lethal mutations or suppressor mutations in common. These are W75D + I94V + M169L, W75E + I94V + N99D, R165K + H210E, and M169L + H210E. These residues, W75, I94, N99, R165, M169, and H210 are shown as stick representations in Figure 6B. In this network, the closest side chain distance between residues in each interaction set is no more than 5 Å away. As improved models of KAT1 are generated, this distance can be decreased (personal communication, Michael Grabe). However, these interaction sets with common conditional lethal or suppressor mutations in this initial model illustrates that these residues are connected.

Residue Y72 in KAT1 S1 is likely to face away from the other transmembrane segments

When searching for conditional lethals in S1, residue Y72 was individually mutated to all other 19 amino acids (Table 4). All substitutions were tolerated as assayed by yeast growth on 0.4 mM K^+ plates though the proline mutant was lethal on 100 mM K^+ plates (see Appendix 2, Part 4). This suggests that this residue is not facing protein since it is not on a high impact face (Minor et al., 1999). The tolerance of mutation at Y72 is in contrast to residue W75 that was also mutated to all other amino acids (Table 4). In this case, only charged residues, W75E, W75D, W75K, and W75R, were conditionally lethal. Indeed, suppressors for W75E and W75D have been isolated as mutations in S2 and S4, respectively (Figure 1, Table 1 and 2) indicating that this site, W75, is protein-facing. The Y72 residue was not specifically restrained during model building and as better models of KAT1 are generated, it will be interesting to see which way Y72 will face, lipid or protein. In the model shown here, it is protein-facing; however, further modeling and refinement is necessary to make a final evaluation. This is one example of how the KAT1 model can be tested with restraint information that was not explicitly introduced in the model building.

Discussion

Six new suppressor/conditional lethal interaction sets were identified in this study and six of the eight total interaction set restraints were used to build a preliminary model of KAT1 in the down state of S4. These interaction sets were obtained using a yeast growth assay for functional channels in the open or down state of KAT1, the state necessary to allow K^+ ions in for yeast growth. Four of the interaction sets indicates close proximity between S1 and S4, S2 and S4, and S4 and S5 through an interaction network of residues that have common conditional lethal or suppressor mutations and which are close in the computational model (Figure 6B). The KAT1 model also suggests that S4 is packed against the pore domain contacting the S5 segments of two adjacent subunits.

An interaction network of residues was discovered between residues in S1 (W75), S2 (I94 and N99), S4 (R165 and M169), and S5 (H210) from four interaction sets that had common conditional lethal or suppressor mutations. To test the interaction network, it will be interesting to see if residues within the network that are not part of the conditional lethal/suppressor sets found in the original screening process can suppress other distant residues in the network. This was partially tested with a double mutant we made, N99D in S1 and H210E in S5 (Table 3). In this case, N99D could not distantly suppress the H210E conditional lethal; however, as these are just two specific mutations in the network, we may be able to find other interrelated residues within the network that affect each other when mutated. It will also be interesting to make the

quadruple mutant, W75D + I94V + M169L + H210E, to see if the suppressor mutation, M169L, in S4 which was common to the W75D + I94V and H210E conditional lethal mutations in S1 and S5, respectively, can suppress both of these simultaneously. If this quadruple mutant can rescue yeast growth, it suggests that these residues are all interacting in the same state. If it cannot rescue yeast growth, it suggests that M169L is positioned differently when it suppresses the conditional lethals, W75D + I94V versus H210E. This set of experiments will test the consistency of the interaction network proposed.

The specificity of the suppressor mutations in all six interaction sets was probed by testing these suppressors against different conditional lethals (Figure 4 and Table 3). This set of experiments found the suppressor mutations to be specific for its original conditional lethal and in the case for suppressor mutations of W75, the suppressors could suppress almost all conditional lethal mutations at the W75 site (Table 3). Further testing for the specificity of these suppressor mutations of the six new interaction sets identified here is currently in progress by screening all codons at an identified suppressor site for each conditional lethal. Since two of these interaction sets, Y86H + D89G + R174E and W75E + I94V + L115P, were not included in the KAT1 model, it would be beneficial to further evaluate whether these sets and any of the other interaction sets have multiple substitutions at the suppressor site that can suppress its original identified conditional lethal mutation. If multiple residues can suppress the original conditional lethal, then the suppression is likely due to allosteric changes.

In the KAT1 model, S4 is packed against the pore domain contacting two S5 segments of adjacent subunits throughout their transmembrane segments. This is in contrast to the $K_v1.2$ structure where S4 and S5 make contacts near the extracellular ends, but not throughout their transmembrane segments (Long et al., 2005a; Long et al., 2005b). The structure of the isolated KvAP voltage-sensor, S1-S4, indicates that this domain can be expressed and crystallized independent of the pore domain (Jiang et al., 2003). Furthermore, a novel protein from *Ciona intestinalis* that has a voltage-sensor-like domain, S1-S4, can gate the catalytic activity of the cytosolic enzyme to which it is connected (Jiang et al., 2003; Murata et al., 2005) suggesting that the voltage-sensor domain is modular. However, the work on KAT1 previously published and presented here suggests that S4 and S5 make intimate contacts in the down state of S4 (Lai et al., 2005). In addition, mutations in the S4 segment of Shaker-type channels severely affect gating in the up or activated state of S4 suggesting a much closer interaction between S4 and S5 (Ledwell and Aldrich, 1999; Pathak et al., 2005).

Experiments testing the putative salt bridges between S2 and S4, and S3 and S4 are currently underway to provide more restraints between these segments. A previous study showed that a charge reversal mutation in S2, D105R, could rescue integration into the membrane of the KAT1 S4 carrying the charge reversal mutation R171D (Sato et al., 2003). This indicates that these charged residues, D105 in S2 and R171 in S4, come into contact during channel biogenesis, but we would like to know how the charged pairs interact in the down state of the channel. Preliminary work starting with conditional lethal mutations in

S4, R171E and R174E, tested for suppression by mutations at D95 and D105 in S2 and D141 in S3 by screening these conditional lethal mutations combined with a randomized codon at the given residue in S2 and S3. Surprisingly, no suppressor mutations were identified in these screens (personal communication, Wei Zhou). Further work making site-directed mutations testing charge reversal mutations at each of the S2, S3, and S4 sites will be necessary to search for the appropriate salt bridge interactions in the KAT1 down state.

Interpolation of this model with a model of KAT1 in the up state (Figure 5B) based on the $K_v1.2$ structure suggests that the S4 segment moves a fair distance between these states with S1, S2, and S3 presumably moving with S4 during channel gating. These movements are consistent with a fair amount of movement of S4 across the electric field - at least that S4 may traverse the outer leaflet of the membrane which has been suggested by measurements of the depth of hanatoxin, a voltage-sensor binding toxin, in the membrane (Phillips et al., 2005). Future work will be focused on verifying the KAT1 structural model through iterative steps of computational model building and experimental testing as well as rationalizing current distance estimates of S4 movement from various K_v channels.

To test the KAT1 model with computational approaches, the most immediate experiment would be to test whether interpolation of the KAT1 down state of S4 to the up state of $K_v1.2$ is consistent with current distance estimates of S4 movement (Ahern and Horn, 2005; Chanda et al., 2005; Phillips et al., 2005; Posson et al., 2005; Ruta et al., 2005). Work in the field has proposed a

very small movement of S4, 1-2 Å, over a localized electric field (Chanda et al., 2005; Posson et al., 2005) to a very large movement, 15-20 Å (Ruta et al., 2005), to anywhere in between (Ahern and Horn, 2005; Phillips et al., 2005). It will be interesting to take these two states and see how well the predicted movement fits these data. In addition, now that there are atomistic models of these two states, we can compute local electric fields around S4 and deduce how much charge is moved between these two states. From this computation, we can determine how well it predicts the measured gating charge movement thereby strengthening the reliability of our model.

For experimental testing of the KAT1 model, a few experiments should be considered. Residues that are found to be in close proximity on the model could be tested with the same conditional lethal/suppressor yeast assay or if conditional lethal mutations cannot be found for the putatively interacting residues, mutations of these interacting pairs can be recorded to see if they independently or cooperatively affect the half activation voltage. These experiments are reminiscent of the double mutant cycles used to determine interacting and non-interacting residues (Wells, 1990). Cysteine crosslinking of residues believed to be in close proximity is also an option; however, due to the difficulty in obtaining crosslinking between residues believed to be deep within the transmembrane segements (see Appendix 2, Part 2), it would be wise to choose residues that interact on the extracellular side. Lastly, once models of the gating charge movement have been made, it should be possible to mutate different residues (candidates include the negative charges in S2 and S3 that

create salt bridges with S4) and record from these mutant channels to see if the model predicts the changes in the current-voltage or gating charge-voltage relationship. If the model predicts the correct changes in these relationships upon mutation, it will reinforce the reliability of our model both of the structure of the down state and the movement of S4.

From the experiments described here, we derived a model of KAT1 in the down state. This is the first atomistic model of the down state of a K_v channel based on experimental data that find connections between transmembrane segments. This model will help address mechanistic questions of voltage-gating such as how the positively charged arginines in S4 transit the electric field during gating, the distance traveled in this movement, and the configuration of the local electric field. In addition, this model provides a framework to understand how this movement couples to pore opening (see Chapter IV).

Figures

Figure 1. Six new conditional lethal and second-site suppressor pairs were discovered.

Conditional lethal mutations are in red and suppressor mutations are in blue. The I94V mutation is in black when made in conjunction with the mutation W75D since it was made as a result of creating a mutation library of S2-S4 and was shown not to be necessary for conditional lethality (see Figure 2). A KAT1 wildtype positive control and KAT1-stuffer negative control are shown. (A) KAT1 conditional lethals in S4 and S5 do not support yeast growth on 0.4 mM K^+ selective plates while the conditional lethal with its suppressor(s) do support yeast growth. (B) KAT1 conditional lethals in S1 do not support yeast growth on 0.2 mM K^+ selective plates while the conditional lethal with its suppressor(s) do support yeast growth.

Figure 1. Six new conditional lethal and second-site suppressor pairs were discovered

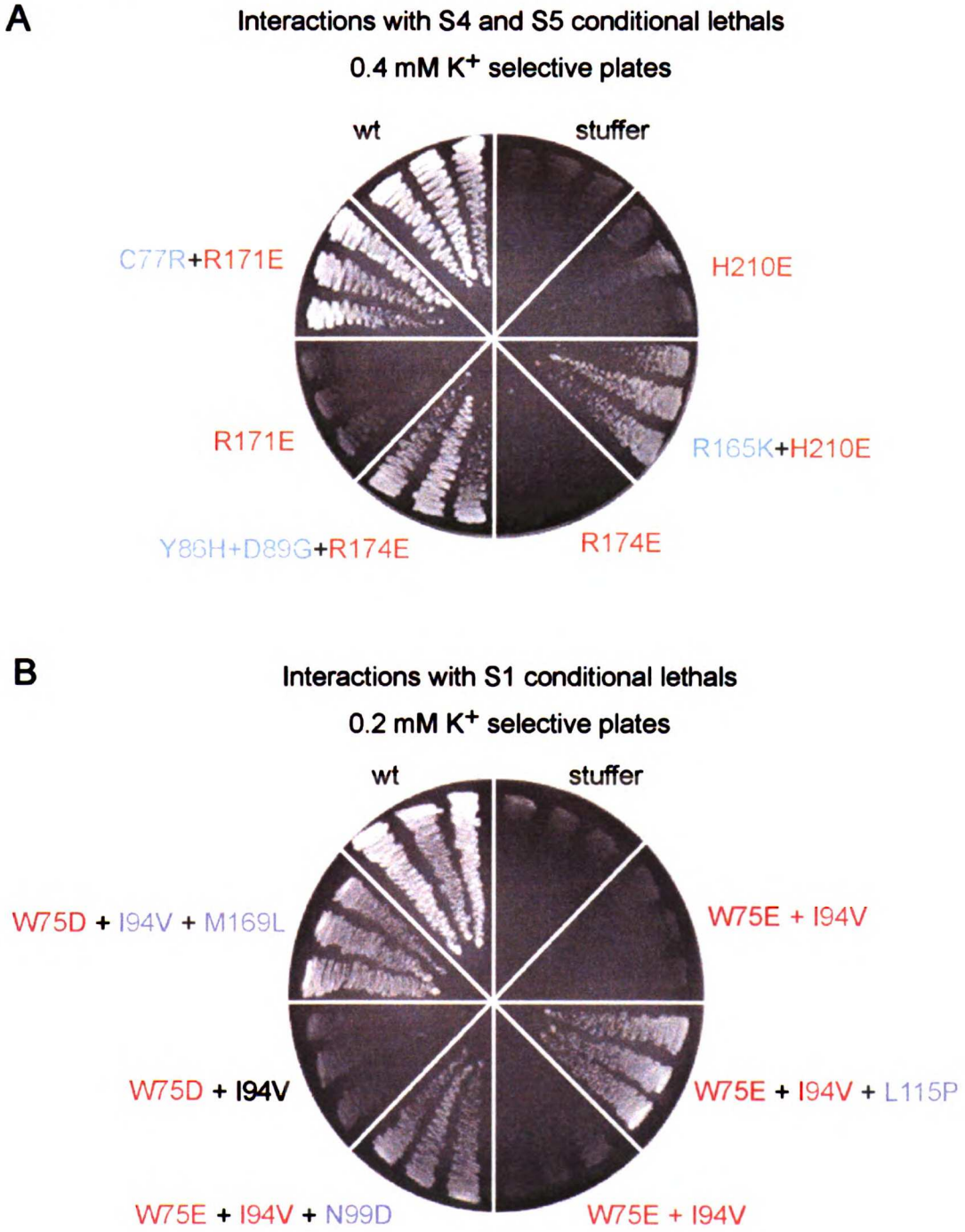

Figure 2. I94V is sometimes necessary in conjunction with other mutations to create a conditional lethal or to suppress a conditional lethal.

Conditional lethal mutations are in red and suppressor mutations are in blue. The I94V mutation is in black when made in conjunction with the mutation W75D since it was made as a result of creating a mutation library of S2-S4 and was shown not to be necessary for conditional lethality. W75E alone still rescues yeast growth on 0.2 mM K^+ selective plates, but addition of the I94V mutation creates a conditional lethal pair of mutations. W75D is conditionally lethal with or without I94V. The suppressor, M169L, was discovered in conjunction with W75D + I94V and it was found that I94V was necessary for suppression.

Figure 2. I94V is sometimes necessary in conjunction with other mutations to create a conditional lethal or to suppress a conditional lethal.

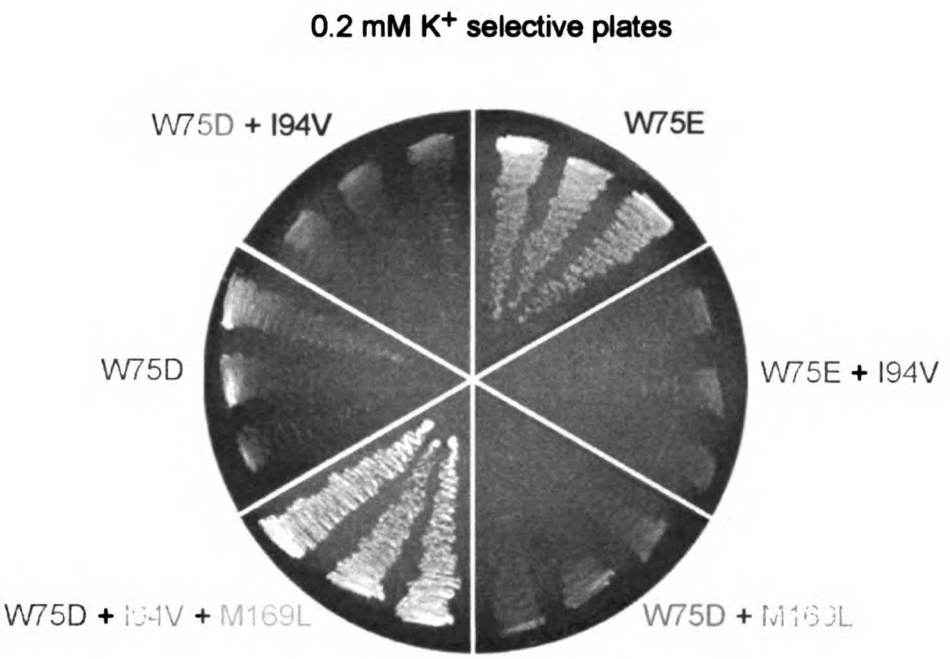

Figure 3. The conditional lethals in S1, S4, and S5 affect channel biogenesis or function.

KAT1 conditional lethals in S4, R171E and R174E do not support yeast growth on 2 mM K^+ selective plates while conditional lethals in S5, V204E and H210E, and conditional lethals in S1, W75E + I94V and W75D, do support yeast growth. A KAT1 wildtype positive control and KAT1-stuffer negative control are shown.

Figure 3. The conditional lethals in S1, S4, and S5 affect channel biogenesis or function.

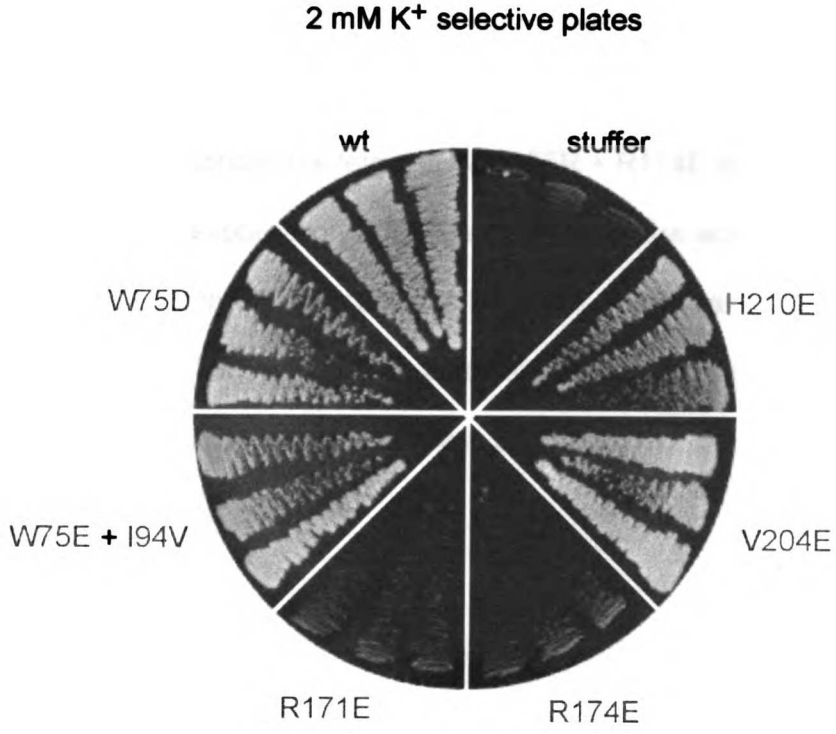

Figure 4. Suppressor mutations are specific for their conditional lethal except for suppressor mutations found for the W75 site.

Suppressors were tested against conditional lethals in the same transmembrane segment as the original suppressor/conditional lethal set. KAT1 wildtype and KAT1-stuffer controls are shown. Suppressors found in S1 do not suppress the other conditional lethal in S4, C77R + R174E and Y86H + D89G + R171E, and the S4 suppressor, R165K, cannot suppress another conditional lethal in S5, V204E on 0.4 mM selective K^+ plates. However, suppressor mutations N99D, L115P, and M169L that were found for conditional lethal mutations at the W75 site, could suppress other conditional lethal mutations at that site.

Figure 4. Suppressor mutations are specific for their conditional lethal except for suppressor mutations found for the W75 site.

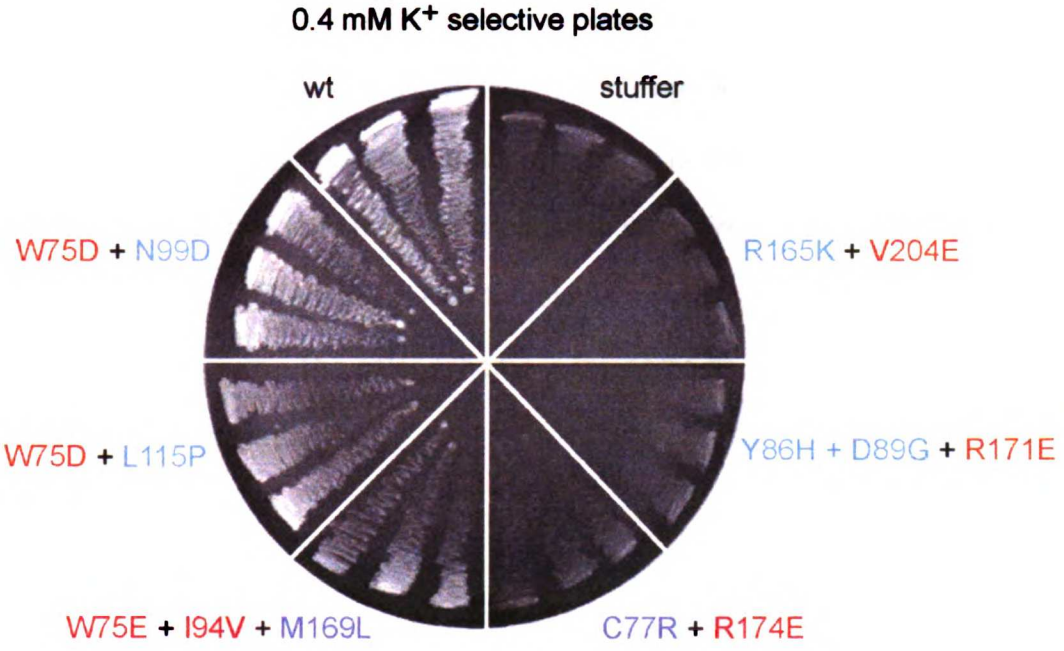

Figure 5. Model of the transmembrane packing of KAT1.

(A) A model of KAT1 in the down state using the K_v1.2 structure to model the pore region and the individual S1, S2, and S4 segments (Long et al., 2005a; Sali and Blundell, 1993). The pore region is shown in grey with the S5 of two adjacent subunits in blue. S1 is in orange, S2 in cyan, and S4 in green. The packing of the individual transmembrane segments is shown for only one subunit. S3 is omitted from this model because there are currently no restraints for this segment. (B) A model of KAT1 in the up state using the KAT1 sequence on the K_v1.2 structure. The color scheme is the same as in A with the S3 segment added in grey.

Figure 5. Model of the transmembrane packing of KAT1.

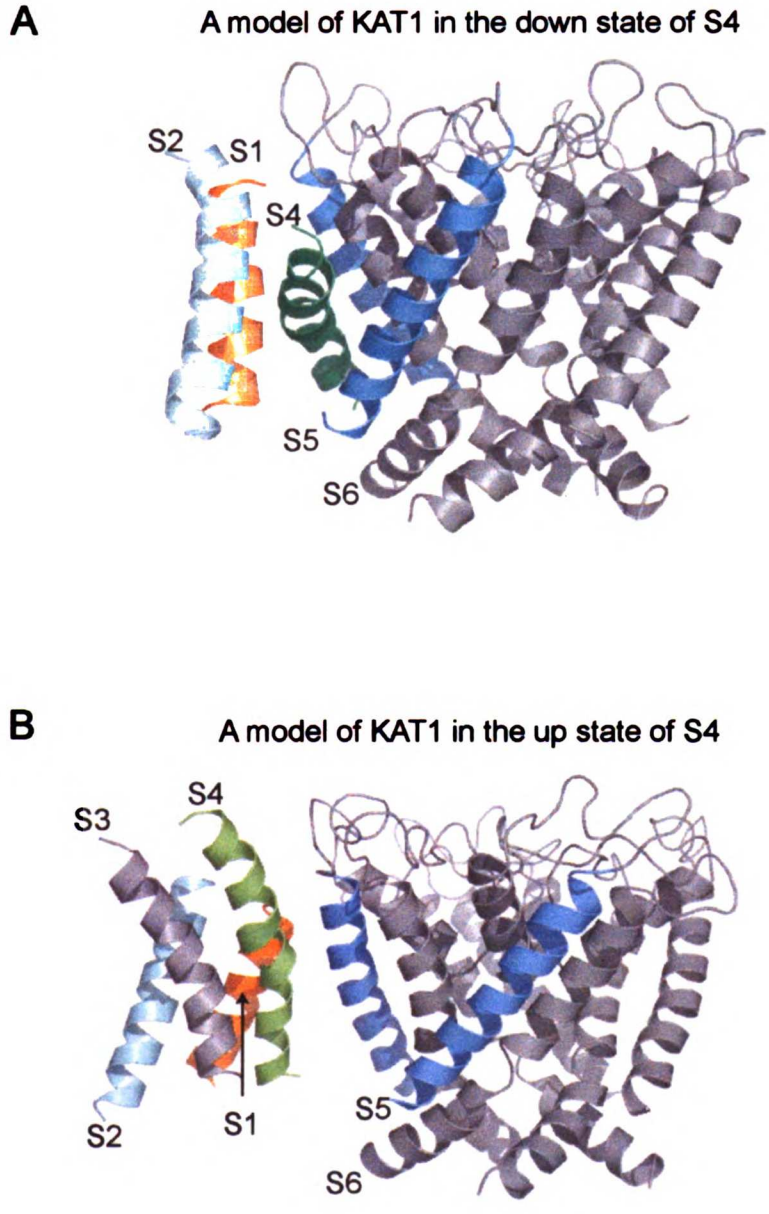

Figure 6. S4 interacts with two adjacent subunits and residues in S1, S2, S4, and S5 form an interaction network.

(A) The N-terminal end of S4 makes contacts with S5 presumably of its own subunit and the C-terminal end makes contacts with the S5 of the adjacent subunit. Residues from the S4 N-terminal end interaction sets, R165K + H210E and M169L + H210E, are highlighted in red. Residues from the S4 C-terminal end interaction set, S179N + V204E, are highlighted in yellow. Two adjacent subunits of the pore domain are shown with the S5 segments in blue and the loop and S6 regions in grey. The S4 segment is in green and S1 and S2 have been omitted for clarity. (B) Interaction sets that had common conditional lethal or suppressor residues are highlighted in red on a model of KAT1 in the down state. Coloring is the same as in Figure 5. This model suggests an interaction network involving these residues.

Figure 6. S4 interacts with two adjacent subunits and residues in S1, S2, S4, and S5 form an interaction network.

A S4 spans the S5 segments of two adjacent subunits

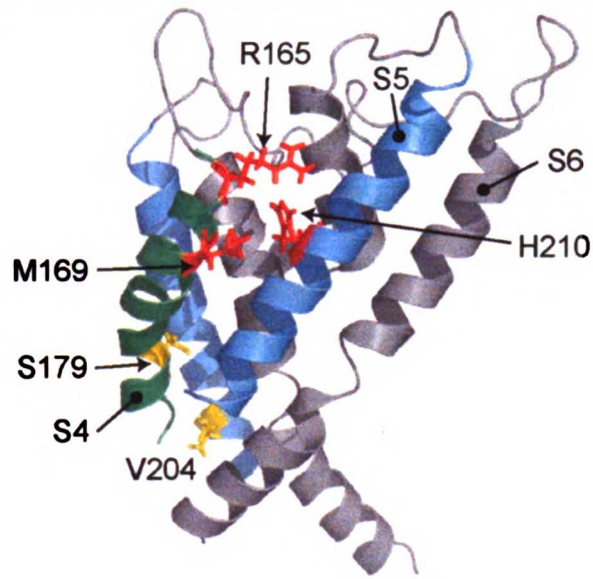

B An interaction network of residues between S1, S2, S4, and S5

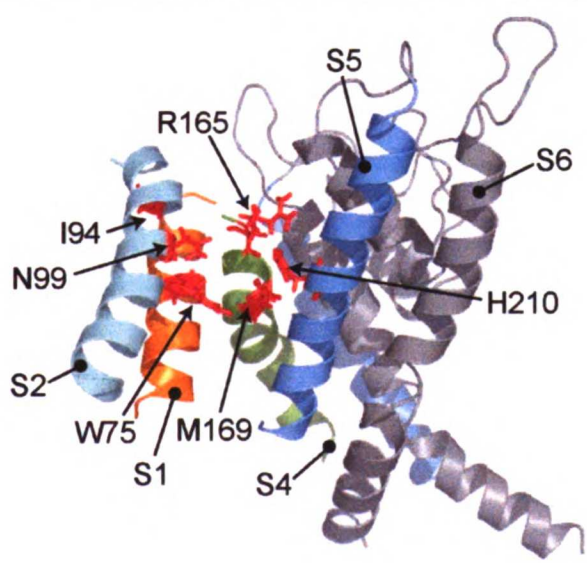

Tables

Table 1. Summary of all the screens identifying interactions between transmembrane segments.

The putative transmembrane region, the conditional lethal, library complexity, number of yeast colonies screened, the estimated percent rescue, the percent amino acid changes in the unselected library, the percent base pair changes in the unselected library, and the specific second-site suppressor mutation are given. Conditional lethal mutations are in red and specific second-site suppressor mutations in blue. Screens of conditional lethal mutations against randomized regions of S1-S3 (A), S4 (B), and S2-S4 (C) are shown. In (D), a summary of the screens performed looking for a second-site suppressor of a particular conditional lethal at a specific site.

Table 1. Summary of all the screens identifying interactions between transmembrane segments.

(A) S1-S3 screen

Putative TM region of Conditional Lethal	Conditional Lethal	Library Complexity	# Screened	Estimated % Rescue	% Unselected AA changes	% Unselected b.p. changes	Specific suppressor
S4	R171E	1.5×10^5	9279	1.70	4.3-6	2.2-3	C77R
S4	R174E	1.2×10^4	10206	0.27	6-6.3	3.0	Y86H + D89G
S4	L175N	9.4×10^3	2067	0.01	6.0	3.0	None
S4	L175H	1.6×10^4	1474	0.00	6.0	3.0	None
S4	L175P	1.1×10^4	1714	0.00	6.0	3.0	None
S4	V178N	1.7×10^4	1948	0.20	6.0	3.0	None
S5	F207D	1.8×10^4	2724	0.00	6.0	3.0	None
S5	F207K	1.0×10^3	531	0.00	6.0	3.0	None
S5	F207R	1.7×10^4	2508	0.00	6.0	3.0	None
S5	F215R	5.2×10^3	1991	0.00	6.0	3.0	None
S6	N284K	3.1×10^3	1720	0.00	6.0	3.0	None
S6	N284R	4.2×10^3	1578	0.00	6.0	3.0	None

(B) S4 screen

Putative TM region of Conditional Lethal	Conditional Lethal	Library Complexity	# Screened	Estimated % Rescue	% Unselected AA changes	% Unselected b.p. changes	Specific suppressor
S5	F207D	1.2×10^3	1007	0.00	5.8	3.1	None
S5	F207K	1.4×10^3	873	0.00	5.8	3.1	None
S5	F207R	8.0×10^2	876	0.00	5.8	3.1	None
S5	F215R	5.2×10^3	4536	0.00	5.8-7.7	3.1-3.5	None
S6	N284K	1.0×10^4	2715	0.00	5.8	3.1	None
S6	N284R	1.5×10^4	2231	0.00	5.8-7.7	3.1-3.5	None
S6	N284P	1.0×10^2	548	0.00	7.7	3.5	None

(C) S2-S4 screen

Putative TM region of Conditional Lethal	Conditional Lethal	Library Complexity	# Screened	Estimated % Rescue	% Unselected AA changes	% Unselected b.p. changes	Specific suppressor
S1	W75E + I94V	8.4×10^2	2620	0.30	5.2	2.6	N99D, L115P
S1	W75D + I94V	4.2×10^3	3646	0.10	5.2	2.6	M169L + I94V
S1	W75K + I94V	1.7×10^3	1777	0.00	5.2	2.6	None
S1	W75R + I94V	3.6×10^3	2697	0.00	5.2	2.6	None

(D) Screens against a specific amino acid

Putative TM region of Conditional Lethal	Conditional Lethal	Library Complexity	# Screened	Estimated % Rescue	Site of Random Mutation	Putative TM region of Site of Random Mutation	Specific suppressor
S4	L175N	960	353	0.00	V204X	S5	None
S4	L175N	1287	133	0.00	F207X	S5	None
S4	L175N	1008	176	0.00	H210X	S5	None
S5	V204E	1035	2481	0.00	R165X	S4	None
S5	V204E	1364	5223	0.00	L172X	S4	None
S5	H210E	128	2405	0.25	R165X	S4	R165K
S5	H210E	59	658	0.00	L172X	S4	None
S6	F283P	638	532	0.00	R165X	S4	None
S6	N284K	842	1114	0.00	M169X	S4	None
S6	N284K	1300	557	0.00	L172X	S4	None
S6	N284P	200	91	0.00	M169X	S4	None
S6	N284P	768	458	0.00	L172X	S4	None
S6	N284R	133	13*	0.00	M169X	S4	None

Table 2. Summary of all interaction sets.

Conditional lethals are in red, suppressor mutations are blue, and I94V is in black for W75D as it was present in the screens against S2-S4 and was not necessary for the conditional lethal phenotype. The putative transmembrane segment for the suppressor and conditional lethal are shown with the S2 segment in parentheses when it refers to I94V in conjunction with W75D and does not contribute to the conditional lethal phenotype. The phenotype in the K^+ transporter deficient yeast strain is shown on 100 mM K^+ and 0.4 mM K^+ plates. + designates yeast growth. Previously published suppressor and conditional lethal pairs are included (Lai et al., 2005).

Table 2. Summary of all interaction sets.

Putative TM Region for Suppressor Mutation(s)	*Suppressor Mutation(s)*	*Putative TM Region for Conditional Lethal Mutation(s)*	*Conditional Lethal*	*100 mM K+*	*0.4 mM K+*
S2+ S4	I94V + M169L	S1 + (S2)	W75D + I94V	+	+
S2	N99D	S1+ S2	W75E + I94V	+	+
S2	L115P	S1+ S2	W75E + I94V	+	+
S1	C77R	S4	R171E	+	+
S1, S1-S2	Y86H + D89G	S4	R174E	+	+
S4	R165K	S5	H210E	+	+
S4	M169L	S5	H210E	+	+
S4	S179N	S5	V204E	+	+

Table 3. Summary of suppressor mutations at the W75 residue site.

Conditional lethals are in red, suppressor mutations are blue, and all other residues are in black when they do not contribute to conditional lethality or suppression. The phenotype in the K^+ transporter deficient yeast strain is shown on 100 mM K^+ and 0.4 mM K^+ plates. + designates yeast growth. – designates no yeast growth. The putative transmembrane region is shown with the S2 segment in parentheses when it refers to I94V and that does not additionally contribute to the phenotype. The table has six sections for the phenotype of: the suppressor mutations alone, the putative conditional lethal mutations with or without I94V, the conditional lethal mutations with the suppressor mutation N99D, the conditional lethal mutations with the suppressor mutation L115P, the conditional lethal mutations with the suppressor mutation M169L, and the suppressor mutations with conditional lethal mutations in S4 and S5.

Table 3. Summary of suppressor mutations at the W75 residue site.

	Putative TM Region	*Mutation*	*100 mM K+*	*0.4 mM K+*
Suppressor mutations alone	S2	I94V	+	+
	S2	N99D	+	+
	S2	L115P	+	+
	S4	M169L	+	+
Putative conditional lethal mutations	S1	W75E	+	+
	S1 + S2	W75E + I94V	+	-
	S1	W75D	+	-
	S1 + (S2)	W75D + I94V	+	-
	S1	W75K	+	-
	S1 + (S2)	W75K + I94V	+	-
	S1	W75R	+	-
	S1 + (S2)	W75R + I94V	+	-
Conditional lethal muations with the suppressor mutation N99D	S1 + S2	W75E + I94V + N99D	+	+
	S1 + S2	W75D+ N99D	+	+
	S1 + S2	W75D + I94V + N99D	+	+
	S1 + S2	W75K+ N99D	+	+
	S1 + S2	W75R+ N99D	+	-
Conditional lethal muations with the suppressor mutation L115P	S1 + S2	W75E + I94V + L115P	+	+
	S1 + S2	W75D+ L115P	+	+
	S1 + S2	W75D + I94V + L115P	+	+
	S1 + S2	W75K+ L115P	+	+
	S1 + S2	W75R+ L115P	+	-
Conditional lethal muations with the suppressor mutation M169L	S1 + S2	W75E + I94V + M169L	+	+
	S1 + S2	W75D+ M169L	+	-
	S1 + S2	W75D + I94V + M169L	+	+
	S1 + S2	W75K+ M169L	+	+
	S1 + S2	W75R+ M169L	+	-
Suppressor mutations with conditional lethal muations in S4 and S5	S2 + S4	N99D + R171E	+	-
	S2 + S5	N99D + H210E	+	-
	S2 + S4	L115P + R171E	+	-
	S2 + S5	L115P + H210E	+	-
	S4 + S5	M169L + F207K	+	-

Table 4. Summary of all mutations at residues Y72 and W75 in S1 in conjunction with the I94V mutation.

Their phenotype in the K^+ transporter deficient yeast strain when plated on to 100 mM K^+ plates and then streaked on to 0.4 mM K^+ plates is shown. + indicates growth, +/- indicates moderate growth, - indicates no growth, and -* indicates decreased growth on 100 mM K^+ plates with "fast" and "slow" growing colonies (see Appendix 2, Part 4). Conditional lethal mutations are in red and specific second-site suppressor mutations are in blue.

Table 4. Summary of all mutations at residues Y72 and W75 in S1 in conjunction with the I94V mutation.

Mutation(s)	*100 mM K+*	*0.4 mM K+*
I94V	+	+
Y72F + I94V	+	+
Y72L + I94V	+	+
Y72I + I94V	+	+
Y72M + I94V	+	+
Y72V + I94V	+	+
Y72S + I94V	+	+
Y72P + I94V	-*	n/a
Y72T + I94V	+	+
Y72A + I94V	+	+
Y72H + I94V	+	+
Y72Q + I94V	+	+
Y72N + I94V	+	+
Y72K + I94V	+	+
Y72D + I94V	+	+
Y72E + I94V	+	+
Y72C + I94V	+	+
Y72R + I94V	+	+
Y72G + I94V	+	+
Y72W + I94V	+	+
W75F + I94V	+	+
W75L + I94V	+	+
W75I + I94V	+	+
W75M + I94V	+	+
W75V + I94V	+	+
W75S + I94V	+	+
W75P + I94V	+	+
W75T + I94V	+	+
W75A + I94V	+	+
W75Y + I94V	+	+
W75H + I94V	+	+
W75Q + I94V	+	+
W75N + I94V	+	+
W75K + I94V	+	-
W75D + I94V	+	-
W75E + I94V	+	-
W75C + I94V	+	+
W75R + I94V	+	-
W75G + I94V	+	+

References

Aggarwal, S. K., and MacKinnon, R. (1996). Contribution of the S4 segment to gating charge in the Shaker K+ channel. Neuron *16*, 1169-1177.

Ahern, C. A., and Horn, R. (2004). Stirring up controversy with a voltage sensor paddle. Trends Neurosci *27*, 303-307.

Ahern, C. A., and Horn, R. (2005). Focused electric field across the voltage sensor of potassium channels. Neuron *48*, 25-29.

Armstrong, C. M., and Bezanilla, F. (1973). Currents related to movement of the gating particles of the sodium channels. Nature *242*, 459-461.

Bezanilla, F. (2002). Voltage sensor movements. J Gen Physiol *120*, 465-473.

Broomand, A., Mannikko, R., Larsson, H. P., and Elinder, F. (2003). Molecular movement of the voltage sensor in a K channel. J Gen Physiol *122*, 741-748.

Cha, A., Snyder, G. E., Selvin, P. R., and Bezanilla, F. (1999). Atomic scale movement of the voltage-sensing region in a potassium channel measured via spectroscopy. Nature *402*, 809-813.

Chanda, B., Asamoah, O. K., Blunck, R., Roux, B., and Bezanilla, F. (2005). Gating charge displacement in voltage-gated ion channels involves limited transmembrane movement. Nature *436*, 852-856.

Cohen, B. E., Grabe, M., and Jan, L. Y. (2003). Answers and questions from the KvAP structures. Neuron *39*, 395-400.

Cuello, L. G., Cortes, D. M., and Perozo, E. (2004). Molecular architecture of the KvAP voltage-dependent K+ channel in a lipid bilayer. Science *306*, 491-495.

Gandhi, C. S., Clark, E., Loots, E., Pralle, A., and Isacoff, E. Y. (2003). The orientation and molecular movement of a k(+) channel voltage-sensing domain. Neuron *40*, 515-525.

Gandhi, C. S., and Isacoff, E. Y. (2002). Molecular models of voltage sensing. J Gen Physiol *120*, 455-463.

Glauner, K. S., Mannuzzu, L. M., Gandhi, C. S., and Isacoff, E. Y. (1999). Spectroscopic mapping of voltage sensor movement in the Shaker potassium channel. Nature *402*, 813-817.

Hille, B. (2001). Ion channels of excitable membranes, 3rd edn (Sunderland, Mass., Sinauer).

Hong, K. H., and Miller, C. (2000). The lipid-protein interface of a Shaker K(+) channel. J Gen Physiol *115*, 51-58.

Jiang, Y., Lee, A., Chen, J., Ruta, V., Cadene, M., Chait, B. T., and MacKinnon, R. (2003). X-ray structure of a voltage-dependent K+ channel. Nature *423*, 33-41.

Lai, H. C., Grabe, M., Jan, Y. N., and Jan, L. Y. (2005). The S4 voltage sensor packs against the pore domain in the KAT1 voltage-gated potassium channel. Neuron *47*, 395-406.

Laine, M., Lin, M. C., Bannister, J. P., Silverman, W. R., Mock, A. F., Roux, B., and Papazian, D. M. (2003). Atomic proximity between S4 segment and pore domain in Shaker potassium channels. Neuron *39*, 467-481.

Larsson, H. P., Baker, O. S., Dhillon, D. S., and Isacoff, E. Y. (1996). Transmembrane movement of the shaker K+ channel S4. Neuron *16*, 387-397.

Latorre, R., Olcese, R., Basso, C., Gonzalez, C., Munoz, F., Cosmelli, D., and Alvarez, O. (2003). Molecular coupling between voltage sensor and pore opening in the Arabidopsis inward rectifier K+ channel KAT1. J Gen Physiol *122*, 459-469.

Ledwell, J. L., and Aldrich, R. W. (1999). Mutations in the S4 region isolate the final voltage-dependent cooperative step in potassium channel activation. J Gen Physiol *113*, 389-414.

Li-Smerin, Y., Hackos, D. H., and Swartz, K. J. (2000a). alpha-helical structural elements within the voltage-sensing domains of a K(+) channel. J Gen Physiol *115*, 33-50.

Li-Smerin, Y., Hackos, D. H., and Swartz, K. J. (2000b). A localized interaction surface for voltage-sensing domains on the pore domain of a K+ channel. Neuron *25*, 411-423.

Long, S. B., Campbell, E. B., and Mackinnon, R. (2005a). Crystal structure of a mammalian voltage-dependent Shaker family K+ channel. Science *309*, 897-903.

Long, S. B., Campbell, E. B., and Mackinnon, R. (2005b). Voltage sensor of Kv1.2: structural basis of electromechanical coupling. Science *309*, 903-908.

Mannikko, R., Elinder, F., and Larsson, H. P. (2002). Voltage-sensing mechanism is conserved among ion channels gated by opposite voltages. Nature *419*, 837-841.

Minor, D. L., Jr., Masseling, S. J., Jan, Y. N., and Jan, L. Y. (1999). Transmembrane structure of an inwardly rectifying potassium channel. Cell *96*, 879-891.

Monks, S. A., Needleman, D. J., and Miller, C. (1999). Helical structure and packing orientation of the S2 segment in the Shaker K+ channel. J Gen Physiol *113*, 415-423.

Murata, Y., Iwasaki, H., Sasaki, M., Inaba, K., and Okamura, Y. (2005). Phosphoinositide phosphatase activity coupled to an intrinsic voltage sensor. Nature *435*, 1239-1243.

Neale, E. J., Elliott, D. J., Hunter, M., and Sivaprasadarao, A. (2003). Evidence for intersubunit interactions between S4 and S5 transmembrane segments of the Shaker potassium channel. J Biol Chem *278*, 29079-29085.

Pathak, M., Kurtz, L., Tombola, F., and Isacoff, E. (2005). The cooperative voltage sensor motion that gates a potassium channel. J Gen Physiol *125*, 57-69.

Phillips, L. R., Milescu, M., Li-Smerin, Y., Mindell, J. A., Kim, J. I., and Swartz, K. J. (2005). Voltage-sensor activation with a tarantula toxin as cargo. Nature *436*, 857-860.

Posson, D. J., Ge, P., Miller, C., Bezanilla, F., and Selvin, P. R. (2005). Small vertical movement of a K+ channel voltage sensor measured with luminescence energy transfer. Nature *436*, 848-851.

Ruta, V., Chen, J., and Mackinnon, R. (2005). Calibrated Measurement of Gating-Charge Arginine Displacement in the KvAP Voltage-Dependent K(+) Channel. Cell *123*, 463-475.

Sali, A., and Blundell, T. L. (1993). Comparative protein modelling by satisfaction of spatial restraints. J Mol Biol *234*, 779-815.

Sato, Y., Sakaguchi, M., Goshima, S., Nakamura, T., and Uozumi, N. (2003). Molecular dissection of the contribution of negatively and positively charged residues in S2, S3, and S4 to the final membrane topology of the voltage sensor in the K+ channel, KAT1. J Biol Chem *278*, 13227-13234.

Shealy, R. T., Murphy, A. D., Ramarathnam, R., Jakobsson, E., and Subramaniam, S. (2003). Sequence-function analysis of the K+-selective family of ion channels using a comprehensive alignment and the KcsA channel structure. Biophys J *84*, 2929-2942.

Starace, D. M., and Bezanilla, F. (2004). A proton pore in a potassium channel voltage sensor reveals a focused electric field. Nature *427*, 548-553.

Swartz, K. J. (2004). Towards a structural view of gating in potassium channels. Nat Rev Neurosci *5*, 905-916.

Tombola, F., Pathak, M., and Isacoff, E. (2005). How Far Will You Go to Sense Voltage? Neuron *48*, 719-725.

Wells, J. A. (1990). Additivity of mutational effects in proteins. Biochemistry *29*, 8509-8517.

CHAPTER IV

Testing Gating Models of Hyperpolarization and Depolarization-Activated Potassium Channels

Abstract

Members of the voltage-gated potassium (K_v) channel family can be activated by either hyperpolarized or depolarized potentials. Understanding how these channels gate, open or close, in response to membrane potential changes remains a challenge. Key structural features responsible for gating are a putative glycine hinge in the S6 pore region creating a kink in this helix to open the pore and coupling of the S4-S5 linker to the end of S6, thereby connecting the S4 voltage-sensor movement to pore opening. A series of mutational and chimeric analyses of depolarization and hyperpolarization-activated channels from *Drosophila melanogaster* and *Arabidopsis thaliana*, specifically Shaker, KAT1, and SKOR, seem to lend support for a model where the S6 segment of the pore kinks to open in both depolarization and hyperpolarization-activated channels. In addition, we find that charged residues in the S4-S5 linker of KAT1 are important for gating.

Introduction

How do voltage-gated channels gate in response to changes in membrane potential? Significant progress in understanding this process has been made due to numerous structural and functional investigations of different types of voltage-gated channels - hyperpolarization and depolarization-activated. To explore the gating mechanism of these channels, findings from the voltage-gated sodium (Na_V), voltage-gated potassium (K_V), and 2-TM channel families will be integrated in this discussion of general features of channel gating. However, it is likely that further evidence will reveal different mechanistic details required for each channel family's particular gating pattern.

We set out to understand how K_V channels gate in response to hyperpolarization or depolarization. To understand this property, we focused on three model channels: Shaker – a depolarization-activated K_v channel from *Drosophila melanogaster* (Tempel et al., 1987), KAT1 – a hyperpolarization-activated K_v channel from *Arabidopsis thaliana* (Anderson et al., 1992), and SKOR – a depolarization-activated K_v channel from *Arabidopsis thaliana* (Gaymard et al., 1998). These channels have similar structural features (6-TM segments, S4 voltage-sensor, salt bridges between S2, S3, and S4) (Bezanilla, 2002; Sato et al., 2003; Seoh et al., 1996; Tempel et al., 1987; Tiwari-Woodruff et al., 1997; Yellen, 2002), orientation in the membrane (Latorre et al., 2003; Mura et al., 2004), and movement of the S4 voltage-sensor (Gandhi and Isacoff, 2002; Horn, 2004; Mannikko et al., 2002) despite their being activated by different voltage ranges, hyperpolarization and depolarization.

Glycine residues have high conformational flexibility due to the lack of a Cβ atom (Creighton, 1993) and are known to create "kinks" or "hinges" in helices that may serve functional roles (Deber and Li, 1995; Jiang et al., 2002). Glycine hinge models of gating focus on a highly conserved glycine in the middle of S6 that creates a hinge, so that the S6 helices can kink to splay apart the lower half of S6 and allow K^+ and blocking agents into the pore (Ding et al., 2005; Jiang et al., 2002; Magidovich and Yifrach, 2004; Shealy et al., 2003). From now on, this conserved glycine will be referred to as the "hinge glycine" as designated by an alignment of the glycine that appears to bend the S6 helix in the MthK crystal structure to other potassium channels (Jiang et al., 2002; Shealy et al., 2003). This model explains some ion conduction properties since mutation of the hinge glycine to alanine decreases the macroscopic ionic current in recordings of Shaker in *Xenopus laevis* oocytes suggesting that the inability of S6 to kink restricts ion conduction. Consistent with this, mutation of the hinge glycine in Shaker to proline, another helix-breaking amino acid that could form a permanent kink (Deber and Li, 1995), creates channels that are more likely to open and more difficult to close (Ding et al., 2005; Magidovich and Yifrach, 2004; Zhao et al., 2004b). However, these studies are complicated by the fact that there is often another glycine approximately seven residues N-terminal of the hinge glycine in almost all other channels (Shealy et al., 2003) and a PVP motif seven residues C-terminal of the hinge glycine in Shaker serving as other possible bending points to gate these channels.

The position of the hinge glycine is important for gating these channels and is tolerated at specific sites in S6. Studies have shown that the hinge glycine can be moved from its very conserved position to other residues in S6 and still gate the channel in a similar manner to wildtype. For example, moving the hinge glycine to one residue toward the C-terminus of S6 in Shaker retains a depolarization-activated channel with similar channel properties, but putting a glycine at other positions in S6 causes the channels to be nonfunctional or not expressed at the surface (Ding et al., 2005; Magidovich and Yifrach, 2004). Similar studies have shown that substitution with proline, which is believed to create a permanent kink, is also tolerated at specific sites in S6. In an archaeal voltage-gated sodium channel, NaChBac, replacing the leucine seven residues C-terminal from the hinge glycine with a proline (L226P) remarkably reverses the channel polarity from a depolarization-activated channel to a hyperpolarization-activated one (Zhao et al., 2004a) suggesting that the position of the kink alone could determine the voltage-activation property of a channel. This proline scan of S6 residues in NaChBac revealed four sites that retained depolarization activation and three that acquired hyperpolarization activation. Furthermore, proline substitution of the hinge glycine, the residue immediately N-terminal of the hinge glycine, and the residue immediately C-terminal of the hinge glycine in NaChBac, all result in depolarization-activated channels. These experiments illustrate that while hinge placement is important for pore opening, how the precise location affects gating polarity is not well understood.

Another description of voltage-gating involves "coupling" models which describe how the S4-S5 linker communicates with the C-terminal end of S6. Mutational analyses of HERG and HCN and chimeric analyses of Shaker with 2-TM channels suggest that these two regions of the channel interact with each other to connect the movement of the S4 voltage-sensor to the S6 gate (Chen et al., 2001; Decher et al., 2004; Lu et al., 2002; Tristani-Firouzi et al., 2002). In addition, direct contact of these two regions is seen in the crystal structure of $K_v1.2$ implicating interactions between these segments in gating (Long et al., 2005a; Long et al., 2005b). Precisely how these regions interact to affect voltage-gating is again not well understood.

We set out to further define the roles of the hinge position and the coupling of the S4-S5 linker and S6 in determining the voltage-dependence of a channel. We aimed to get at the precise structural components involved in reversing the voltage-dependence of these channels by making a series of mutations and chimeras that probed these structural features. In conjunction with the KAT1 model from Chapter III and the $K_v1.2$ structure, we hoped to eventually determine how these specific mutations and chimeras could affect the channel conformation to gain a mechanistic understanding of voltage-dependence from a structural perspective.

Two models derived from these ideas are a "hinge position" gating model and a "coupling" gating model of voltage-dependence. These models are not necessarily mutually exclusive, but we will treat them individually for now to gain some insight into how a particular model might accurately predict voltage-

dependent gating. In addition, we will start to talk about the open and closed states of a channel since we are now referring to this aspect of channel gating.

In the hinge position model, the position of the glycine that creates the kink in S6 is what determines voltage-dependent gating (Figure 1). The movement of S4 is similar for both depolarization and hyperpolarization-activated channels (Bezanilla, 2002; Gandhi and Isacoff, 2002; Horn, 2002; Mannikko et al., 2002) and the hinge is also similar in that S6 is straight in the hyperpolarized state, but kinked in the depolarized state. However, in this model, when the S6 helix is straight, the pore is closed for depolarization-activated channels and open for hyperpolarization-activated channels. This could be due to structural differences between these types of channels that make the ends of S6 closer to each other in a helical bundle like in KcsA for depolarization-activated channels (Doyle et al., 1998) or farther apart in hyperpolarization-activated channels with a big enough space to let ions through. In addition, it was noted that the hinge glycine in KAT1 is placed two residues N-terminal of the hinge glycine in SKOR based on an alignment using ClustalW (Figure 7B) lending to this idea that the kink is positioned differently in these channels. In depolarization-activated channels (i.e. SKOR), the hinge kinks open to allow ion conduction at depolarized potentials similar to the models suggested by the MthK and $K_v1.2$ structures (Jiang et al., 2002; Long et al., 2005a). However, in hyperpolarization-activated channels (i.e. KAT1), since the glycine hinge is positioned on a different face of the helix (two residues N-terminal of the hinge glycine in SKOR), these

positional differences would change the kinking angle such that the ends of S6 would kink and close the channel (Figure 1A).

In the "coupling" gating model, the coupling of the S4-S5 linker to the pore region is what determines voltage-dependence. In this model, it assumes the hinge glycine will always kink to open the channel and when the S6 helices are straight, the channel is always closed. Therefore the open state with the hinge glycine kinked is at depolarized potentials for depolarization-activated channels and at hyperpolarized potentials for hyperpolarization-activated channels. Since the movement of S4 is the same for depolarization and hyperpolarization-activated channels (Mannikko et al., 2002), this means that the way in which the S4-S5 linker interacts with the pore domain – most likely S6 given chimeric analyses and structural evidence (Chen et al., 2001; Decher et al., 2004; Long et al., 2005b; Lu et al., 2002; Tristani-Firouzi et al., 2002) – is the deterministic factor in how the channel opens and closes. Note that the way the pore kinks open in this model is the same as in the hinge position model for depolarization-activated channels, Shaker and SKOR. For hyperpolarization-activated channels (i.e. KAT1), the kink in the open and closed states are different in these models.

In an effort to examine these models, mutations in either the hinge glycine of KAT1 or Shaker and an alanine scan of the S4-S5 linker of KAT1 have been tested to see how these mutations affect gating of the channel. In addition, we tried to reverse the voltage-dependence of KAT1 from a hyperpolarization-activated channel to a depolarization-activated one through a series of chimeras. Given the high sequence similarity between KAT1 and SKOR, we made

chimeras replacing sections of the KAT1 S6 with residues or regions of SKOR S6 to identify the regions necessary for turning a hyperpolarization-activated channel into a depolarization-activated one. This approach was reasonable for these two channels since their S4-S5 linkers are highly homologous (Figure 7 A) suggesting that the reason for their difference in voltage-dependence is due to regions in S6.

Materials and Methods

Molecular Biology

KAT1 with its 5' and 3' UTRs was amplified by PCR and cloned into the HindIII-XhoI sites of a modified pYES2 vector containing a Met-25 promoter (Minor et al., 1999). Site-directed mutations and chimeras were made using the QuikChange site-directed mutagenesis kit (Stratagene, LaJolla, CA). *KAT1* wt or mutation constructs were subcloned into the oocyte pLin (Yi et al., 2001) vector via the HindIII-XhoI cloning sites. *KAT1* with the Shaker S4-S5 linker sequence was generously provided by Dr. Ramon Latorre (unpublished results) and cloned into pLin via the HindIII-XhoI cloning sites. In this chimera, the KAT1 S4-S5 linker, R184 to K200 (184 – RLEKDIRFNYFWIRCTK – 200, 17 residues), is replaced with the Shaker S4-S5 linker, G381 to E395 (381 – GLQILGRTLKASMRE – 395, 15 residues).

Yeast Selection

Plasmids containing *KAT1* wt, mutants, or chimeras in the modified pYES2 vector were transformed into the yeast strain SGY1528 via lithium acetate transformation and plated onto nonselective 100 mM K^+ -URA/-MET yeast media plates (Minor et al., 1999). After three days growth, three colonies of each construct were successively streaked onto plates containing 2 mM K^+, 0.5 mM K^+, and finally 0.2 mM K^+ with 1-3 days of growth between restreaking.

Electrophysiology

Wildtype, mutant, and chimeric *KAT1* in the pLin vector was transcribed using the AmpliCap T7 High Yield Message Maker Kit (Epicentre Technologies, Madison, WI) to generate cRNA. Stage V-VI *Xenopus laevis* oocytes were injected with RNA and recorded by two-electrode voltage clamp (GeneClamp 500B, Axon Instruments, Foster City, CA). The amount of RNA injection, voltage protocols, and recording solutions are given in the Figure legends. The pClamp software (Axon Instruments, Foster City, CA) was used for recording and analysis and the Origin (Northampton, MA) or Microsoft Excel (Redmond, WA) software were used for plotting graphs, traces, and data analysis.

Results

Mutation of the hinge glycine in KAT1

If the hinge position gating model is correct (Figure 1A), then mutation of the glycine hinge to a less flexible residue should stabilize the open conformation of KAT1. There are two glycines in the KAT1 S6. The hinge glycine, G293, was assigned according to an alignment of KAT1 to KcsA and then MthK, the structure of which suggested a glycine hinge model of gating (Jiang et al., 2002; Shealy et al., 2003). There is another glycine seven residues N-terminal of the hinge glycine, G286. While mutation of hinge glycine, G293, to alanine and tryptophan did not yield any currents (Table 1), mutation of G293 to proline significantly increased the time to activation and time to closure of the channel as seen from the kinetics of activation and deactivation (Figure 2B compared to A). One possible explanation for these results is that mutation of the hinge glycine to alanine and tryptophan, residues that have more helix-stabilizing propensity than helix-breaking tendency (Creighton, 1993; Deber and Li, 1995), stabilize a closed conformation which is inconsistent with the hinge position gating model and more consistent with coupling gating model. This interpretation assumes that the mutant channels are expressed to the same degree on the surface as the wildtype channel. It is possible that these mutations affect channel biogenesis which has been seen with mutations of the hinge glycine in Shaker (Ding et al., 2005; Magidovich and Yifrach, 2004). Moreover, the proline mutation appears to slow both the activation and deactivation time suggesting that the transition state

of this mutant channel is more energetically unfavorable and this finding does not necessarily support or refute either model.

Mutation of the hinge glycine in Shaker

According to the hinge position model and the coupling model, mutation of the glycine in Shaker to less flexible residues should stabilize the closed state of the channel. There are two glycines in the Shaker S6 and the hinge glycine, G466, was assigned based on an alignment of Shaker to KcsA and then MthK (Jiang et al., 2002; Shealy et al., 2003). The other glycine, G459, is seven residues N-terminal of the hinge glycine similar to KAT1. Mutant channels with the hinge glycine, G466, replaced with alanine, cysteine, serine, lysine, tryptophan, and proline did not yield any currents under the same conditions as wildtype (Table 1). However, injection of 100 times more RNA (50 ng) of constructs containing G466A or G466C mutations caused the oocytes to exhibit an outwardly rectifying current (Figure 3). Assuming that these currents are not due to overexpression artifacts, they suggest that the channel can gate even without the hinge glycine. This indicates that the hinge glycine is not the only part of S6 that controls gating - perhaps other regions such as the other glycine, G459, or the PVP motif seven residues C-terminal of the hinge glycine also have important roles (Webster et al., 2004). Another possibility is that these mutated residues, alanine and cysteine, have some degree of flexibility that allows the channel to open slightly, but decreases the conductance of the channel so that the current can only be detected upon overexpression. These observations are

[redacted]

compatible with both models for depolarization-activated channels where a kink in the S6 helix is needed to open the channel.

Alanine scan of the KAT1 S4-S5 linker

The S4-S5 linker is important for coupling the voltage-sensor to the gate (Chen et al., 2001; Decher et al., 2004; Long et al., 2005b; Lu et al., 2002; Tristani-Firouzi et al., 2002). An alanine scan of this region identified residues critical for this coupling. R184, L185, E186, K187, D188, I189, and R190 of the KAT1 S4-S5 linker were individually mutated to alanine. The functional effects of these mutations were determined by evaluation in the K^+-transporter deficient yeast strain and by recording in *Xenopus laevis* oocytes via two-electrode voltage clamp (TEVC). Each residue mutated to alanine supports yeast growth on 0.2 mM K^+ yeast plates (Figure 4), so small differences in functionality cannot be assessed by this method. Electrophysiological recording reveals that the threshold to channel activation and macroscopic ionic current is reduced by alanine substitution of E186, K187, D188, I189, and to a lesser degree R190 (Figure 5 and Figure 6). This suggests that particular residues in the S4-S5 linker are important for channel gating.

Chimeras of KAT1 and SKOR

In an effort to distinguish between the hinge position and coupling gating models, we noted that KAT1, a hyperpolarization-activated channel, and SKOR, a depolarization-activated channel, both from *Arabidopsis thaliana*, are highly

homologous with approximately 40% identity in the transmembrane regions and 50% identity in the S4-S5 linkers (Figure 7A). These similarities could allow us to identify structural components that are required for changes in gating. Given the high sequence identity in the S4-S5 linker, we focused on regions of S6 that were different in chemical composition between KAT1 and SKOR to determine the affects of these regions on voltage-dependent gating.

We generated various chimeras and mutations in the KAT1 S6 with sequences derived from SKOR S6. The second half of the KAT1 S6, H301 to T308, was replaced with the SKOR S6, K329 to R338 (329 – KGSKTER – 338), causing an increase in the time to activation and deactivation (Figure 7D). Mutation of N287 in KAT1 to alanine significantly reduced the amount of current compared to wildtype under the same conditions (Figure 7E). Moving the other glycine in KAT1, G286, down two residues to the placement in SKOR, creating the double mutant, G286I + T288G, for KAT1, gave an inwardly rectifying channel although with a severely reduced current (Figure 7F). These chimeras and mutations were also tested at more positive potentials and no outwardly rectifying currents were detected except for the endogenous current (unpublished data and see Figure 8). These data suggest that S6 is important for gating; however, the specific region of S6 responsible for depolarization or hyperpolarization activation has not been identified.

Chimera of KAT1 with the S4-S5 linker of Shaker

A chimera of KAT1 with the S4-S5 linker of Shaker (see Materials and Methods for details) was generously provided by Dr. Ramon Latorre (unpublished data). Recording of this chimera in *Xenopus* oocytes by TEVC revealed an outwardly rectifying current above +50 mV; however, this current is also seen in water injected negative control oocytes (Figure 8A). Quantification of these currents illustrates that the oocytes injected with the chimera construct give less current than water injected control oocytes, but due to the presence of an endogenous channel or channels the current of the chimera construct could not be isolated. In addition, the endogenous outwardly rectifying current is likely to be conducted by K^+ or H^+ since there are no Cl^- or Na^+ ions in the extracellular recording solution.

Discussion

How the voltage-sensor couples to the gate, the structural determinants of this property, and how these features lead to differences in the voltage-dependence of different ion channels are still unanswered questions in the field. While electrophysiological and structural analyses have pointed to the S4-S5 linker and the hinge to C-terminal end of S6 as major features of coupling and gating, the precise interactions that occur between these structural elements and the movement of these elements between the open and closed states of both hyperpolarization and depolarization-activated channels remains a fascinating area of research. We considered two models, the hinge position gating model and the coupling gating model, to help frame this research. While the experiments in this section were inconclusive, they set the framework for further work addressing how different K_v channels with similar topology, orientation in the membrane, and movement of the voltage-sensor can activate at either hyperpolarized or depolarized potentials. In addition, they provide a framework to think about gating and may lead to other ideas of how coupling and gating may work. Indeed, the experiments suggest that voltage-gating may be more complicated than these two simple models illustrate.

To test the hinge position gating model, the hinge glycine in KAT1, G293, and Shaker, G466, were mutated to various residues (Table 1) that should stabilize either an open or closed state, respectively. The results showed that the hinge glycine may not be the only hinge in the S6 gate and may not solely be responsible for channel opening and closing. For KAT1, mutation of G293 to

alanine and tryptophan did not result in current when compared to wildtype under identical conditions (Table 1). Assuming the channels are expressed at the surface in equal numbers compared to wildtype, the Ala and Trp mutations do not support the hinge position model since an open state was not stabilized as would be predicted by this model. However, these mutations may affect channel folding or biogenesis and experiments determining the number of channels at the surface will help address this issue. In addition, mutation of G293 to proline appears to affect the transition state since there is a longer time to activation and deactivation (Figure 2). The KAT1 glycine hinge mutations appear to support the coupling gating model where the S6 gate must kink open to allow ion conduction similar to the paradigm for Shaker and $K_v1.2$. However, this is confounded by the fact that proline mutations in the S6 of NaChBac as described in the Introduction can reverse the voltage-dependence of this channel suggesting that the position alone of a helix-breaking residue can affect voltage-dependent gating.

For Shaker, mutation of the hinge glycine, G466, to alanine or tryptophan resulted in currents, but not under the same conditions as wildtype (Table 1). Overexpression of these mutants resulted in an outwardly rectifying current suggesting that the hinge glycine is not the only hinge along the S6 helix (Figure 3). A second glycine seven residues N-terminal of the hinge glycine, G459, as well as the PVP motif seven residues C-terminal (P473-V474-P475) may be responsible for gating in the pore region as suggested by other groups (Webster et al., 2004). Another possibility is that these mutated residues, alanine and

cysteine, have some degree of flexibility that allows the channel to open slightly, but decreases the conductance of the channel; therefore, the currents can only be detected upon overexpression. These experiments are compatible with both the hinge position and coupling models in that the pore must kink to open.

Work by Ding et al. has shown that the G466A mutant is expressed at the surface in tsA201 cells (Ding et al., 2005). However, there appears to be a biogenesis defect since these channels are not as well glycosylated as wildtype in oocytes (Ding et al., 2005; Magidovich and Yifrach, 2004). Given these findings, overexpression of this mutant may be necessary to overcome the biogenesis defect or on a functional level, a smaller conductance or open probability, so that enough channels will be expressed for a macroscopic current to be detected. Single channel recordings of the mutant channels and quantification of the amount of surface expression in oocytes will help address these questions. The detection of current by the Shaker G466A mutant is in direct contradiction to currently published results (Ding et al., 2005; Magidovich and Yifrach, 2004) where the G466A mutation did not yield currents despite the same amount of RNA injection (50 ng) as tested here (Magidovich and Yifrach, 2004). It will be important to repeat these experiments with a pore blocking toxin to validate these currents.

To test the coupling gating model, an alanine scan of the KAT1 S4-S5 linker revealed the importance of a highly charged segment of the linker that significantly affects channel properties. Individual mutation of each E186, K187, D188, I189, and R190 to alanine reduces the amount of current elicited under the

same recording conditions as wildtype demonstrating the importance of these residues in gating (Figure 5). Preliminary structural models of KAT1 by Dr. Michael Grabe (unpublished data) suggest that the S4-S5 linkers may interact with the end of S6 by electrostatic interactions. Since the S4-S5 linker of KAT1 and SKOR are similarly highly charged and the distribution of positive and negative charges at the end of S6 is different (see Figure 7), this suggests that these two regions may interact electrostatically to influence the type of voltage-gating that occurs as suggested in studies of HERG and HCN (Chen et al., 2001; Decher et al., 2004; Tristani-Firouzi et al., 2002). Replacement of the end of KAT1 S6 with the differently charged SKOR end of S6 (Figure 7D) did not switch the voltage-activation properties of KAT1, but did result in a channel with slowed activation and deactivation properties. These data identify key residues in the KAT1 S4-S5 linker that are important for coupling and start to suggest that electrostatic interactions may be responsible for this coupling, although the precise contacts between the S4-S5 linker and the end of S6 have yet to be determined. Chimeras of Shaker and KcsA also suggest that interactions between the S4-S5 linker and S6 could also couple S4 to the S6 gate (Caprini et al., 2005; Lu et al., 2002). In this case, we would posit that since the Shaker S4-S5 linker is an amphipathic helix, depending on the state of the channel, either the hydrophobic or charged side of the helix could make different contacts with the end of S6 to couple the voltage-sensor to the gate. Taken together, these data indicate that different channels may have employed different strategies for the types of interactions that could couple the voltage-sensor to the gate.

In addition to mutation of the KAT1 hinge glycine, G293, described above, the other glycine in S6, G286 – seven residues N-terminal of G293, was tested for its importance in voltage-dependent gating by moving it two residues C-terminal to the placement of this glycine in SKOR. Currents detected by this KAT1 double mutant, G286I + T288G, were severely decreased compared to wildtype suggesting that the hinge glycine, G293, alone is not responsible for voltage-gating (Figure 7F) and that the position of the other glycine in KAT1 is critical to channel function. This is also evidenced by the fact that the previously tested hinge glycine, G293, (Figure 5 and Table 1) is conserved in SKOR (Figure 7B) and therefore this glycine is likely not responsible for the differences in voltage-dependence between these channels despite the identification of this residue as the hinge glycine based on the alignment of this residue to the hinge glycine in KcsA and MthK (Jiang et al., 2002; Shealy et al., 2003).

Interestingly, a triple mutant of SKOR which mutates residues in the SKOR S6 to residues in KAT1, D312N + M313L + I314G, by the Dreyer group (Poree et al., 2005) led to an open channel at all potentials. This triple mutant results in two glycines, the glycine from the I314G mutation and the endogenous SKOR glycine at position 316, suggesting that the positioning of the glycine and conformational flexibility in S6 is important for voltage-dependent gating. Additionally, in their study, the single mutants, I314G and G316I, in SKOR resulted either in non-functional channels or a similar gating to SKOR; however, this data was not shown by Porée et al. and should be further tested.

Work on NaChBac identified that mutating S6 residues to proline created channels that were hyperpolarization-activated and this channel is normally depolarization-activated. Interestingly, the placement of this proline was approximately on the same helical face as the hinge glycine (i+3, i+7, i+10) from the hinge glycine, indicating that the placement of this proline to a different location on the same face can somehow reverse the voltage-dependence of the channel. This appears to lend support for the hinge position gating model.

This work illustrates that understanding how voltage-dependent gating works may be more complicated than the simple models shown here since some evidence supports the hinge position model while other data support the coupling gating model. The support for the coupling gating model comes from the findings that mutation of the hinge glycine in KAT1 to alanine and tryptophan appears to create non-functional channels contrary to the hinge position gating model and that an alanine scan of the KAT1 S4-S5 linker identified key residues that affect gating. Support for the importance of the hinge position is given by the KAT1-SKOR chimeras described above and other chimeras previously published (Poree et al., 2005) as well as work in the NaChBac channel (Zhao et al., 2004a). Indeed, there may be aspects of both models that are relevant and more work will need to be done to make sense of all the data.

Further experiments that are worth pursuing involve probing the structural differences between KAT1 and SKOR given that these channels are highly homolgous. A glycine or proline scan of KAT1 would be informative as these scans have only been done on depolarization-activated channels to date and

insight into how the placement of the hinge affects voltage-gating in a hyperpolarization-activated channel would give additional insights into the conformational changes of S6 and their relation to gating. In addition, assessing properties of chimeras between KAT1 and SKOR in both the S4-S5 linker region and S6 region may provide useful insights into coupling and how these regions contribute to voltage-dependent gating. Lastly, for the hinge glycine mutants that gave currents, G293P for KAT1, and G466A and G466C for Shaker, it will be interesting to probe the accessibility of the pore region to different sized tetraalkylammonium cations that block the pore. Presumably, the larger the pore size, the larger the blocker cation that will be let through, so one could get an estimate of whether the mutation widens or restricts the pore opening.

The experiments described in this Chapter illustrates that while it is possible to determine the residues in the S4-S5 linker and S6 that affect voltage-dependent gating, it is difficult to interpret the effect of these mutations without a structural context that could lend some insight into the mechanism. We are now in a position to better assess this using the experimental evidence obtained here and the KAT1 model from Chapter III. In future work, computational modeling of how these mutations affect the structure of the channel will provide insights into the mechanism of voltage-dependent gating.

Figures

Figure 1. Two models of voltage-gating.

The voltage-sensor is represented by a blue blob with positive charges in it represented as red plus signs, the S4-S5 linker by a black or orange line, the pore region (S5-S6) by a grey region, the potassium ions by blue circles, and the region important for gating (hinge or S4-S5 linker) is orange. (A) In the "hinge position" gating model, the positioning of a hinge in the S6 region, notably a glycine, is responsible for determining whether the pore is open or closed. (B) In the "coupling" gating model, the open state of any channel is "kinked" open and the closed state is "straight" closed and the gating of these states by voltage is dependent on the interaction of the S4-S5 linker with the pore region.

Figure 1. Two models of voltage-gating.

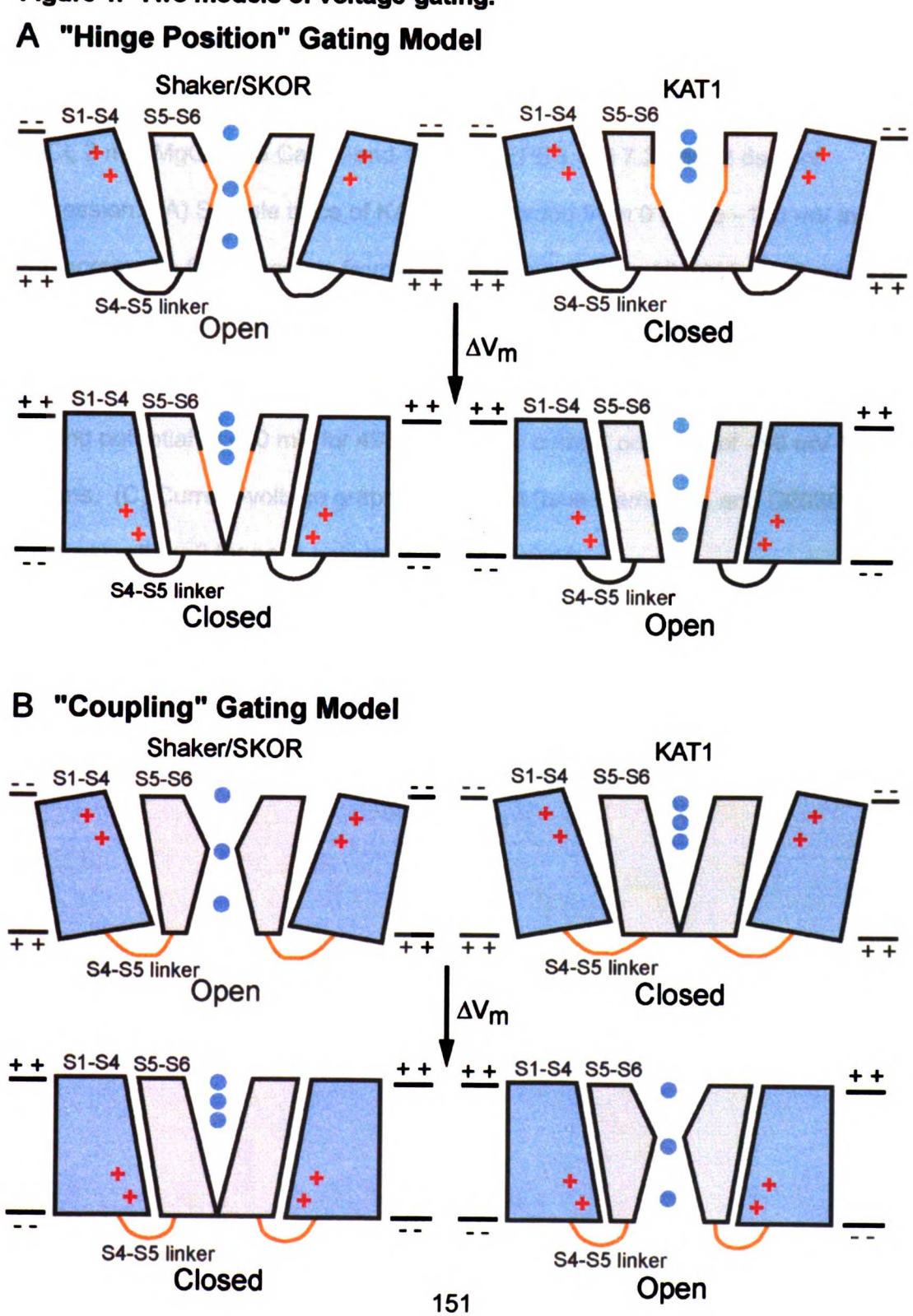

Figure 2. Mutation of the hinge glycine in KAT1 to proline, G293P, slows activation and deactivation.

Ooctyes were injected with 5 ng RNA and recorded in 50 mM KCl, 90 mM NaCl, 2 mM $MgCl_2$, 0.5 $CaCl_2$, and 10 mM HEPES, pH 7.2 after 2 days of expression. (A) Sample trace of KAT1 wt recorded from 0 mV to –140 mV in 10 mV increments for 4 seconds from a holding potential of –10 mV for 400 ms to a tail current potential of –50 mV for 800 ms. (B) Sample trace of KAT1 G293P recorded from 0 mV to –140 mV in 10 mV increments for 23.3 seconds from a holding potential of –10 mV for 496 ms to a tail current potential of –50 mV for 992 ms. (C) Current-voltage graph of KAT1 wt (blue diamonds) and G293P (pink squares) with n=2 for each construct. SEM is given.

Figure 2. Mutation of the hinge glycine in KAT1 to proline, G293P, slows activation and deactivation.

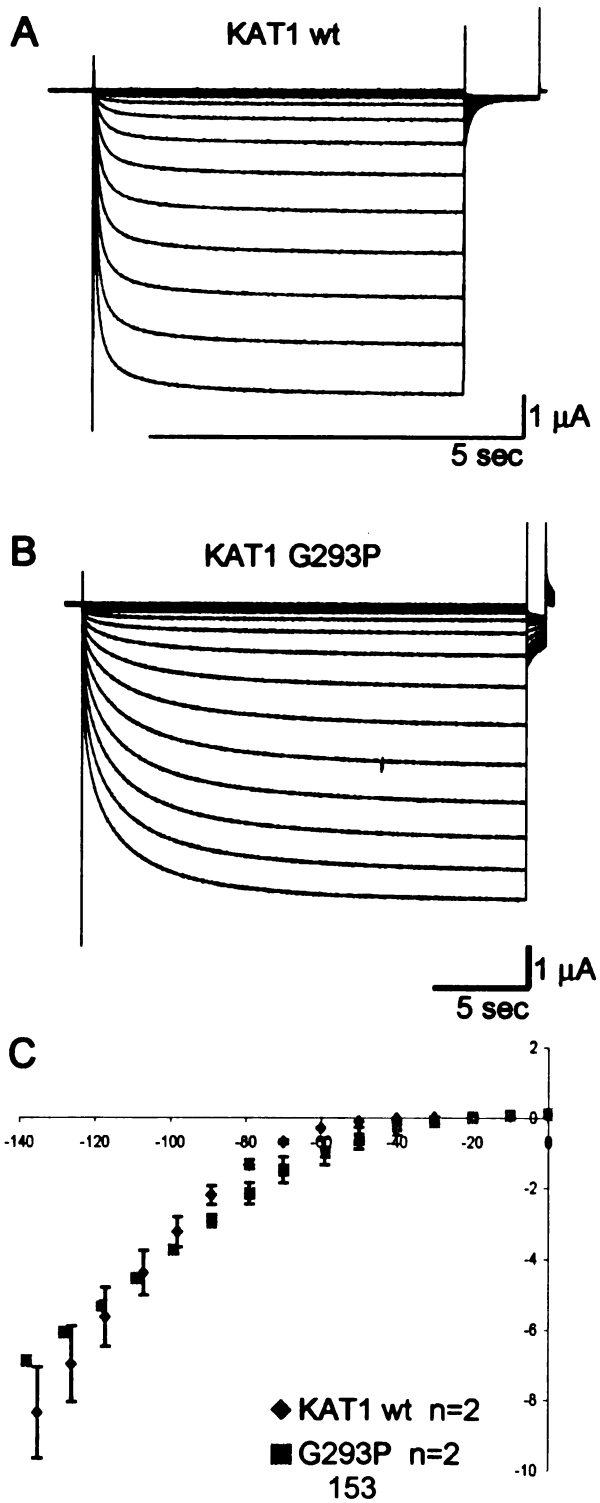

Figure 3. Mutation of the hinge glycine in Shaker ΔN6-46, G466A or G466C, upon overexpression reveals an outwardly rectifying current.

All currents were recorded in ND96: 96 mM NaCl, 2 mM KCl, 1 mM $MgCl_2$, 1.8 mM $CaCl_2$, 5 mM HEPES, pH 7.4 with a voltage protocol pulsing from –100 mV to +40 mV in 10 mV increments for 200 ms from a holding potential of –100 mV for 50 ms to a tail current of –120 mV for 50 ms after 2 days expression. (A) Sample trace of a 50 nL water injected negative control oocyte. (B) Sample trace of a Shaker ΔN6-46 positive control oocyte (0.5 ng RNA injected) showing an outwardly rectifying current. (C) Sample trace of currents from an oocyte injected with 50 ng RNA of Shaker ΔN6-46 G466A revealing an outwardly rectifying current upon overexpression. (D) Sample trace of currents from an oocyte injected with 50 ng RNA of Shaker ΔN6-46 G466C revealing an outwardly rectifying current upon overexpression.

Figure 3. Mutation of the hinge glycine in Shaker ΔN6-46, G466A or G466C, upon overexpression reveals an outwardly rectifying current.

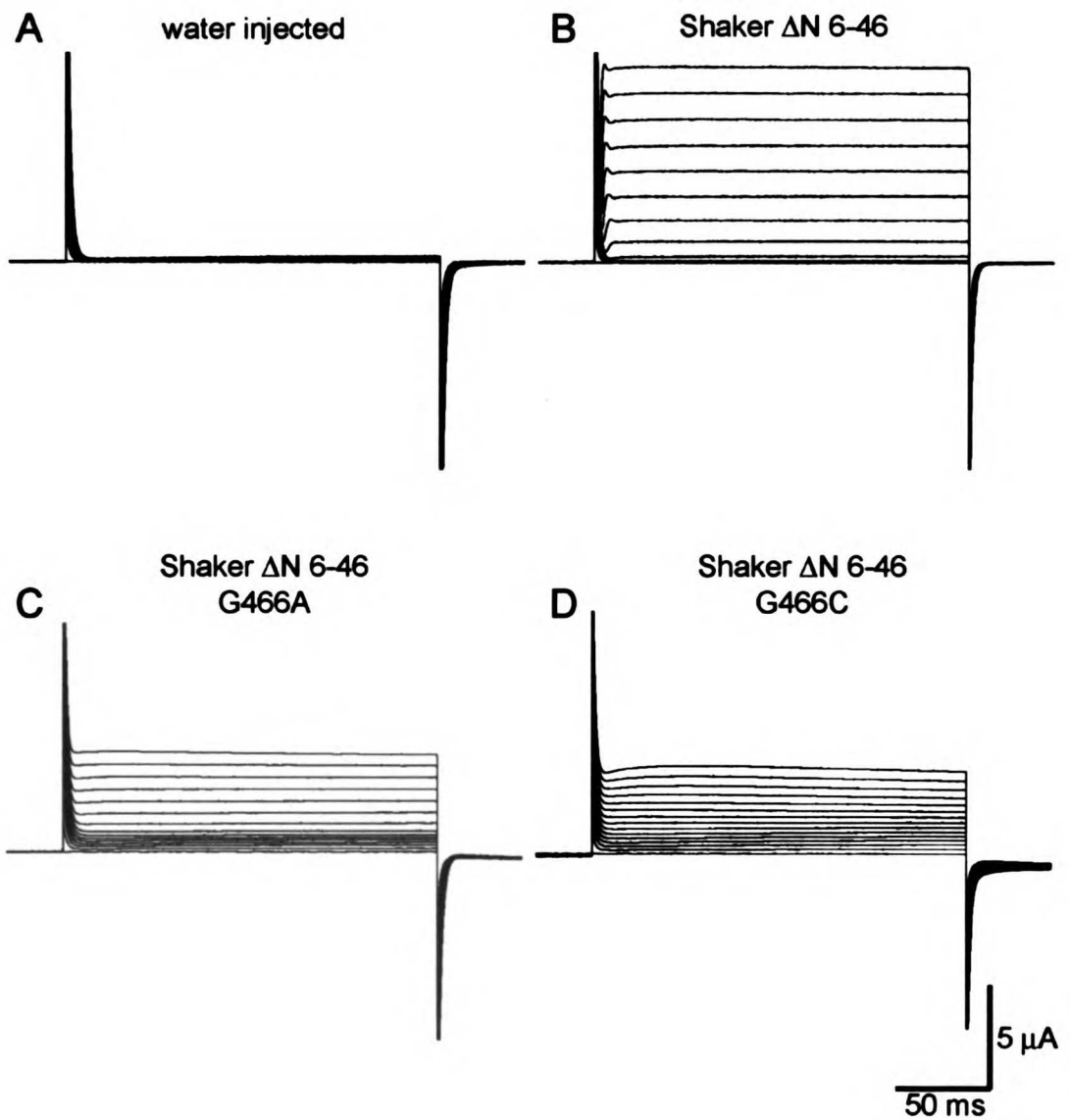

Figure 4. Mutation of each residue in the KAT1 S4-S5 linker to alanine rescues the K^+ transporter deficient yeast strain on 0.2 mM K^+ yeast plates.

Figure 4. Mutation of each residue in the KAT1 S4-S5 linker to alanine rescues the K+ transporter deficient yeast strain on 0.2 mM K+ yeast plates

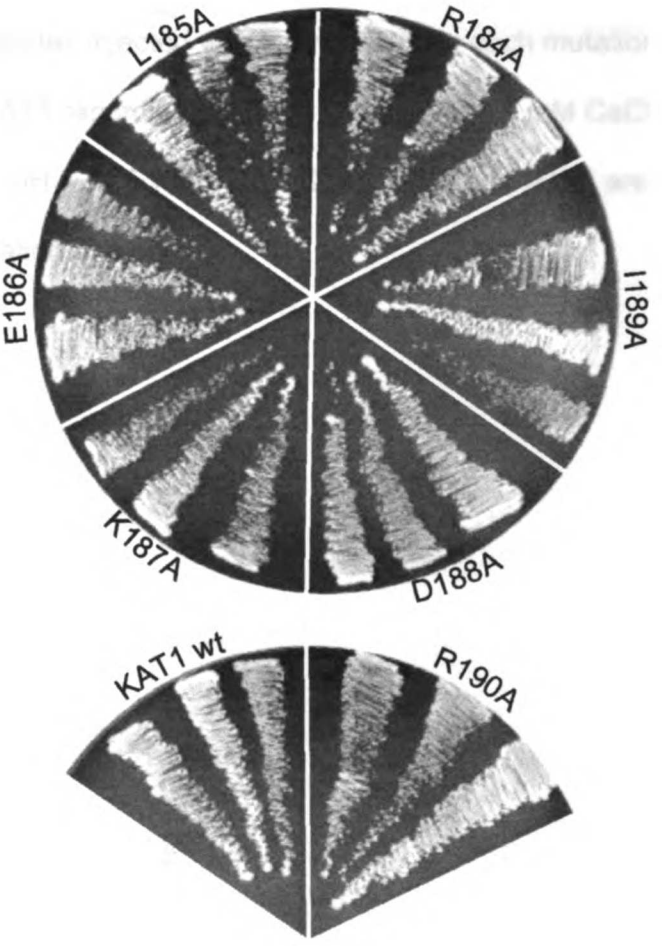

Figure 5. Sample traces of an alanine scan of the KAT1 S4-S5 linker.

Sample traces are shown for KAT1 wt (A), R184A (B), L185A (C), E186A (D), K187A (E), D188A (F), I189A (G), R190A (H). Currents were elicited from +60 mV to –160 mV in 20 mV increments for 1500 ms from a holding potential of –10 mV from oocytes injected with 2.3 ng RNA for each mutation after 2 days expression in KAT1 recording solution: 115 mM KCl, 1 mM $CaCl_2$, 2 mM $MgCl_2$, 10 mM HEPES, pH 7.2. E186, K187, D188, I189, and R190 are the most affected by mutation to alanine.

Figure 5. Sample traces of an alanine scan of the KAT1 S4-S5 linker.

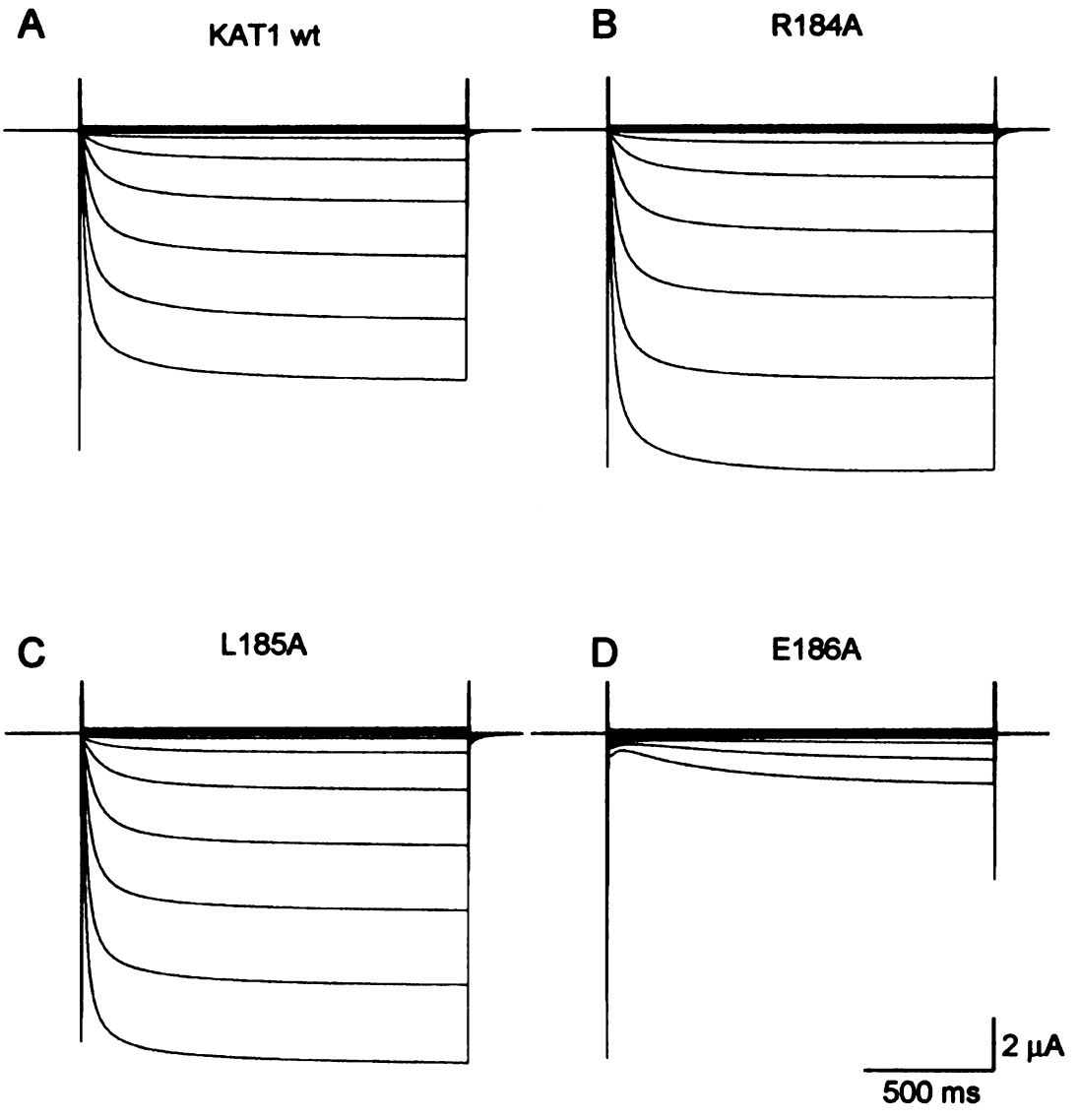

Figure 5 (continued). Sample traces of an alanine scan of the KAT1 S4-S5 linker.

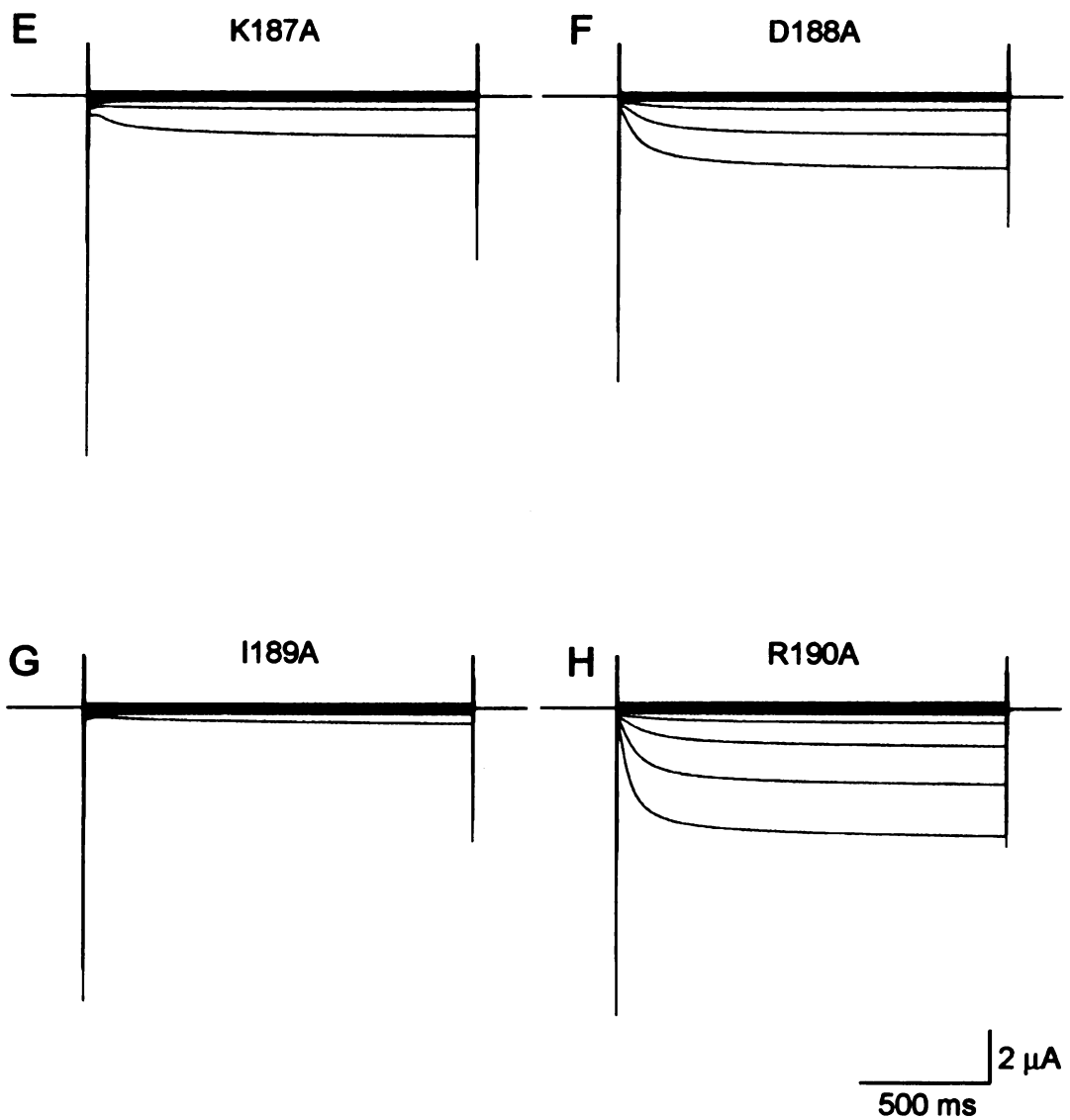

Figure 6. E186, K187, D188, I189, and R190 are the most affected by mutation to alanine.

Current-voltage graph of an alanine scan of the KAT1 S4-S5 linker. SEM are shown and the number of oocytes recorded given. Recording conditions are the same as in Figure 5.

Figure 6. E186, K187, D188, I189, and R190 are the most affected by mutation to alanine.

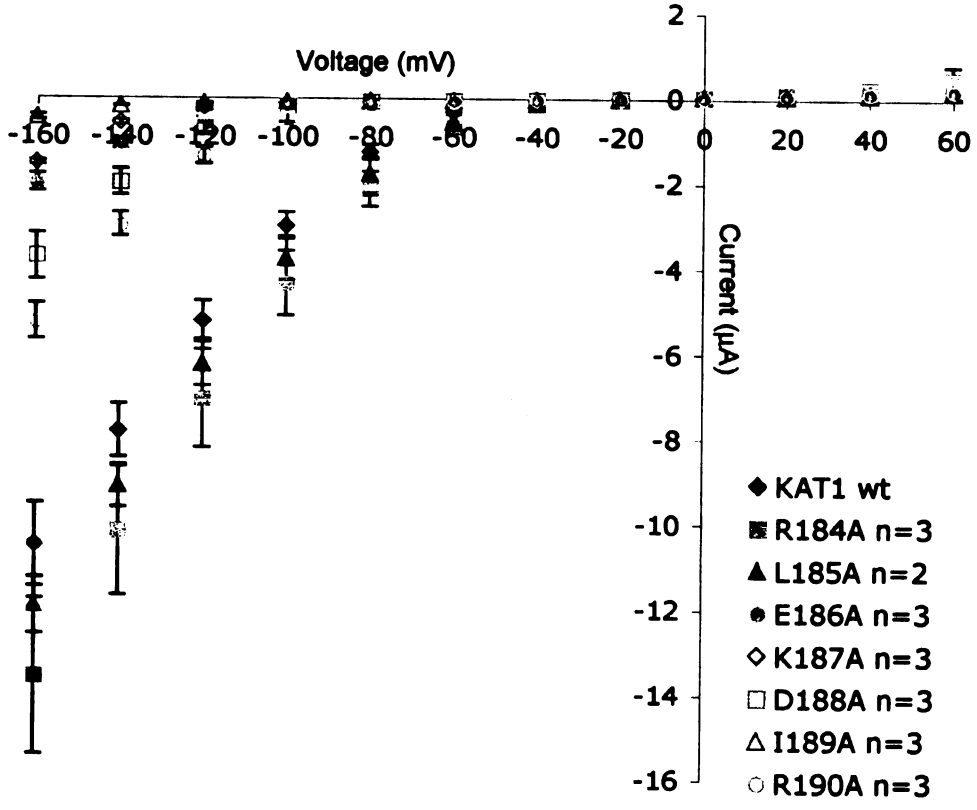

Figure 7. Currents from chimeras and mutations of KAT1 and SKOR.

All currents were recorded 1 day after injection with 5 ng RNA for each construct. Currents were elicited from +20 mV to –180 mV in 10 mV increments for 5 seconds from a holding potential of –10 mV for 600 ms and to a tail current potential of –50 mV for 1 second in the 90K(MES) recording solution: 90 mM K(MES), 1 mM $Mg(MES)_2$, 1.8 mM $Ca(MES)_2$, 10 mM HEPES, pH 7.4. (A) Alignment of the KAT1 and SKOR S4-S5 linkers. Identical residues are boxed in grey. (B) Alignment of KAT1 and SKOR around S6. Boundary of KAT1 S6 by Anderson et al. is designated by a black bar (Anderson et al., 1992). The alignment was made using the default ClustalW parameters. Identical residues are boxed in grey. Glycine residues that were tested are in orange. Mutation of KAT1 N297 to alanine (SKOR A325) is in green. The SKOR region (KGSKTER) that was replaced into KAT1 is in red. Replacement of D312 to I314 in SKOR with N284 to G286 of KAT1 tested previously (Poree et al., 2005) is in blue. (C) Currents from an oocyte expressing KAT1 wt as a positive control. (D) Sample trace of a chimera where H301 to T308 of KAT1 is replaced with K329 to R338 of SKOR. Activation and closing of the channel are slower in this chimera compared to KAT1 wt. (E) Currents elicited from the mutation N297A in KAT1. Currents are significantly reduced compared to KAT1 wt. (F) Currents elicited from the mutations G286I + T288G in KAT1 which replaces G286 of KAT1 with the Ile in SKOR and the KAT1 T288 with the Gly of SKOR, moving a putative glycine hinge in KAT1 S6 down by 2 residues. Currents are significantly reduced compared to KAT1 wt.

Figure 7. Currents from chimeras and mutations of KAT1 and SKOR.

A Alignment of KAT1 and SKOR S4-S5 region

KAT1 184 RLEKDIRFNYFWIRCTK 200
SKOR 204 KMEKDIRINYLFTRIVK 220

B Alignment of KAT1 and SKOR S6 region

KAT1
273 EMLFDIFFMMFNLGLTAYLIGNMTNLVVHWTSRTRTFRD 311
301 EMIFAMVYISFDMILGAYLIGNMTALIVKG-SKTERFRD 338
SKOR

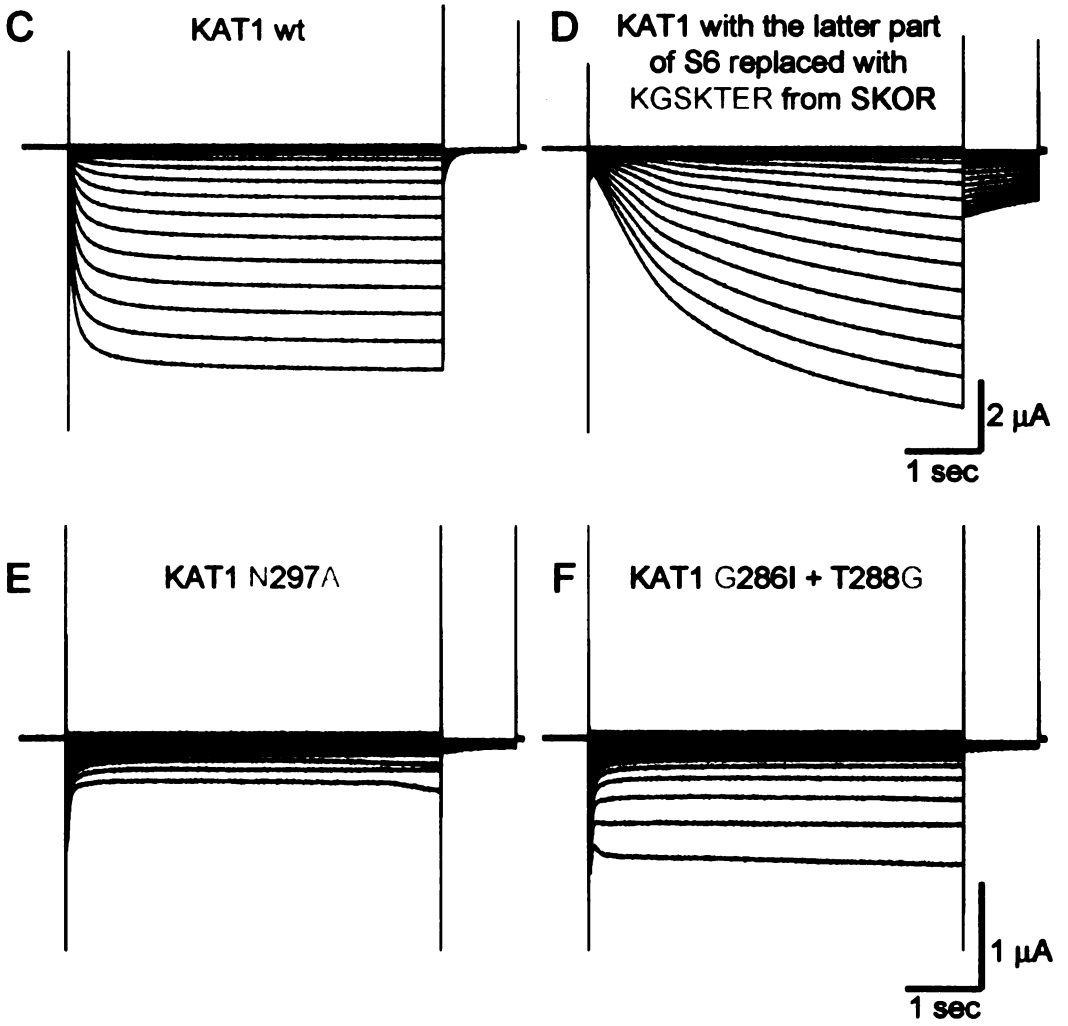

Figure 8. An endogenous outwardly rectifying current in *Xenopus* oocytes is significantly activated at potentials more positive than +50 mV.

(A) Sample traces of a 50 nL water injected oocyte (left) and an oocyte injected with 5 ng of KAT1 chimera containing the S4-S5 linker of Shaker. Currents were recorded in 90K(MES): 90 mM K(MES), 1 mM $Mg(MES)_2$, 1.8 mM $Ca(MES)_2$, 10 mM HEPES, pH 7.4 and pulsed from –10 mV to +100 mV in 10 mV increments for 5 seconds from a holding potential of –10 mV for 600 ms and to a tail current potential of +50 mV for 1 sec. (B) Quantitation of recordings as in (A) in a current-voltage curve reveals a strong outwardly rectifying current above +50 mV. SEM and the number of oocytes recorded is given.

Figure 8. An endogenous outwardly rectifying current in *Xenopus* oocytes is significantly activated at potentials more positive than +50 mV.

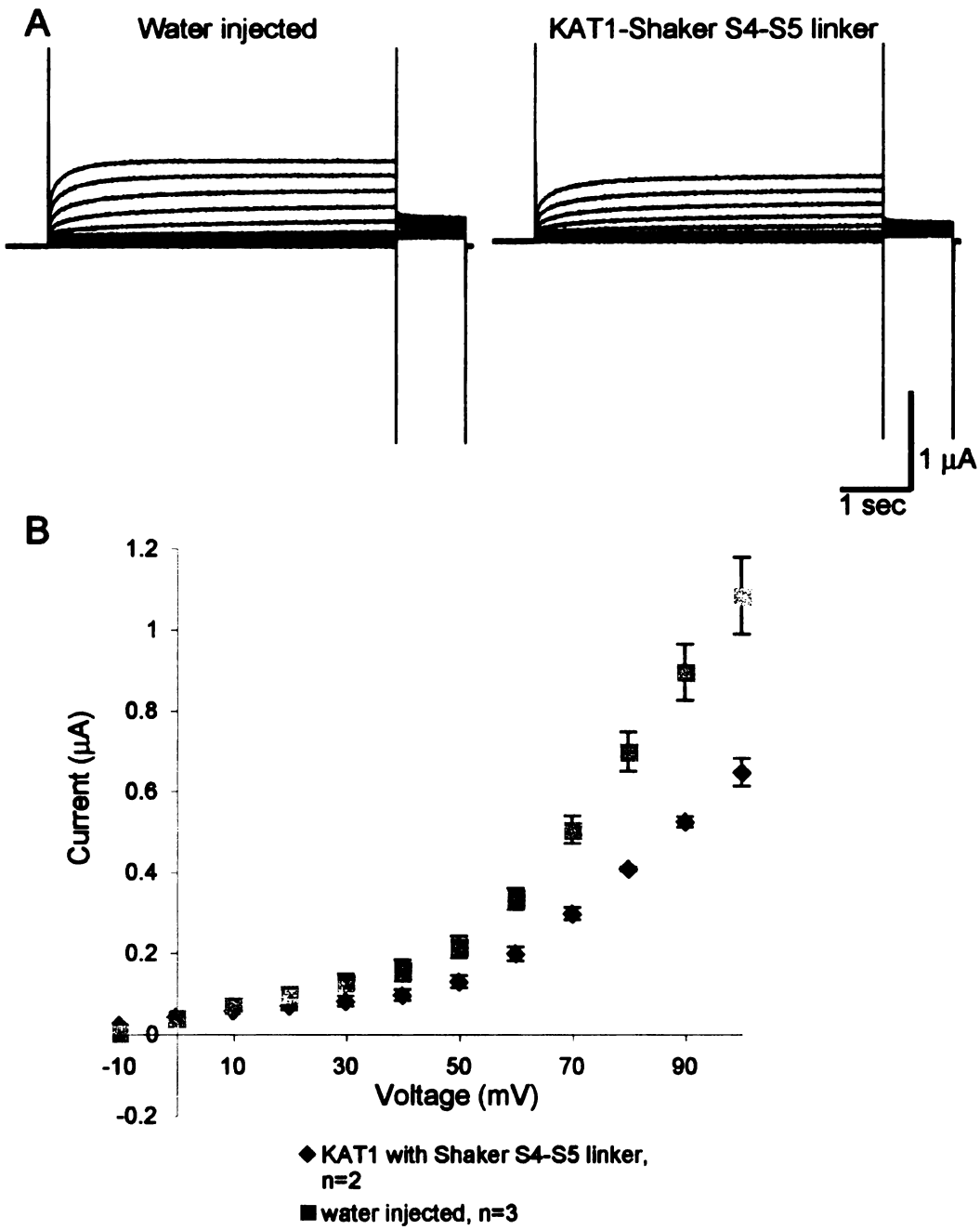

Tables

Table 1. Summary table of hinge glycine mutations made in Shaker ΔN6-46 and KAT1 and the conditions under which currents were or were not detected.

The channel, mutation, whether currents were elicited under conditions given in Figure 5, how much RNA was injected, and the number of days allowed for expression are given. Shaker ΔN6-46 G466A and G466C did not elicit currents when 0.5 ng RNA was injected, but did when 100 times more RNA (50 ng) was injected.

Table 1. Summary table of hinge glycine mutations made in Shaker ΔN6-46 and KAT1 and conditions under which currents were or were not detected.

Channel	Mutation	Currents	ng injected	Days expressed
Shaker ΔN6-46	wt	yes	0.5	1-3
Shaker ΔN6-46	G466A	no	0.5	3
Shaker ΔN6-46	G466C	no	0.5	2
Shaker ΔN6-46	G466S	no	0.5	2
Shaker ΔN6-46	G466K	no	0.5	2
Shaker ΔN6-46	G466W	no	0.5	3
Shaker ΔN6-46	G466P	no	0.5	3
Shaker ΔN6-46	G466A	yes	50	2
Shaker ΔN6-46	G466C	yes	50	2

Channel	Mutation	Currents	ng injected	Days expressed
KAT1	wt	yes	5	1-3
KAT1	G293A	no	5	3
KAT1	G293W	no	5	3
KAT1	G293P	yes	5	2

References

Anderson, J. A., Huprikar, S. S., Kochian, L. V., Lucas, W. J., and Gaber, R. F. (1992). Functional expression of a probable Arabidopsis thaliana potassium channel in Saccharomyces cerevisiae. Proc Natl Acad Sci U S A *89*, 3736-3740.

Bezanilla, F. (2002). Voltage sensor movements. J Gen Physiol *120*, 465-473.

Caprini, M., Fava, M., Valente, P., Fernandez-Ballester, G., Rapisarda, C., Ferroni, S., and Ferrer-Montiel, A. (2005). Molecular compatibility of the channel gate and the N terminus of S5 segment for voltage-gated channel activity. J Biol Chem *280*, 18253-18264.

Chen, J., Mitcheson, J. S., Tristani-Firouzi, M., Lin, M., and Sanguinetti, M. C. (2001). The S4-S5 linker couples voltage sensing and activation of pacemaker channels. Proc Natl Acad Sci U S A *98*, 11277-11282.

Creighton, T. E. (1993). Proteins: Structures and Molecular Properties, Second edn (New York, W. H. Freeman and Company).

Deber, C. M., and Li, S. C. (1995). Peptides in membranes: helicity and hydrophobicity. Biopolymers *37*, 295-318.

Decher, N., Chen, J., and Sanguinetti, M. C. (2004). Voltage-dependent gating of hyperpolarization-activated, cyclic nucleotide-gated pacemaker channels: molecular coupling between the S4-S5 and C-linkers. J Biol Chem *279*, 13859-13865.

Ding, S., Ingleby, L., Ahern, C. A., and Horn, R. (2005). Investigating the putative glycine hinge in Shaker potassium channel. J Gen Physiol *126*, 213-226.

Doyle, D. A., Morais Cabral, J., Pfuetzner, R. A., Kuo, A., Gulbis, J. M., Cohen, S. L., Chait, B. T., and MacKinnon, R. (1998). The structure of the potassium channel: molecular basis of K+ conduction and selectivity. Science *280*, 69-77.

Gandhi, C. S., and Isacoff, E. Y. (2002). Molecular models of voltage sensing. J Gen Physiol *120*, 455-463.

Gaymard, F., Pilot, G., Lacombe, B., Bouchez, D., Bruneau, D., Boucherez, J., Michaux-Ferriere, N., Thibaud, J. B., and Sentenac, H. (1998). Identification and disruption of a plant shaker-like outward channel involved in K+ release into the xylem sap. Cell *94*, 647-655.

Horn, R. (2002). Coupled movements in voltage-gated ion channels. J Gen Physiol *120*, 449-453.

Horn, R. (2004). How S4 segments move charge. Let me count the ways. J Gen Physiol *123*, 1-4.

Jiang, Y., Lee, A., Chen, J., Cadene, M., Chait, B. T., and MacKinnon, R. (2002). The open pore conformation of potassium channels. Nature *417*, 523-526.

Latorre, R., Munoz, F., Gonzalez, C., and Cosmelli, D. (2003). Structure and function of potassium channels in plants: some inferences about the molecular origin of inward rectification in KAT1 channels (Review). Mol Membr Biol *20*, 19-25.

Long, S. B., Campbell, E. B., and Mackinnon, R. (2005a). Crystal structure of a mammalian voltage-dependent Shaker family K+ channel. Science *309*, 897-903.

Long, S. B., Campbell, E. B., and Mackinnon, R. (2005b). Voltage sensor of Kv1.2: structural basis of electromechanical coupling. Science *309*, 903-908.

Lu, Z., Klem, A. M., and Ramu, Y. (2002). Coupling between voltage sensors and activation gate in voltage-gated K+ channels. J Gen Physiol *120*, 663-676.

Magidovich, E., and Yifrach, O. (2004). Conserved gating hinge in ligand- and voltage-dependent K+ channels. Biochemistry *43*, 13242-13247.

Mannikko, R., Elinder, F., and Larsson, H. P. (2002). Voltage-sensing mechanism is conserved among ion channels gated by opposite voltages. Nature *419*, 837-841.

Minor, D. L., Jr., Masseling, S. J., Jan, Y. N., and Jan, L. Y. (1999). Transmembrane structure of an inwardly rectifying potassium channel. Cell *96*, 879-891.

Mura, C. V., Cosmelli, D., Munoz, F., and Delgado, R. (2004). Orientation of Arabidopsis thaliana KAT1 channel in the plasma membrane. J Membr Biol *201*, 157-165.

Poree, F., Wulfetange, K., Naso, A., Carpaneto, A., Roller, A., Natura, G., Bertl, A., Sentenac, H., Thibaud, J. B., and Dreyer, I. (2005). Plant K(in) and K(out) channels: approaching the trait of opposite rectification by analyzing more than 250 KAT1-SKOR chimeras. Biochem Biophys Res Commun *332*, 465-473.

Sato, Y., Sakaguchi, M., Goshima, S., Nakamura, T., and Uozumi, N. (2003). Molecular dissection of the contribution of negatively and positively charged residues in S2, S3, and S4 to the final membrane topology of the voltage sensor in the K+ channel, KAT1. J Biol Chem *278*, 13227-13234.

Seoh, S. A., Sigg, D., Papazian, D. M., and Bezanilla, F. (1996). Voltage-sensing residues in the S2 and S4 segments of the Shaker K+ channel. Neuron *16*, 1159-1167.

Shealy, R. T., Murphy, A. D., Ramarathnam, R., Jakobsson, E., and Subramaniam, S. (2003). Sequence-function analysis of the K+-selective family of ion channels using a comprehensive alignment and the KcsA channel structure. Biophys J *84*, 2929-2942.

Tempel, B. L., Papazian, D. M., Schwarz, T. L., Jan, Y. N., and Jan, L. Y. (1987). Sequence of a probable potassium channel component encoded at Shaker locus of Drosophila. Science *237*, 770-775.

Tiwari-Woodruff, S. K., Schulteis, C. T., Mock, A. F., and Papazian, D. M. (1997). Electrostatic interactions between transmembrane segments mediate folding of Shaker K+ channel subunits. Biophys J *72*, 1489-1500.

Tristani-Firouzi, M., Chen, J., and Sanguinetti, M. C. (2002). Interactions between S4-S5 linker and S6 transmembrane domain modulate gating of HERG K+ channels. J Biol Chem *277*, 18994-19000.

Webster, S. M., Del Camino, D., Dekker, J. P., and Yellen, G. (2004). Intracellular gate opening in Shaker K+ channels defined by high-affinity metal bridges. Nature *428*, 864-868.

Yellen, G. (2002). The voltage-gated potassium channels and their relatives. Nature *419*, 35-42.

Yi, B. A., Lin, Y. F., Jan, Y. N., and Jan, L. Y. (2001). Yeast screen for constitutively active mutant G protein-activated potassium channels. Neuron *29*, 657-667.

Zhao, Y., Scheuer, T., and Catterall, W. A. (2004a). Reversed voltage-dependent gating of a bacterial sodium channel with proline substitutions in the S6 transmembrane segment. Proc Natl Acad Sci U S A *101*, 17873-17878.

Zhao, Y., Yarov-Yarovoy, V., Scheuer, T., and Catterall, W. A. (2004b). A gating hinge in Na+ channels; a molecular switch for electrical signaling. Neuron *41*, 859-865.

CHAPTER V

Discussion and Future Directions

Discussion and Future Directions

Since the beginning of this thesis work, many groups have used a variety of techniques to get at these same questions of K_v channel structure and gating. More definitive structural constraints were provided by the identification of residues on the extracellular side of S4 and S5 in Shaker that could be cysteine crosslinked (Broomand et al., 2003; Gandhi et al., 2003; Laine et al., 2003; Neale et al., 2003). In addition, crystal structures of two K_v channels, KvAP from archaebacteria and rat K_v1.2 (Jiang et al., 2003a; Long et al., 2005), were published. The structure of KvAP was controversial due to the proposal of a "paddle model" where the latter half of S3, S3b, and S4, form a helix-turn-helix structure that moves as a unit at the protein-lipid interface. The structural contacts proposed by this structure were not entirely consistent with the functional data performed on Shaker (Cohen et al., 2003). Further studies on KvAP, EPR studies, another crystal structure in a detergent-like lipid, and biotin-avidin binding assays of S4 from the extracellular side with different length biotin tethers, raise the possibility that the paddle model may be specific to the KvAP channel (Cuello et al., 2004; Lee et al., 2005; Ruta et al., 2005).

The K_v1.2 structure with the T1 and β2 subunits, presumably in the open state of the channel based on the open pore formation, is more consistent with the general packing arrangement determined from functional data in that S4 is closer to S5 and S1-S3 are packed around S4; however, it is difficult to determine the precise arrangement of S1-S3 around S4 since the side chains and linker regions of these segments are not well-resolved (Long et al., 2005). In

addition, the precise contacts between S4 and S5 and whether there may be lipid or water in between the two segments cannot be fully addressed for the same reason (Long et al., 2005). The general arrangement of the segments suggests that the voltage-sensor region, S1-S4, and the pore region, S5-S6 act as modular components (Long et al., 2005). The idea that the voltage-sensing region works as an independent domain is supported by the discovery of a voltage-dependent enzyme from *Ciona intestinalis* (Murata et al., 2005) that couples a transmembrane voltage-sensor domain, S1-S4, to a cytosolic enzyme.

The environment surrounding S4 is still a matter of debate since the crystal structure of KvAP, the voltage-dependent enzyme from *C. intestinalis*, and EPR studies of KvAP indicate that it is at the protein-lipid interface (Cuello et al., 2004; Jiang et al., 2003a; Murata et al., 2005). However, mutation of the arginines in Shaker S4 create a proton or cation current that flows independent of the pore region suggesting that there is a proteinaceous, water, or some combination of the two, pathway for the arginines during the gating process (Sokolov et al., 2005; Starace and Bezanilla, 2004; Tombola et al., 2005b). In addition, computer modeling of an S4 helix through a low dielectric representing the lipid bilayer found that this interaction would be energetically costly (Grabe et al., 2004).

Studies addressing the movement of S4 have also been under intense examination (Tombola et al., 2005a). For Shaker, FRET and LRET studies suggest a small movement of S4 (~2 Å) across a localized electric field (Chanda et al., 2005; Posson et al., 2005) and studies of charge movement of different

length MTS reagents also suggests a small movement of S4 (~4 Å). Biotin-avidin binding assays of KvAP suggest a larger movement of 15-20 Å (Ruta et al., 2005). As more molecular models become available in the different up and down, closed and open states of these channels, these data may be reconciled and the limitations of each technique elucidated. We may find that the data can be reconciled depending on the local protein environment or we may find that inherent errors in each measurement account for the apparent discrepancy.

Crucial to mechanistic understanding of voltage-gated ion channels is the acquisition of several structural models of different channels in different states. This will provide a framework in which to understand the precise movements of the voltage-sensor upon changes in membrane potential and exactly how the voltage-sensor couples this movement to open the pore in hyperpolarization and depolarization-activated channels. The goal of this thesis was to lend some insight into the structure and gating of K_v channels that could help address some of the issues described above. We aimed to establish a structural model of KAT1, a hyperpolarization-activated channel, using a novel genetic approach and to determine which regions of K_v channels are responsible for the gating properties of hyperpolarization and depolarization-activated channels.

In Chapter II, we used an unbiased conditional lethal/suppressor approach to screen for interactions between S5 and the voltage-sensor, S1-S4. This approach identified two highly specific interactions between S4 and S5 suggesting close apposition of these segments throughout their transmembrane region. This is consistent with evidence in Shaker where mutations in S4 can

affect cooperative interactions between the voltage-sensor and the pore region indicating intimate interaction between these two regions (Ledwell and Aldrich, 1999; Pathak et al., 2005; Smith-Maxwell et al., 1998). However, in the structures of K_v 1.2 and KvAP, S4 and S5 make few contacts in the up state of these channels (Jiang et al., 2003a; Jiang et al., 2003b; Lee et al., 2005; Long et al., 2005). As work in this field progresses, we will be able to determine whether these differences are due to experimental conditions or reflect differences in the states of S4 (up and down). This work validates the yeast screening as a method that can give structural information and lays the groundwork for the work in Chapter III.

In Chapter III, we continued the screening process finding more conditional lethals and screened these against mutagenized segments of the channel for more interaction sets. Six new sets were identified and using six of the eight total identified interaction sets, a model of KAT1 in the down state was determined. An interaction network of residues suggests that S1, S2, S4, and S5 are closely packed for KAT1 in the down state; S4 packs against two S5 segments of adjacent subunits of the pore domain, and S1 and S2 are packed against S4. Interestingly, one study based on cysteine crosslinking in different states of Shaker has suggested that S4 contacts two subunits in the down state and makes contacts with just one subunit in the up state (Elliott et al., 2004). In the KAT1 model, we find that S4 may interact with S5 of two subunits in the down state and based on the K_v1.2 structure, it may then interact with S5 of the neighboring subunit in the up state. While the specifics of which subunit S4

interacts with in the up state are different, the general idea that S4 may switch subunits during the gating process is consistent with Elliott et al. Interpolation of the KAT1 down state model to a model of KAT1 on $K_v1.2$ suggests there is a fair amount of movement of the voltage-sensor; at least that S4 may transit the membrane outer leaflet as previously suggested (Phillips et al., 2005). We must be careful when comparing these models since KAT1 is a hyperpolarization-activated channel and $K_v1.2$ is a depolarization-activated channel, but given the similar movement of S4 determined from the gating currents and cysteine-accessibility studies (Aggarwal and MacKinnon, 1996; Broomand et al., 2003; Larsson et al., 1996; Latorre et al., 2003), this is the simplest interpretation for now. Further experimental and computational testing will help reinforce the reliability of the KAT1 model (see Chapter III).

It is important for this work to evaluate the extent to which the conditional lethal/suppressor mutations are directly interacting. Disulfide crosslinking experiments were attempted to address this concern with little success (see Appendix 2, Part 2). One way to further corroborate the extent of these interactions is to create models using these interactions as restraints and through iterative cycles of computational model building and experimental testing verify the consistency of the mutations involved in either the yeast functional assay or by electrophysiological recording in oocytes. The experiments can be used to either test direct interactions in the models or to test how well a model predicts the gating charge-voltage or current-voltage relationship. Another approach would be to obtain a high resolution crystal structure of KAT1 in the down state.

Both approaches are technically challenging. The disulfide crosslinking between putatively interacting residues may be limited to residues near the extracellular side since it seems to be difficult to create oxidizing conditions within the membrane necessary for thiol reactivity (Mordoch et al., 1999). As for obtaining a crystal structure, only recently have the techniques matured enough to make this approach more feasible for membrane proteins. At the beginning of this thesis work, all the crystal structures of membrane proteins were from native sources. Now, development of heterologous expression systems that generate membrane proteins in large quantities, notably the *Pichia pastoris* expression system (Macauley-Patrick et al., 2005) and work in this area indicating the need to crystallize these proteins with lipids that form bilayers (Lee et al., 2005; Long et al., 2005) have made crystallization of membrane proteins more tractable. In addition, during the process of identifying conditional lethal mutations, one mutant, R177E, was found to be open at all potentials suggesting it is locked in an open state (see Appendix 2, Part 3). A crystal structure of KAT1 wildtype in the down state of S4 and R177E in the up state of S4 are goals currently being pursued in the Jan lab.

In addition, we argue for the proximity of the interaction based on the specificity of the interaction sets. The converse of this hypothesis is evidenced by the finding of suppressor mutations that suppress multiple conditional lethal mutations and are thus non-specific and likely not to be closely interacting (Lai et al., 2005). We can further test this idea by taking suppressor mutations we believe to be non-interacting and testing all possible mutations at the suppressor

site. If our hypothesis is true, suppressor mutations that can suppress multiple conditional lethal mutations should have a variety of residues at the suppressor site suggesting its non-specificity. An initial evaluation of this is currently underway in the Jan lab.

It is also important for this work to determine which state (presumably the down state) of KAT1 we are truly evaluating. As for interpreting precisely which state we are assaying, burst analysis of single channel recordings and accurate conductance-voltage relationships for the conditional lethal/suppressor sets compared to wildtype will be necessary to know if the mutations destabilize or stabilize various closed or open states. Acquiring single channel recordings of KAT1 is also technically challenging. KAT1 has been recorded in the cell-attached and inside-out patch configurations. KAT1 has a small single channel conductance, ~7.5 pS, and experiences rundown although this can be reversed by internal application of ATP (Hoshi, 1995; Zei and Aldrich, 1998). Six times more RNA was necessary to produce detectable macroscopic currents of the KAT1 mutants and it is unknown whether this is due to a decrease in single channel conductance, open probability, or the number of channels at the surface of the membrane. Single channel recordings will help address the former two possibilities and quantification of the channel surface expression will address the latter. These recordings may also give accurate conductance-voltage curves that we were unable to produce in intact oocytes since it was necessary to pulse to voltages more negative than –180 mV to obtain these curves. In addition, recording in yeast might be a possibility to assess the channel function in the

system in which we are analyzing it, but again this is technically challenging (Bertl et al., 1995). Nonetheless, recordings of these mutant channels may be useful for further interpretation of the KAT1 models.

Chapter IV is a set of experiments aimed at determining which channel regions, S4-S5 or S6, are responsible for the voltage-dependence of hyperpolarization and depolarization-activated channels. An alanine scan of the KAT1 S4-S5 linker identified E186, K187, D188, I189, and R190 as being important for gating. Previous studies in HERG and HCN have indicated that the S4-S5 linker and the bottom half of S6 interact electrostatically (Chen et al., 2001; Tristani-Firouzi et al., 2002). The distribution of charges at the end of S6 in SKOR is different from that in KAT1 while their S4-S5 linkers are highly homologous. This suggests that differences near the end of S6 might be responsible for the difference in voltage-dependence of these channels. While chimeras were made in an attempt to validate this hypothesis, the results of these were inconclusive and more chimeras between KAT1 and SKOR may prove helpful in addressing this question. In particular, a chimera of the SKOR A305 to I327 entirely replacing the KAT1 S6 would be an appropriate starting point. If this chimera switched KAT1 to a depolarization-activated channel, the particular region involved in determining this voltage-dependence could be narrowed down from there.

In addition, mutations of the glycine hinge in Shaker and KAT1 and moving the glycine in KAT1 to the position in SKOR were made in an attempt to evaluate the hinge position and coupling gating models predictions of voltage-

dependent gating. These experiments were inconclusive with some support for the coupling gating model over the hinge position gating model (see Chapter IV). Overexpression of mutations in Shaker, G466A and G466C, resulted in outwardly rectifying currents and should be retested since they were not seen by other groups under the same conditions (Magidovich and Yifrach, 2004). However, if our results prove to be accurate, this suggests that Shaker has other hinging points besides glycine 466, either glycine 459 or the PVP motif seven residues downstream of G466, as suggested by other groups (Webster et al., 2004). Furthermore, a glycine or proline scan of KAT1 S6 might lend insight into the property of hyperpolarization-activation much as a proline scan of NaChBac gave mutants that switched this channel from a depolarization to a hyperpolarization-activated channel (Zhao et al., 2004).

The appendices are a compilation of the work presented in the main text of the thesis as well as a set of experiments that led to interesting or negative results that may prove useful for future work on KAT1, Kir 3.2, and membrane proteins in general.

The work described in this thesis sets the foundation toward understanding how voltage-gated channels respond differently to depolarization and hyperpolarization. The structural model of KAT1, the down state of a hyperpolarization-activated channel, is a significant contribution toward the structural and mechanistic understanding of these channels. In addition, it improves our understanding of how the voltage-sensor moves between the up

and down states in a dynamic sense and will contribute to our understanding of how mutations in the S4-S5 loop and S6 affect gating.

This body of work probing the structure of K_v channels has left us with as many questions as answers at this juncture. How intimate are the contacts between S4 and S5? Are they different for channels from different species or are they different for different types of voltage-gated channels (depolarization or hyperpolarization activated)? How does the channel move as it goes through the gating transition? What contacts does it make during this process and how far a distance does it move? These questions are very difficult to answer with the current techniques available since we are asking for a structural framework of a very dynamic process (gating) for a membrane protein. More studies on different types of channels from different species using all the techniques available to us: spectroscopy, mutagenesis, electrophysiology, crystallography, computation, binding studies, and cysteine accessibility, are needed to fully address these questions. As work in the field continues, people will come up with new and creative ways using these same approaches to help answer these questions. Certainly, both structural and functional data will be needed to address the mechanism of voltage-gating.

References

Aggarwal, S. K., and MacKinnon, R. (1996). Contribution of the S4 segment to gating charge in the Shaker K+ channel. Neuron *16*, 1169-1177.

Bertl, A., Anderson, J. A., Slayman, C. L., and Gaber, R. F. (1995). Use of Saccharomyces cerevisiae for patch-clamp analysis of heterologous membrane proteins: characterization of Kat1, an inward-rectifying K+ channel from Arabidopsis thaliana, and comparison with endogeneous yeast channels and carriers. Proc Natl Acad Sci U S A *92*, 2701-2705.

Broomand, A., Mannikko, R., Larsson, H. P., and Elinder, F. (2003). Molecular movement of the voltage sensor in a K channel. J Gen Physiol *122*, 741-748.

Chanda, B., Asamoah, O. K., Blunck, R., Roux, B., and Bezanilla, F. (2005). Gating charge displacement in voltage-gated ion channels involves limited transmembrane movement. Nature *436*, 852-856.

Chen, J., Mitcheson, J. S., Tristani-Firouzi, M., Lin, M., and Sanguinetti, M. C. (2001). The S4-S5 linker couples voltage sensing and activation of pacemaker channels. Proc Natl Acad Sci U S A *98*, 11277-11282.

Cohen, B. E., Grabe, M., and Jan, L. Y. (2003). Answers and questions from the KvAP structures. Neuron *39*, 395-400.

Cuello, L. G., Cortes, D. M., and Perozo, E. (2004). Molecular architecture of the KvAP voltage-dependent K+ channel in a lipid bilayer. Science *306*, 491-495.

Elliott, D. J., Neale, E. J., Aziz, Q., Dunham, J. P., Munsey, T. S., Hunter, M., and Sivaprasadarao, A. (2004). Molecular mechanism of voltage sensor movements in a potassium channel. Embo J *23*, 4717-4726.

Gandhi, C. S., Clark, E., Loots, E., Pralle, A., and Isacoff, E. Y. (2003). The orientation and molecular movement of a k(+) channel voltage-sensing domain. Neuron *40*, 515-525.

Grabe, M., Lecar, H., Jan, Y. N., and Jan, L. Y. (2004). A quantitative assessment of models for voltage-dependent gating of ion channels. Proc Natl Acad Sci U S A *In press*.

Hoshi, T. (1995). Regulation of voltage dependence of the KAT1 channel by intracellular factors. J Gen Physiol *105*, 309-328.

Jiang, Y., Lee, A., Chen, J., Ruta, V., Cadene, M., Chait, B. T., and MacKinnon, R. (2003a). X-ray structure of a voltage-dependent K+ channel. Nature *423*, 33-41.

Jiang, Y., Ruta, V., Chen, J., Lee, A., and MacKinnon, R. (2003b). The principle of gating charge movement in a voltage-dependent K+ channel. Nature *423*, 42-48.

Lai, H. C., Grabe, M., Jan, Y. N., and Jan, L. Y. (2005). The S4 voltage sensor packs against the pore domain in the KAT1 voltage-gated potassium channel. Neuron *47*, 395-406.

Laine, M., Lin, M. C., Bannister, J. P., Silverman, W. R., Mock, A. F., Roux, B., and Papazian, D. M. (2003). Atomic proximity between S4 segment and pore domain in Shaker potassium channels. Neuron *39*, 467-481.

Larsson, H. P., Baker, O. S., Dhillon, D. S., and Isacoff, E. Y. (1996). Transmembrane movement of the shaker K+ channel S4. Neuron *16*, 387-397.

Latorre, R., Olcese, R., Basso, C., Gonzalez, C., Munoz, F., Cosmelli, D., and Alvarez, O. (2003). Molecular coupling between voltage sensor and pore opening in the Arabidopsis inward rectifier K+ channel KAT1. J Gen Physiol *122*, 459-469.

Ledwell, J. L., and Aldrich, R. W. (1999). Mutations in the S4 region isolate the final voltage-dependent cooperative step in potassium channel activation. J Gen Physiol *113*, 389-414.

Lee, S. Y., Lee, A., Chen, J., and Mackinnon, R. (2005). Structure of the KvAP voltage-dependent K+ channel and its dependence on the lipid membrane. Proc Natl Acad Sci U S A *102*, 15441-15446.

Long, S. B., Campbell, E. B., and Mackinnon, R. (2005). Crystal structure of a mammalian voltage-dependent Shaker family K+ channel. Science *309*, 897-903.

Macauley-Patrick, S., Fazenda, M. L., McNeil, B., and Harvey, L. M. (2005). Heterologous protein production using the Pichia pastoris expression system. Yeast *22*, 249-270.

Magidovich, E., and Yifrach, O. (2004). Conserved gating hinge in ligand- and voltage-dependent K+ channels. Biochemistry *43*, 13242-13247.

Mordoch, S. S., Granot, D., Lebendiker, M., and Schuldiner, S. (1999). Scanning cysteine accessibility of EmrE, an H+-coupled multidrug transporter from Escherichia coli, reveals a hydrophobic pathway for solutes. J Biol Chem *274*, 19480-19486.

Murata, Y., Iwasaki, H., Sasaki, M., Inaba, K., and Okamura, Y. (2005). Phosphoinositide phosphatase activity coupled to an intrinsic voltage sensor. Nature *435*, 1239-1243.

Neale, E. J., Elliott, D. J., Hunter, M., and Sivaprasadarao, A. (2003). Evidence for intersubunit interactions between S4 and S5 transmembrane segments of the Shaker potassium channel. J Biol Chem *278*, 29079-29085.

Pathak, M., Kurtz, L., Tombola, F., and Isacoff, E. (2005). The cooperative voltage sensor motion that gates a potassium channel. J Gen Physiol *125*, 57-69.

Phillips, L. R., Milescu, M., Li-Smerin, Y., Mindell, J. A., Kim, J. I., and Swartz, K. J. (2005). Voltage-sensor activation with a tarantula toxin as cargo. Nature *436*, 857-860.

Posson, D. J., Ge, P., Miller, C., Bezanilla, F., and Selvin, P. R. (2005). Small vertical movement of a K+ channel voltage sensor measured with luminescence energy transfer. Nature *436*, 848-851.

Ruta, V., Chen, J., and Mackinnon, R. (2005). Calibrated Measurement of Gating-Charge Arginine Displacement in the KvAP Voltage-Dependent K(+) Channel. Cell *123*, 463-475.

Smith-Maxwell, C. J., Ledwell, J. L., and Aldrich, R. W. (1998). Uncharged S4 residues and cooperativity in voltage-dependent potassium channel activation. J Gen Physiol *111*, 421-439.

Sokolov, S., Scheuer, T., and Catterall, W. A. (2005). Ion permeation through a voltage- sensitive gating pore in brain sodium channels having voltage sensor mutations. Neuron *47*, 183-189.

Starace, D. M., and Bezanilla, F. (2004). A proton pore in a potassium channel voltage sensor reveals a focused electric field. Nature *427*, 548-553.

Tombola, F., Pathak, M., and Isacoff, E. (2005a). How Far Will You Go to Sense Voltage? Neuron *48*, 719-725.

Tombola, F., Pathak, M. M., and Isacoff, E. Y. (2005b). Voltage-sensing arginines in a potassium channel permeate and occlude cation-selective pores. Neuron *45*, 379-388.

Tristani-Firouzi, M., Chen, J., and Sanguinetti, M. C. (2002). Interactions between S4-S5 linker and S6 transmembrane domain modulate gating of HERG K+ channels. J Biol Chem *277*, 18994-19000.

Webster, S. M., Del Camino, D., Dekker, J. P., and Yellen, G. (2004). Intracellular gate opening in Shaker K+ channels defined by high-affinity metal bridges. Nature *428*, 864-868.

Zei, P. C., and Aldrich, R. W. (1998). Voltage-dependent gating of single wild-type and S4 mutant KAT1 inward rectifier potassium channels. J Gen Physiol *112*, 679-713.

Zhao, Y., Scheuer, T., and Catterall, W. A. (2004). Reversed voltage-dependent gating of a bacterial sodium channel with proline substitutions in the S6 transmembrane segment. Proc Natl Acad Sci U S A *101*, 17873-17878.

APPENDIX 1

Tables of KAT1 screens, mutations, rescues, chimeras, and tags

Appendix 1

Appendix 1 is a set of Tables summarizing the data from the KAT1 screens, mutations, rescues, chimeras and tags.

Table 1. Summary of all the screens of randomized regions against different conditional lethals.

The putative transmembrane region, the conditional lethal, library complexity, number of yeast colonies screened, the estimated percent rescue, the percent amino acid changes in the unselected library, the percent base pair changes in the unselected library, and the specific second-site suppressor mutation are given. Conditional lethal mutations are in red and specific second-site suppressor mutations in blue. A summary of the screens of conditional lethals with randomized regions of S1-S3 (A), S4 (B), and S2-S4 (C) are shown. In (D), a summary of the screens for a second-site suppressor of a particular conditional lethal at a specific site is shown.

Table 1. Summary of all the screens of randomized regions against different conditional lethals.

(A) S1-S3 screens

Putative TM region of Conditional Lethal	*Conditional Lethal*	*Library Complexity*	*# Screened*	*Estimated % Rescue*	*% Unselected AA changes*	*% Unselected b.p. changes*	*Specific suppressor*
None	None	5.7×10^3	2916	11.00	6.9	3.3	n/a
S4	R171E	1.5×10^5	9279	1.70	4.3-6	2.2-3	C77R
S4	R174E	1.2×10^4	10206	0.27	6-6.3	3.0	Y86H + D89G
S4	L175N	9.4×10^3	2067	0.01	6.0	3.0	None
S4	L175H	1.6×10^4	1474	0.00	6.0	3.0	None
S4	L175P	1.1×10^4	1714	0.00	6.0	3.0	None
S4	V178N	1.7×10^4	1948	0.20	6.0	3.0	None
S5	Y193E	5.9×10^5	3144	0.25	4.7	2.4	None
S5	R197E	6.0×10^4	8500	0.31	4.7	2.4	None
S5	V204E	5.8×10^4	5796	0.50	4.7	2.4	None
S5	F207D	1.8×10^4	2724	0.00	6.0	3.0	None
S5	F207K	1.0×10^3	531	0.00	6.0	3.0	None
S5	F207R	1.7×10^4	2508	0.00	6.0	3.0	None
S5	H210E	1.2×10^5	6757	0.18	4.6-4.7	2.1-2.4	None
S5	F215R	5.2×10^3	1991	0.00	6.0	3.0	None
S6	N284K	3.1×10^3	1720	0.00	6.0	3.0	None
S6	N284R	4.2×10^3	1578	0.00	6.0	3.0	None

(B) S4 screen

Putative TM region of Conditional Lethal	*Conditional Lethal*	*Library Complexity*	*# Screened*	*Estimated % Rescue*	*% Unselected AA changes*	*% Unselected b.p. changes*	*Specific suppressor*
None	None	8.8×10^4	12000	46.00	5.3	3.0	n/a
S2	D141N	4.0×10^4	3700	0.00	4.7	2.3	None
S5	Y193E	4.4×10^4	3083	0.13	5.3	3.0	None
S5	R197Q	1.7×10^4	7748	0.15	5.3	3.0	None
S5	V204E	1.0×10^4	8988	2.10	5.3	3.0	S179N
S5	F207D	1.2×10^3	1007	0.00	5.8	3.1	None
S5	F207K	1.4×10^3	873	0.00	5.8	3.1	None
S5	F207R	8.0×10^2	876	0.00	5.8	3.1	None
S5	H210E	2.1×10^4	6840	1.10	5.3	3.0	M169L
S5	F215R	5.2×10^3	4536	0.00	5.8-7.7	3.1-3.5	None
S6	N284K	1.0×10^4	2715	0.00	5.8	3.1	None
S6	N284R	1.5×10^4	2231	0.00	5.8-7.7	3.1-3.5	None
S6	N284P	1.0×10^2	548	0.00	7.7	3.5	None

Table 1 (continued).

(C) S2-S4 screen

Putative TM region of Conditional Lethal	Conditional Lethal	Library Complexity	# Screened	Estimated % Rescue	% Unselected AA changes	% Unselected b.p. changes	Specific suppressor
S1	W75E + I94V	8.4×10^4	2620	0.30	5.2	2.6	N99D, L115P
S1	W75D + I94V	4.2×10^3	3646	0.10	5.2	2.6	M169L + I94V
S1	W75K + I94V	1.7×10^3	1777	0.00	5.2	2.6	None
S1	W75R + I94V	3.6×10^3	2697	0.00	5.2	2.6	None

(D) Screens against a specific amino acid

Putative TM region of Conditional Lethal	Conditional Lethal	Library Complexity	# Screened	Estimated % Rescue	Site of Random Mutation	Putative TM region of Site of Random Mutation	Specific suppressor
S4	R171E	149	1024	7.60	C77X	S1	C77R
S4	R171D	228	2143	17.00	C77X	S1	C77R
S5	V204E	272	1040	5.70	S179X	S4	S179N
S5	V204D	2904	2361	0.00	S179X	S4	None
S5	H210E	288	958	14.00	M169X	S4	M169L
S5	H210D	609	2113	6.40	M169X	S4	M169L
S4	L175N	960	353	0.00	V204X	S5	None
S4	L175N	1287	133	0.00	F207X	S5	None
S4	L175N	1008	176	0.00	H210X	S5	None
S5	V204E	1035	2481	0.00	R165X	S4	None
S5	V204E	1364	5223	0.00	L172X	S4	None
S5	H210E	128	2405	0.25	R165X	S4	R165K
S5	H210E	59	658	0.00	L172X	S4	None
S6	F283P	638	532	0.00	R165X	S4	None
S6	N284K	842	1114	0.00	M169X	S4	None
S6	N284K	1300	557	0.00	L172X	S4	None
S6	N284P	200	91	0.00	M169X	S4	None
S6	N284P	768	458	0.00	L172X	S4	None
S6	N284R	133	13*	0.00	M169X	S4	None

Table 2. Summary of mutations made in KAT1 and their phenotype in the K^+ transporter deficient yeast strain.

Conditions tested are 100 mM K^+ plates, 2 mM K^+, and/or 0.4 mM K^+ plates. + indicates yeast growth, +/- indicates moderate growth, - indicates no growth, and -* indicates decreased growth on 100 mM K^+ plates with "fast" and "slow" growing colonies (see Appendix 2, Part 4). Conditional lethal mutations are in red and specific second-site suppressor mutations are in blue. Conditions not tested are blocked out in grey. Mutations for the same residue are boxed in dark lines. Transmembrane regions are separated by a double line.

Table 2. Summary of mutations made in KAT1 and their phenotype in the K^+ transporter deficient yeast strain.

Putative TM region	*Mutation(s)*	*100 mM K+*	*2 mM K+*	*0.4 mM K+*
	wt	+	+	+
S1	C77R	-*		n/a
S1	Y72F + I94V	+		+
S1	Y72L + I94V	+		+
S1	Y72I + I94V	+		+
S1	Y72M + I94V	+		+
S1	Y72V + I94V	+		+
S1	Y72S + I94V	+		+
S1	Y72P + I94V	-*		n/a
S1	Y72T + I94V	+		+
S1	Y72A + I94V	+		+
S1	Y72H + I94V	+		+
S1	Y72Q + I94V	+		+
S1	Y72N + I94V	+		+
S1	Y72K + I94V	+		+
S1	Y72D + I94V	+		+
S1	Y72E + I94V	+		+
S1	Y72C + I94V	+		+
S1	Y72R + I94V	+		+
S1	Y72G + I94V	+		+
S1	Y72W + I94V	+		+
S1	W75F + I94V	+		+
S1	W75L + I94V	+		+
S1	W75I + I94V	+		+
S1	W75M + I94V	+		+
S1	W75V + I94V	+		+
S1	W75S + I94V	+		+
S1	W75P + I94V	+		+
S1	W75T + I94V	+		+
S1	W75A + I94V	+		+
S1	W75Y + I94V	+		+
S1	W75H + I94V	+		+
S1	W75Q + I94V	+		+
S1	W75N + I94V	+		+
S1	W75K + I94V	+		-
S1	W75D + I94V	+		-
S1	W75E + I94V	+		-
S1	W75C + I94V	+		+
S1	W75R + I94V	+		-
S1	W75G + I94V	+		+
S1	W75E	+		+
S1	W75D	+		-
S1	W75K	+		-
S1	W75R	+		-
S1	W75E + N99D	+		+
S1	W75E + L115P	+		+
S1	W75E + M169L	+		+
S1	I84V	+		+
S1	T85A	+		+
S1	Y86H	+		+

Table 2 (continued)

Putative TM region	Mutation(s)	100 mM K+	2 mM K+	0.4 mM K+
S1-S2	K87E	+	+	+
S1-S2	K88N	+		+
S1-S2	D89G	+		+
S1	I84V + T85A	+		+
S1	I84V + Y86H	+		+
S1,S1-S2	I84V + D89G	+		+
S1	T85A + Y86H	+		+
S1,S1-S2	T85A + D89G	+		+
S1,S1-S2	Y86H + D89G	+/-		+
S1,S1-S2	I84V + T85A + D89G	+		+
S1,S1-S2	I84V + Y86H + D89G	+		+
S1,S1-S2	T85A + Y86H + D89G	-*		n/a
S1	I84V + T85A + Y86H	+		+
S1,S1-S2	I84V + T85A + Y86H + D89G	-*		n/a
S2	I94V	+		+
S2	D95N	+	+	+
S2	N99D	+		+
S2	D105N	+	+	+
S2	L115P	+		+
S2	L115R	+	+	+
S2-S3	Y120H	+	+	+
S3	F138L	+		+
S3	D141N	+	-	-

Table 2 (continued)

Putative TM region	Mutation(s)	100 mM K+	2 mM K+	0.4 mM K+
S4	R165K	+		+
S4	L167N	+		+
S4	L167G	+		+
S4	M169L	+	+	+
S4	M169T	+	+	+
S4	L170P	+		+
S4	L170S	+		+
S4	L170E	+	+	+
S4	R171L	+	+	+
S4	R171E	+	-	-
S4	R171D	+	-	+
S4	W173A	+	+	+
S4	W173Y	+		+
S4	W173S	+		+
S4	R174E	+	-	-
S4	R174D	+	-	-
S4	L175A	+	+	+
S4	L175F	+		+
S4	L175S	+		+
S4	L175H	+		-
S4	L175N	+		-
S4	L175P	+		-
S4	R176E	+	+	+
S4	R176D	+		+
S4	R176N	+		+
S4	**R177E**	+	+	+
S4	R177F	+		+
S4	R177K	+		+
S4	V178L	+		+
S4	V178T	+		+
S4	V178F	+		+
S4	V178N	+		-
S4	S179N	+	+	+
S4	S179Q	+	+	+
S4	F182E	+	+	+
S4	R184A	+	+	+
S4-S5	L185A	+	+	+
S4-S5	E186A	+	+	+
S4-S5	K187A	+	+	+
S4-S5	D188A	+	+	+
S4-S5	I189A	+	+	+
S4-S5	R190A	+	+	+

Table 2 (continued)

Putative TM region	Mutation(s)	100 mM K+	2 mM K+	0.4 mM K+
S5	Y193E	+	+/-	-
S5	R197E	+	+	-
S5	R197Q	+	+	-
S5	L201E	+	+	+
S5	V204E	+	+	-
S5	V204D	+	+	-
S5	F207E	+	+	+
S5	F207A	+		+
S5	F207D	+		-
S5	F207G	+		+
S5	F207K	+		-
S5	F207P	+		-
S5	F207R	+		-
S5	F207V	+		+
S5	I209G	+		+
S5	I209L	+		+
S5	I209P	+		+
S5	I209T	+		+
S5	H210E	+	+	-
S5	H210D	+	+	-
S5	A212P	+		-
S5	A212F	+		+
S5	A212K	+		-
S5	A212V	+		+
S5	F215L	+		+
S5	F215S	+		+
S5	F215G	+		+
S5	F215V	+		+
S5	F215K	+		+
S5	F215P	+		-
S5	F215A	+		+
S5	F215R	+		-

Table 2 (continued)

Putative TM region	*Mutation(s)*	*100 mM K+*	*2 mM K+*	*0.4 mM K+*
S6	F283P	+		-
S6	F283A	+		+
S6	F283C	+		+
S6	F283D	+		+
S6	F283E	+		+
S6	F283L	+		+
S6	F283S	+		+
S6	F283T	+		+
S6	F283V	+		+
S6	N284K	+		-
S6	N284R	+		-
S6	N284P	+		-
S6	N284H	+		-
S6	N284A	+		+
S6	N284C	+		+
S6	N284D	+		+
S6	N284F	+		+
S6	N284G	+		+
S6	N284I	+		+
S6	N284L	+		+
S6	N284Q	+		+
S6	N284S	+		+
S6	N284T	+		+
S6	L287F	+		+
S6	L287V	+		+
S6	L287S	+		+
S6	L287E	+		+
S6	N297A	+		+

Table 3. Summary of suppressor and conditional lethal mutants and their phenotype in the K^+ transporter deficient yeast strain.

Conditions tested are 100 mM K^+ and 0.4 mM K^+ plates. + indicates growth, +/- indicates moderate growth, - indicates no growth, and -* indicates decreased growth on 100 mM K^+ plates with "fast" and "slow" growing colonies (see Appendix 2, Part 4). Conditional lethal mutations are in red and specific second-site suppressor mutations are in blue. Evaluation of different sets of screens are separated by a double line.

Table 3. Summary of suppressor and conditional lethal mutants and their phenotype in the K^+ transporter deficient yeast strain.

Putative TM Region	*Mutation*	*100 mM K+*	*0.4 mM K+*
S1 + S2	W75E +I94V + N99D	+	+
S1 + S2	W75D+ N99D	+	+
S1 + S2	W75D + I94V + N99D	+	+
S1 + S2	W75K+ N99D	+	+
S1 + S2	W75R+ N99D	+	-
S1 + S2	W75E + I94V + L115P	+	+
S1 + S2	W75D+ L115P	+	+
S1 + S2	W75D + I94V + L115P	+	+
S1 + S2	W75K+ L115P	+	+
S1 + S2	W75R+ L115P	+	-
S1 + S2	W75E + I94V + M169L	+	+
S1 + S2	W75D+ M169L	+	-
S1 + S2	W75D + I94V + M169L	+	+
S1 + S2	W75K+ M169L	+	+
S1 + S2	W75R+ M169L	+	-
S2 + S4	N99D + R171E	+	-
S2 + S5	N99D + H210E	+	-
S2 + S4	L115P + R171E	+	-
S2 + S5	L115P + H210E	+	-
S4 + S5	M169L + F207K	+	-

Table 3 (continued).

Putative TM Region	*Mutation*	*100 mM K+*	*0.4 mM K+*
S1 + S4	I84V + R174E	+	-
S1 + S4	T85A + R174E	+	-
S1 + S4	Y86H + R174E	+	-
S1-S2 + S4	K87E + R174E	+	-
S1-S2 + S4	D89G + R174E	+	-
S2 + S4	L115R + R174E	+	-
S2-S3 + S4	Y120H + R174E	+	-
S3 + S4	F138L + R174E	+	-
S1 + S4	I84V + T85A + R174E	+	-
S1 +S4	I84V + Y86H + R174E	+	-
S1,S1-S2 + S4	I84V + D89G + R174E	+	-
S1 + S4	T85A + Y86H + R174E	+	+/-
S1 + S4	T85A + Y86H + R174D	+	-
S1,S1-S2 + S4	T85A + D89G + R174E	+	-
S1,S1-S2 + S4	Y86H + D89G + R174E	+	+
S1,S1-S2 + S4	Y86H + D89G + R174D	+	-
S1,S1-S2 + S4	Y86H + D89G + R171E	+	-
S1,S1-S2 + S4	I84V + T85A + D89G + R174E	+	-
S1,S1-S2 + S4	I84V + Y86H + D89G + R174E	+	+
S1,S1-S2 + S4	I84V + Y86H + D89G + R174D	+	+/-
S1 + S4	I84V + T85A + Y86H + R174E	+	+/-
S1 + S4	I84V + T85A + Y86H + R174D	+	-
S1,S1-S2 + S4	T85A + Y86H + D89G + R174E	+	+
S1,S1-S2 + S4	T85A + Y86H + D89G + R174D	+	-
S1,S1-S2 + S4	I84V + T85A + Y86H + D89G + R174E	+	+
S1,S1-S2 + S4	I84V + T85A + Y86H + D89G + R174D	+	+/-
S1,S2-S3,S3 + S4	T85A + Y120H + S135T + R174E	+	+
pre-S1, S1-S2, S2-S3,S3-S4 + S4	A61V + K87E + Y120H + Q149L + R174E	+	+
S1,S2 + S4	V67A + T85A + L115R + R174E	+	+
S1 + S4	C77R + R171E	+	+
S1 + S4	C77R + R171D	+	+
S1 + S4	C77R + R174E	+	-
S4 + S5	S179N + V204E	+	+
S4 + S5	S179N + V204D	+	-
S4 + S5	S179Q + V204D	+	-
S4 + S5	S179N + H210E	+	-
S4 + S5	R165K + H210E	+	+
S4 + S5	R165K + V204E	+	-
S4 + S5	M169L + H210E	+	+
S4 + S5	M169L + H210D	+	+
S4 + S5	M169L + V204E	+	-
S4 + S5	M169T + H210E	+	-

Table 4. Summary of chimeras and tags made with KAT1 and their phenotype in the K^+ transporter deficient yeast strain.

Conditions tested are 100 mM K^+, 2 mM K^+, and 0.4 mM K^+ plates. + indicates growth and a - indicates no growth. KXS5 and KXH5 are chimeras of KAT1 made with the *Xenopus* Shaker by Cao et al. and generously provided to us by Dr. Julian I. Schroeder (Cao et al., 1995). N-terminal and C-terminal 6xHis tagged constructs with a TEV protease site between the 6xHis tag and KAT1 were evaluated. HA tagged constructs at the C-terminus, in the S5 to P-loop, and in the S1 to S2 loop were also tested. Data for the stuffer constructs as described in Chapter I in the Materials and Methods section and the KAT1-SKOR chimeras as described in Chapter IV are shown.

Table 4. Summary of chimeras and tags made with KAT1 and their phenotype in the K^+ transporter deficient yeast strain.

Description	*100 mM K+*	*2 mM K+*	*0.4 mM K+*
KXS5 (Cao et al. 1995)	+	-	-
KXH5 (Cao et al. 1995)	+	-	-
6xHis-TEV--KAT1	+	+	+
KAT1-TEV-6xHis	+	+	+
KAT1-HA	+	+	+
KAT1 S5-HA-P	+	+	+
KAT1 S1-HA-S2	+	+	+
KAT1-S1-S3 stuffer	+	-	n/a
KAT1-S4 stuffer	+	-	n/a
KAT1 ShB S4-S5	+	-	-
KAT1 G286I + T288G	+		+
KAT1 N297A	+		+
KAT1-SKOR end of S6	+		+

References

Cao, Y., Crawford, N. M., and Schroeder, J. I. (1995). Amino terminus and the first four membrane-spanning segments of the Arabidopsis K+ channel KAT1 confer inward-rectification property of plant-animal chimeric channels. J Biol Chem *270*, 17697-17701.

APPENDIX 2

A Compilation of Several Investigations

Appendix 2

Appendix 2 is a compilation of several investigations that resulted in significant results that might prove useful for future work on KAT1 and GIRK2.

1. *Evaluation of different blockers of hyperpolarization-activated currents in* Xenopus laevis *oocytes.*

Endogenous currents in *Xenopus laevis* ooctyes were activated at membrane potentials more negative than –140 mV to –160 mV. These currents are due in part to Ca^{2+}-activated chloride currents and a nonselective cation current (Kuruma et al., 2000). These currents are partially blocked by 500 μM Niflumic acid and 50 μM Gd^{3+} (Gadolinium ion) (Figure 1 A and B). Axolotl, *Ambystoma mexicanum*, oocytes also had this endogenous current (Figure 1 C). It was found that replacement of the chloride ions with MES (2-(N-Morpholino)ethanesulfonic acid) and external application of 1 mM Ba^{2+}, blocked these endogenous currents (see Chapter I, Figure 3). These currents are highly variable from batch to batch of oocytes. Some oocyte batches do not contain any endogenous currents while some contain a high amount. Testing of these conditions were derived from various sources (Kowdley et al., 1994; Kuruma et al., 2000; Tokimasa and North, 1996; Tzounopoulos et al., 1995).

2. *Examination of crosslinking cysteine residues in transmembrane segments.*

Many attempts to crosslink putatively interacting residues in transmembrane segments of KAT1 proved unsuccessful. If two residues interact

between subunits, when these residues are mutated to cysteine and crosslinked, one would expect a dimer or tetramer band when the protein is run on a gel and detected by Western. KAT1 wildtype with ten endogenous cysteines was used as a negative control. Crosslinking was attempted under reducing conditions and conditions where oxidizing agent was not added (Laine et al., 2003), under oxidizing conditions (0.1% H_2O_2 (Schulteis et al., 1996) and 2 μM $CuSO_4$/100 μM 1,10-phenanthroline (Broomand et al., 2003)), and with various crosslinkers of different lengths, membrane permeability, and type of chemical reactivity (Methanethiosulfonate deriviatives: MTS-2-MTS (5.2 Å, expected membrane impermeable) and MTS-6-MTS (10.4 Å, expected membrane impermeable) – Toronto Research Chemicals (Loo and Clarke, 2001); Maleimide derivatives: BMB (10.9 Å, expected membrane permeable) and BM[PEO]$_3$ (14.7 Å, expected membrane impermeable) – Pierce). *Xenopus* oocytes were injected with 5 ng RNA of C-terminally HA-tagged KAT1 wt, S179C + V204C, or M169C + H210C and treated with one of the above crosslinking reagents, as per the references cited, 2-3 days after injection. A summary of the results are given in Table 1. The double mutants gave a similar oligomer pattern compared to wildtype indicating no increase in crosslinking of the double mutants.

In addition, crosslinking between putatively interacting residues when mutated to cysteine were tested by Two-Electrode Voltage Clamp (TEVC). Wildtype and mutated channels were expressed in *Xenopus laevis* oocytes and the current was recorded with external application of 0.2% H_2O_2 (Gandhi et al., 2003) (Figure 2), 1 μM Cd^{2+} (Laine et al., 2003) (Figure 3), or 2 μM $CuSO_4$/100

μM 1,10-phenanthroline (Broomand et al., 2003) (Figure 4). No significant change in current was seen for the double mutant, S179C + V204C, compared to wildtype.

The KAT1 double mutant M169C + H210C did not give any current in oocytes 3-4 days after 5 ng RNA injection. This could be because the cysteines have a preformed disulfide bond that interferes with the current similar to disulfide bridges found in Shaker (Laine et al., 2003). Application of 10 mM DTT to reduce a possible disulfide bond also yielded no current (Figure 5). The reasons for seeing no current in this double mutant could be because not enough of the channel is expressed, the channel is not expressed at the surface, or that DTT cannot access the disulfide bond that might have formed during biogenesis of the channel. However, westerns of oocytes injected with M169C + H210C with a C-terminal HA tag showed that the protein was expressed.

These results indicate three possibilities for the inability to crosslink cysteines believed to be in transmembrane regions: 1) The double mutant residues interact within the same subunit and therefore a significant increase in dimer or tetramer formation compared to wildtype is not detected. 2) The conditions are not oxidizing enough for the thiols to react in the membrane. Previous studies have also described the inability of sulfhydryls to form an anion needed for reactivity (Mordoch et al., 1999). 3) The double mutants from which these cysteine mutants were derived do not directly interact and are part of an allosteric network that allows suppression of the conditional lethal.

3. *The KAT1 mutant channel with R177E in the S4 segment is open at all potentials.*

One mutation, R177E, in the S4 segment of KAT1 appears to cause the channel to stay open at all potentials (Figure 6 A & B). This mutation may stabilize the channel in an open state and provides a good candidate for X-ray crystallography as it has been shown that membrane proteins that are difficult to crystallize can be stabilized in a particular conformation to allow crystal growth (Abramson et al., 2003). This mutant conducts a linear current that is Ba^{2+} insensitive (Figure 6 C) and can conduct Na^{+} (Figure 6 C).

4. *Some KAT1 mutants grow more slowly on unselective 100 mM K^{+} plates.*

An interesting phenomenon was observed for certain mutants of KAT1. For mutants C77R, Y72P, T85A + Y86H + D89G, and I84V + T85A + Y86H + D89G occurring in S1 or the S1-S2 loop, growth of these in the K^{+} transporter deficient yeast strain, SGY1528, resulted in very few colonies on unselective 100 mM K^{+} yeast plates after 3 days of growth which normally results in growth even when nonfunctional channels are expressed (Figure 7 – compare the 3 day growth for KAT1 R171E-stuffer (A, left), a nonfunctional channel, and the KAT1 C77R mutant (B, left)). Colonies of the C77R mutant growing in 3 days at 30°C are designated as "fast" growing colonies and after 5 days, smaller colonies appear, termed "slow" growing colonies (Figure 7 B, right).

This phenotype might be due to the mutant channels conducting Na^+ thereby causing toxicity to the yeast as seen with mutants in GIRK2 (Yi et al., 2001). When the selectivity was tested in a 90 mM K^+ solution versus a 90 mM Na^+ solution (Figure 8B and 9A), it was seen that KAT1 wildtype had a significant sodium current that is unlikely to be due to the C-terminal HA tag (unpublished observation). The I_{Na}/I_K was 0.22 at –130 mV (n=2) at the end of 5 second pulses which is significantly different from a published % K^+ conductance for KAT1 in a sodium solution at 7±8% at –130 mV (n=4) at the end of 1.5 second pulses (Schachtman et al., 1992). The recording conditions were different for these two evaluations of the KAT1 K^+ selectivity which may account for this discrepancy. Another possibility is that the oocyte vectors may be different. The 5' and 3' UTR regions of the *Xenopus* β-globin gene was used to enhance expression (Liman et al., 1992) and the 5' and 3' UTR of KAT1 was retained in the vector used here. It is of note that Schachtman et al. report a P_{NH4+}/P_{K+} value of 0.42 indicating that there is a case where the K^+ selectivity is decreased. Experiments recording KAT1 tail currents will be necessary to get accurate measurements of E_{Na} and E_K for accurate values for P_{Na}/P_K and recording KAT1 with the various 5' and 3' UTRs removed will help resolve this discrepancy. As for the C77R mutant, it is difficult to evaluate the selectivity given that the currents in a 90 mM Na^+ solution are low and that this mutant does not give any tail currents suggesting that closing this mutant channel closes much more quickly (Figure 8C and 9B).

Another possibility for the yeast phenotype of these mutants is that they cause a slowing of channel biogenesis, causing them to be trapped in the ER/Golgi by which aggregation or channel activity in the ER/Golgi causes toxicity. This is a reasonable hypothesis considering that all these mutations occur in the S1 segment or S1-S2 loop which are the first regions to become integrated into the membrane in channel biogenesis. In addition, the mutations would seemingly affect the charge (C77R) or flexibility (Y72P or T85A + Y86H + D89G) of this region thereby affecting the recognition of this region as a transmembrane segment and integration into the membrane. A C-terminally GFP tagged KAT1 C77R mutant in the SGY1528 yeast strain was cultured in 0.4 mM K^+ SD –URA/-MET media, fixed, and imaged with epifluorescence microscopy. While it was evident that C77R mutant channels exhibited a reduced surface peripheral fluorescence, this effect was not quantitatively measured.

To further evaluate the yeast phenotype, a set of experiments was pursued on the mutant KAT1 C77R to determine the nature of the "fast" and "slow" growing colonies and ensure that they were not contaminants (Table 2). The fast colonies grew after 3 days and the slow colonies grew after 5 days on 100 mM K^+ yeast plates (Figure 7B). When six sample colonies of the fast and slow growing yeast were streaked onto 0.4 mM K^+, most of the original fast colonies grew within 2 days (5 of 6) while the slow ones did not grow in 2 days (0 of 6). This is consistent with results in culture where 2 fast colonies and 2 slow colonies were cultured in 100 mM K^+ and 0.4 mM K^+ SD –URA/-MET media.

The fast growing ones grew in 2 days in the 100 mM K^+ media while the slow growing ones took 6 days to grow in 100 mM K^+ media and 3 days to grow in 0.4 mM K^+ media. Therefore, the fast colonies are consistently fast growing and the slow colonies consistently slow growing whether on plates or in culture at 100 mm K^+ concentration. However, the toxicity of the C77R mutation appears to be related to the potassium concentration either as a direct result of potassium or osmolarity since the slow colonies grew more quickly in 0.4 mM K^+ media compared to 100 mM K^+ media when plated or in culture. Streaks of C77R from glycerol stocks further support this finding since colonies grew on 0.4 mM K^+ plates after 3 days and did not grow on 100 mM K^+ plates after 7 days. In addition, when C77R was transformed into the SGY1528 yeast strain and directly plated on to 0.4 mM K^+ plates, 17 colonies grew compared to 6 when directly plated on 100 mM K^+ plates.

Furthermore, the plasmids from the fast growing colonies were extracted and sequenced revealing that they contained other mutations in addition to C77R, G38E and R177L. This may be due to the yeast mutagenizing it's own genome and plasmid to compensate for its inability to grow (Heidenreich and Wintersberger, 2001; Steele and Jinks-Robertson, 1992). By contrast, the slow growing colonies contained only the original mutation, C77R, and perhaps reveal the true phenotype of this mutation in this assay without further mutation. However, more samples will need to be tested to verify this and compensatory mutations in the yeast genome independent of the KAT1 gene must also be considered.

In summary, the phenotype of these mutants on 100 mM K^+ yeast plates could be caused by aggregation or channel activity in the ER/Golgi that is related to the potassium concentration either directly due to potassium itself or to the change in osmolarity.

5. *Two extracellular cysteines in Kir 3.2 (GIRK2) may form a disulfide bond, but it is not necessary for function.*

An extracellular disulfide bond was found in Kir 2.1 (IRK1) (Cho et al., 2000) that affected channel function and we wanted to test if a similar bond was present in Kir 3.2 between two extracellular cysteines (C134 and C166). While these two residues may form a disulfide bond, it was not necessary for channel function as mutation of these two residues to alanine has the same inward rectification property as Kir 3.2 wildtype (Figure 10). Interestingly, mutation of these two residues to serine does affect channel properties, possibly due to the polar nature of serine.

Figures

Figure 1. Blocking of endogenous hyperpolarization-activated currents in *Xenopus laevis* oocytes.

(A) Left, Endogenous currents from a water injected *Xenopus laevis* oocyte elicited from + 20 mV to –180 mV in 10 mV increments for 4960 ms from a holding potential of –10 mV for 496 ms to a tail current potential of – 50 mV for 992 ms. The recording solution was 50 mM KCl, 90 mM NaCl, 2 mM $MgCl_2$, 0.5 mM $CaCl_2$, and 10 mM HEPES pH 7.2. Right, Inhibition of the endogenous currents by addition of the same recording solution with 500 μM Niflumic acid on the same oocyte. (B) Left, Endogenous currents from a water injected *Xenopus laevis* oocyte from + 20 mV to –200 mV in 10 mV increments for 4960 ms from a holding potential of –10 mV for 496 ms to a tail current potential of – 50 mV for 992 ms. The recording solution is the same as in A. Right, Inhibition of the endogenous currents by addition of the same recording solution with 50 μM Gd^{3+} on the same oocyte. (C) Endogenous hyperpolarization-activated currents in uninjected Axolotl, *Ambystoma mexicanum*, salamander oocytes are similar to *Xenopus laevis* oocytes. The recording protocol was the same as in B and the recording solution was the same as in A.

Figure 1. Blocking of endogenous hyperpolarization-activated currents in *Xenopus laevis* oocytes.

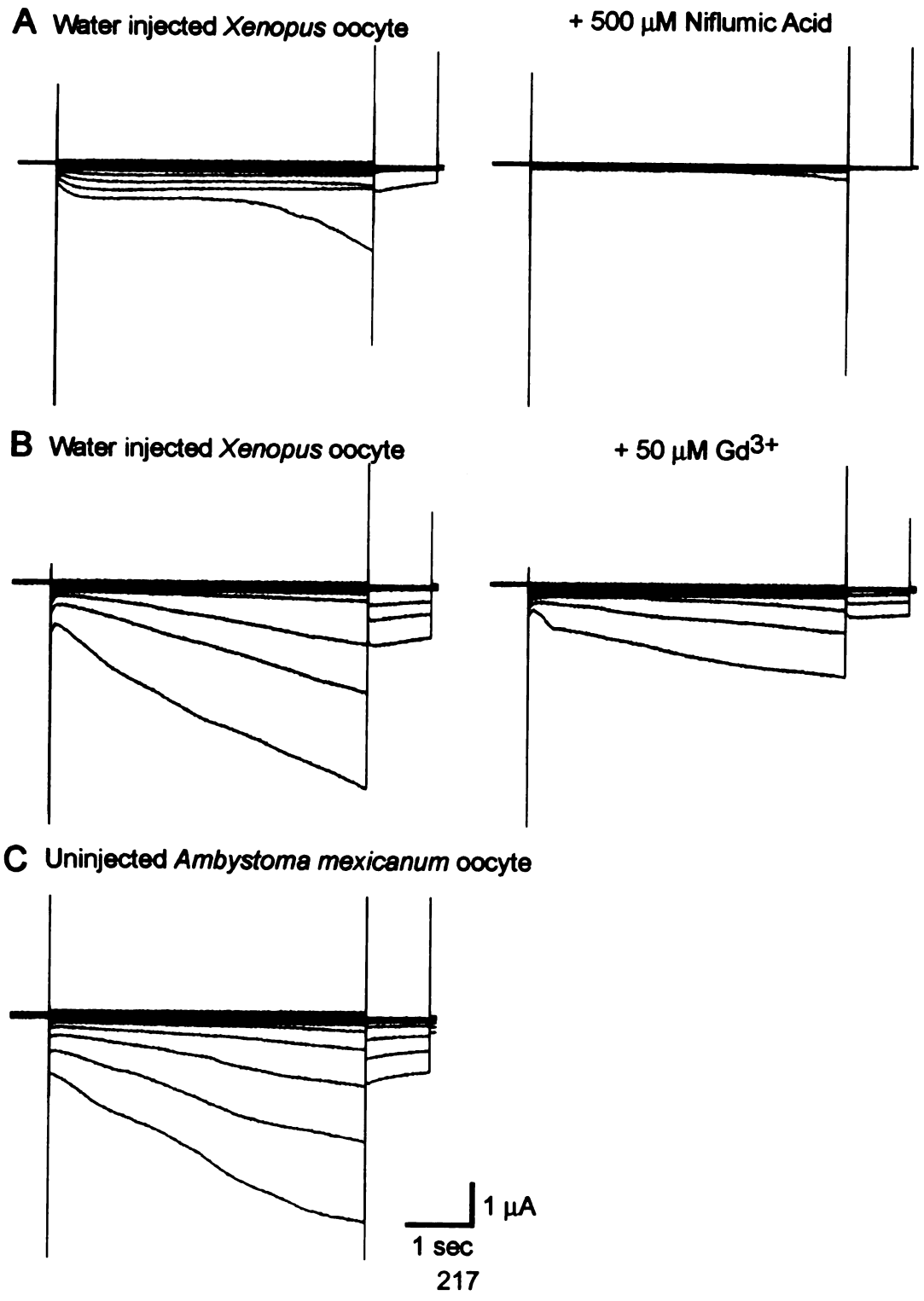

Figure 2. Hydrogen peroxide does not significantly affect KAT1 wildtype and cysteine mutant currents.

Current traces of C-terminally HA tagged (A) KAT1 wt, (B) KAT1 S179C + V204C, and (C) KAT1 M169C + H210C with (right) and without (left) external application of 0.2% H_2O_2. Oocytes were pulsed from + 20 mV to –160 mV in 10 mV increments for 4960 ms from a holding potential of –10 mV for 496 ms to a tail current potential of – 50 mV for 992 ms in 50 mM KCl, 90 mM NaCl, 2 mM $MgCl_2$, 0.5 mM $CaCl_2$, and 10 mM HEPES pH 7.2. Oocytes were injected with 5 ng RNA for each construct and recorded after 3 days of expression.

Figure 2. Hydrogen peroxide does not significantly affect KAT1 wildtype and cysteine mutant currents.

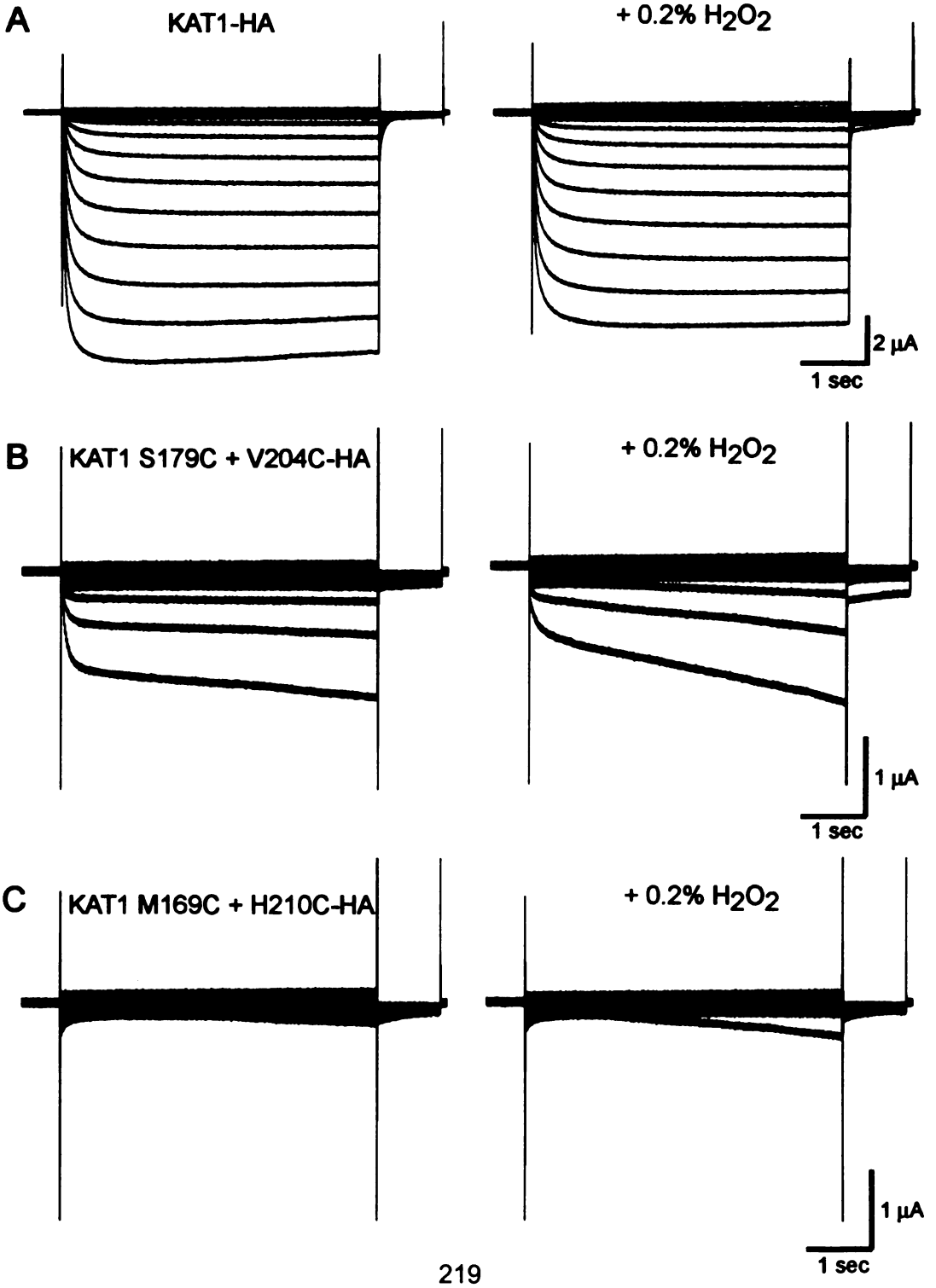

Figure 3. Cd^{2+} does not significantly affect KAT1 wildtype and cysteine mutant currents.

Current traces of C-terminally HA tagged (A) KAT1 wt, (B) KAT1 S179C + V204C, and (C) KAT1 M169C + H210C with (right) and without (left) external application of 10 μM Cd^{2+}. The voltage protocol was the same as in Figure 2 and the recording solution was 50 mM K(MES), 90 mM Na(MES), 2 mM $Mg(MES)_2$, 0.5 mM $Ca(MES)_2$, and 10 mM HEPES pH 7.2. Oocytes were injected with 5 ng RNA for each construct and recorded after 4 days of expression.

Figure 3. Cd^{2+} does not significantly affect KAT1 wildtype and cysteine mutant currents.

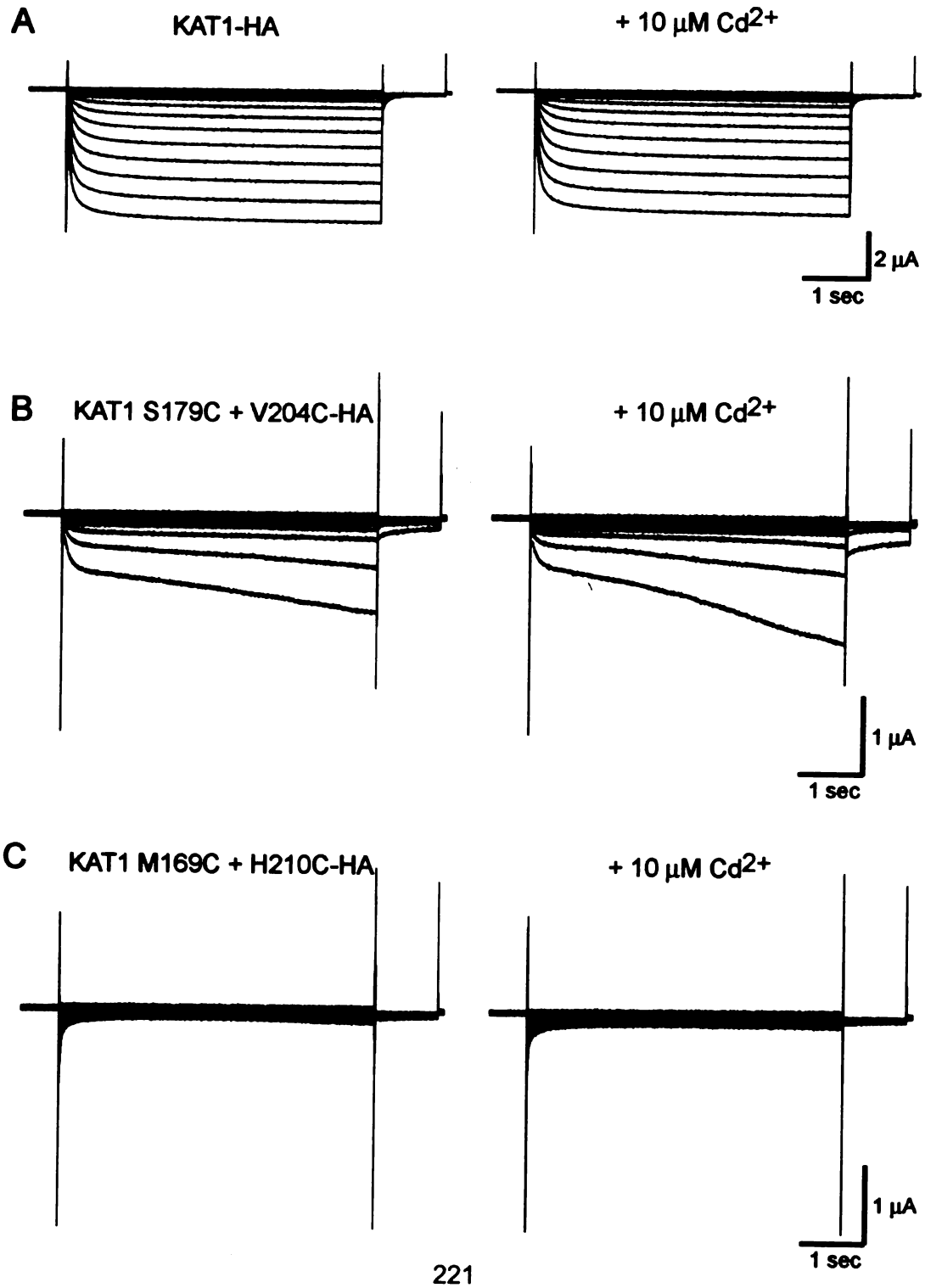

Figure 4. Copper phenanthraline does not significantly affect KAT1 wildtype and cysteine mutant currents.

Current traces of C-terminally HA tagged (A) KAT1 wt, (B) KAT1 S179C + V204C, and (C) KAT1 M169C + H210C with (right) and without (left) external application of 2 μM $CuSO_4$/ 10 μM Phenanthroline. Oocytes were pulsed from + 20 mV to –180 mV in 10 mV increments for 4960 ms from a holding potential of –10 mV for 496 ms to a tail current potential of – 50 mV for 992 ms in 115 mM K(MES), 1 mM $Mg(MES)_2$, 1.8 mM $Ca(MES)_2$, and 10 mM HEPES pH 7.4. Oocytes were injected with 5 ng RNA for each construct and recorded after 3 days of expression.

Figure 4. Copper phenanthraline does not signifcantly affect KAT1 wildtype and cysteine mutant currents.

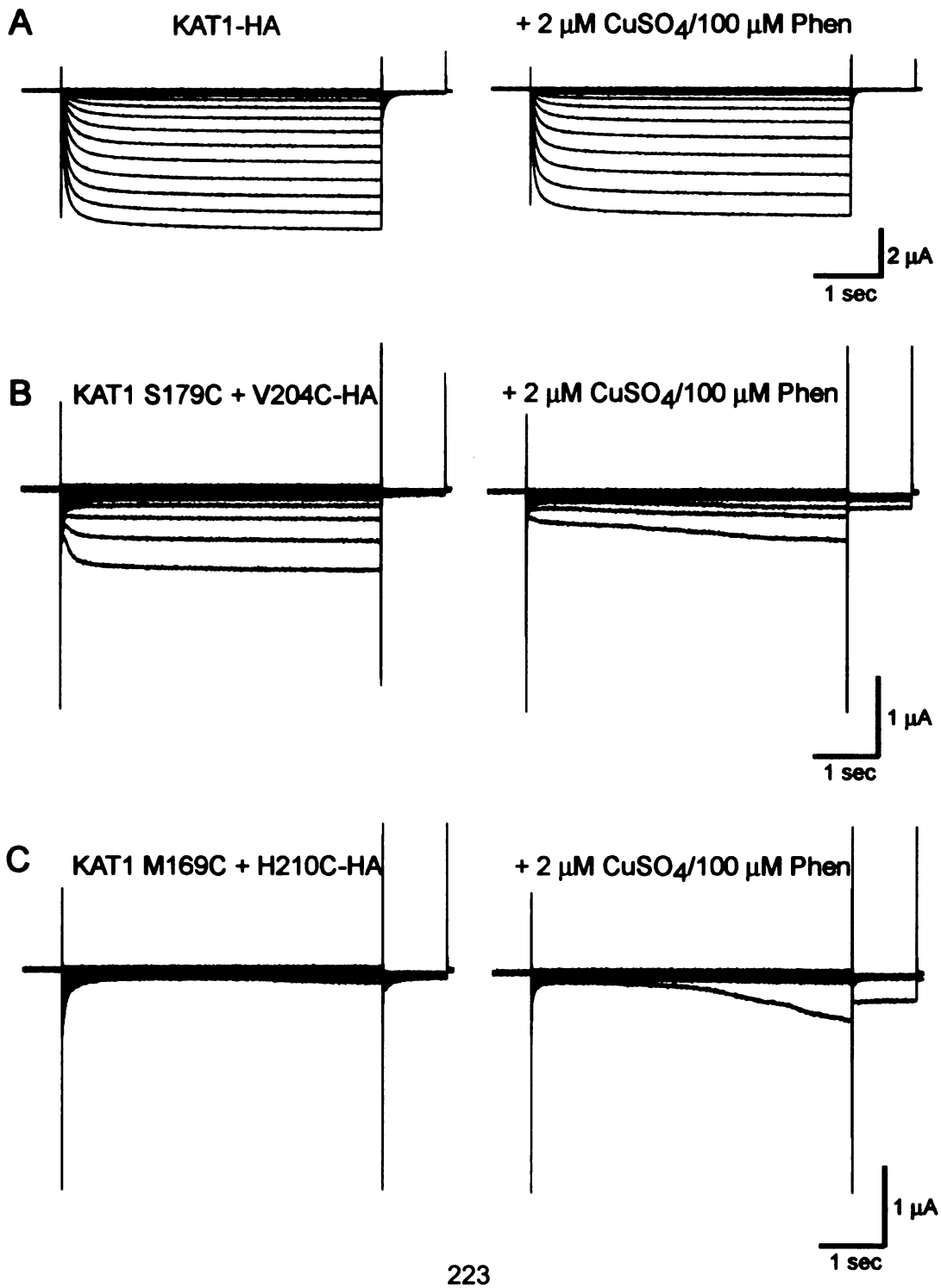

Figure 5. Dithiothreitol does not affect KAT1 wt and the double mutant M169C + H210C.

Current traces of C-terminally HA tagged (A) KAT1 wt and (B) KAT1 M169C + H210C with (right) and without (left) external application of 10 mM DTT. The voltage protocol was the same as in Figure 2 and the recording solution was 50 mM KCl, 90 mM NaCl, 2 mM $MgCl_2$, 0.5 mM $CaCl_2$, and 10 mM HEPES pH 7.2. Oocytes were injected with 5 ng RNA for each construct and recorded after 3 days of expression.

Figure 5. Dithiothreitol does not affect KAT1 wt and the double mutant M169C + H210C.

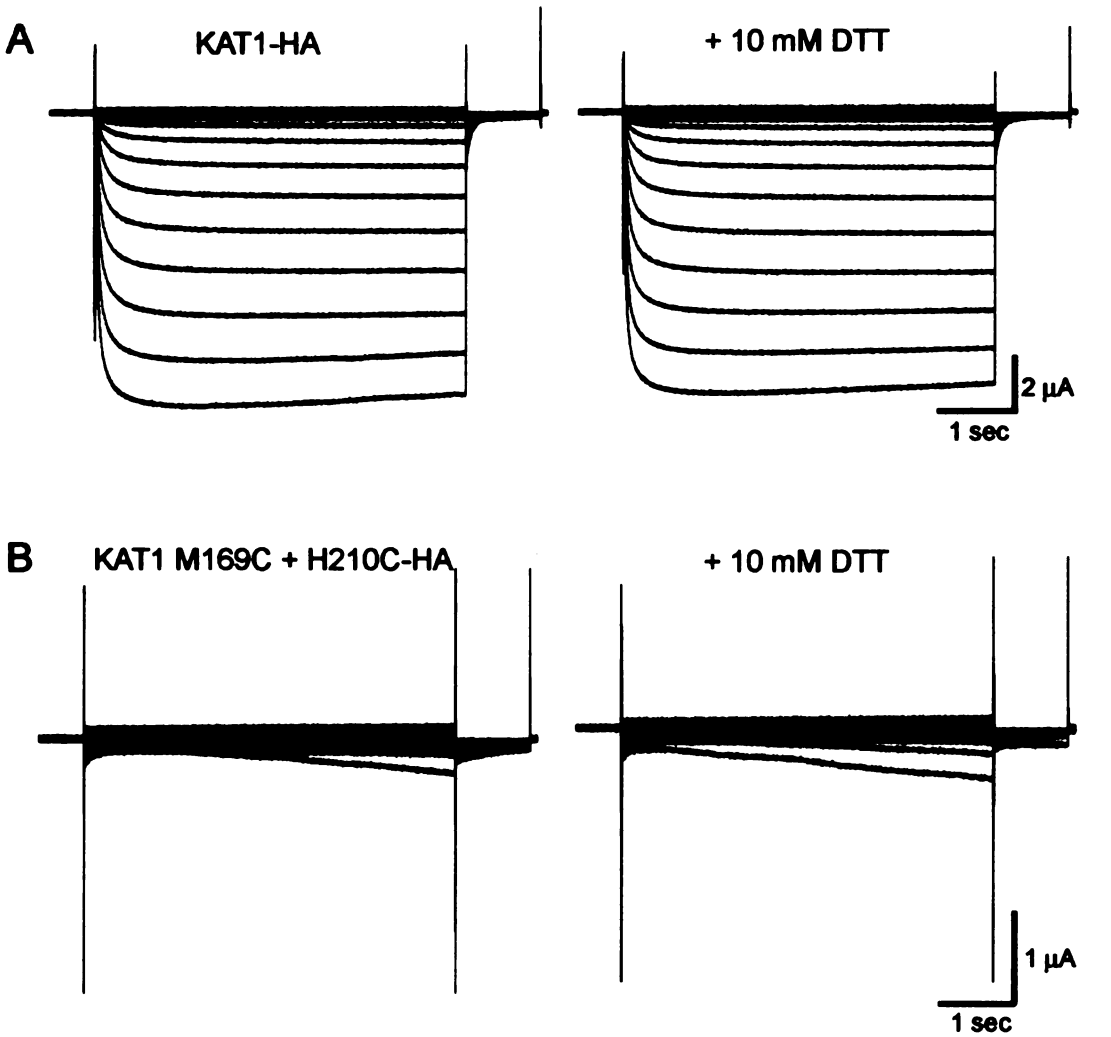

Figure 6. The KAT1 R177E mutant conducts a linear current.

(A) KAT1 R177E recorded in 90K(MES) recording solution: 90 mM K(MES), 1 mM $Mg(MES)_2$, 1.8 mM $Ca(MES)_2$, 10 mM HEPES pH 7.4 from a holding potential of –10 mV pulsing from +20 mV to –180 mV for 5 sec in 10 mV increments to a tail potential of –50 mV. (B) KAT1 R177E recorded in 90K(MES) recording solution as in A from a holding potential of –10 mV pulsing from –10 mV to +100 mV for 5 sec in 10 mV increments to a tail potential of +50 mV. (C) KAT1 R177E recorded from –60 mV to +50 mV from a holding potential of –10 mV in 10 mV intervals for 500 ms in 90K(MES), 90K(MES) + 1 mM Ba^{2+}, and in 90Na(MES) which is the same formulation as 90K(MES) except the K^+ is replaced with Na^+.

Figure 6. The KAT1 R177E mutant conducts a linear current.

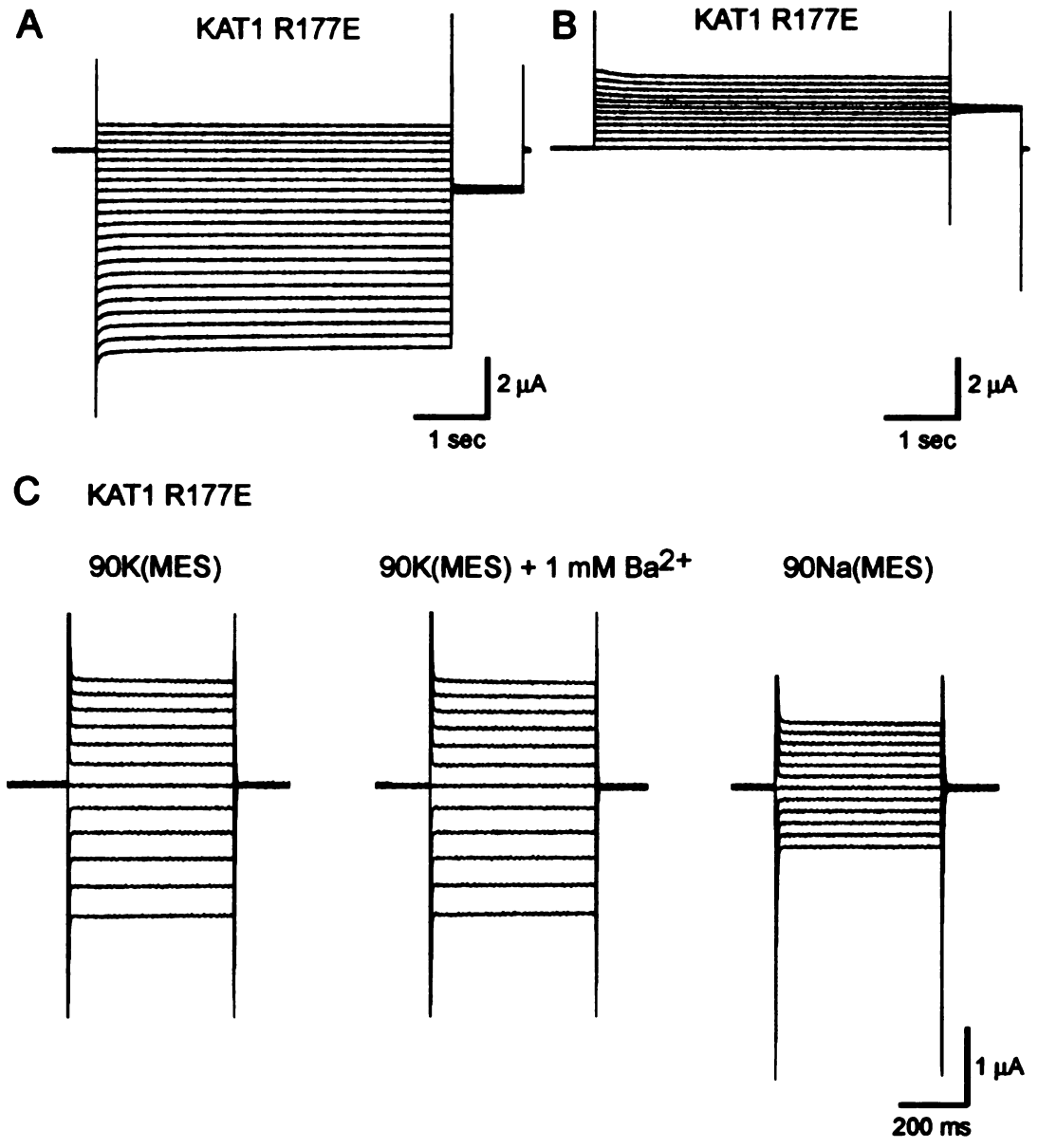

Figure 7. The KAT1 C77R mutation decreases growth on unselective plates.

Examples of (A) KAT1 R171E-stuffer (a nonfunctional channel) and (B) KAT1 C77R when transformed into the SGY1528 yeast strain with 100 ng DNA plasmid and grown on 100 mM K^+ yeast plates after 3 and 5 days incubation at 30°C.

Figure 7. The KAT1 C77R mutation decreases growth on unselective plates.

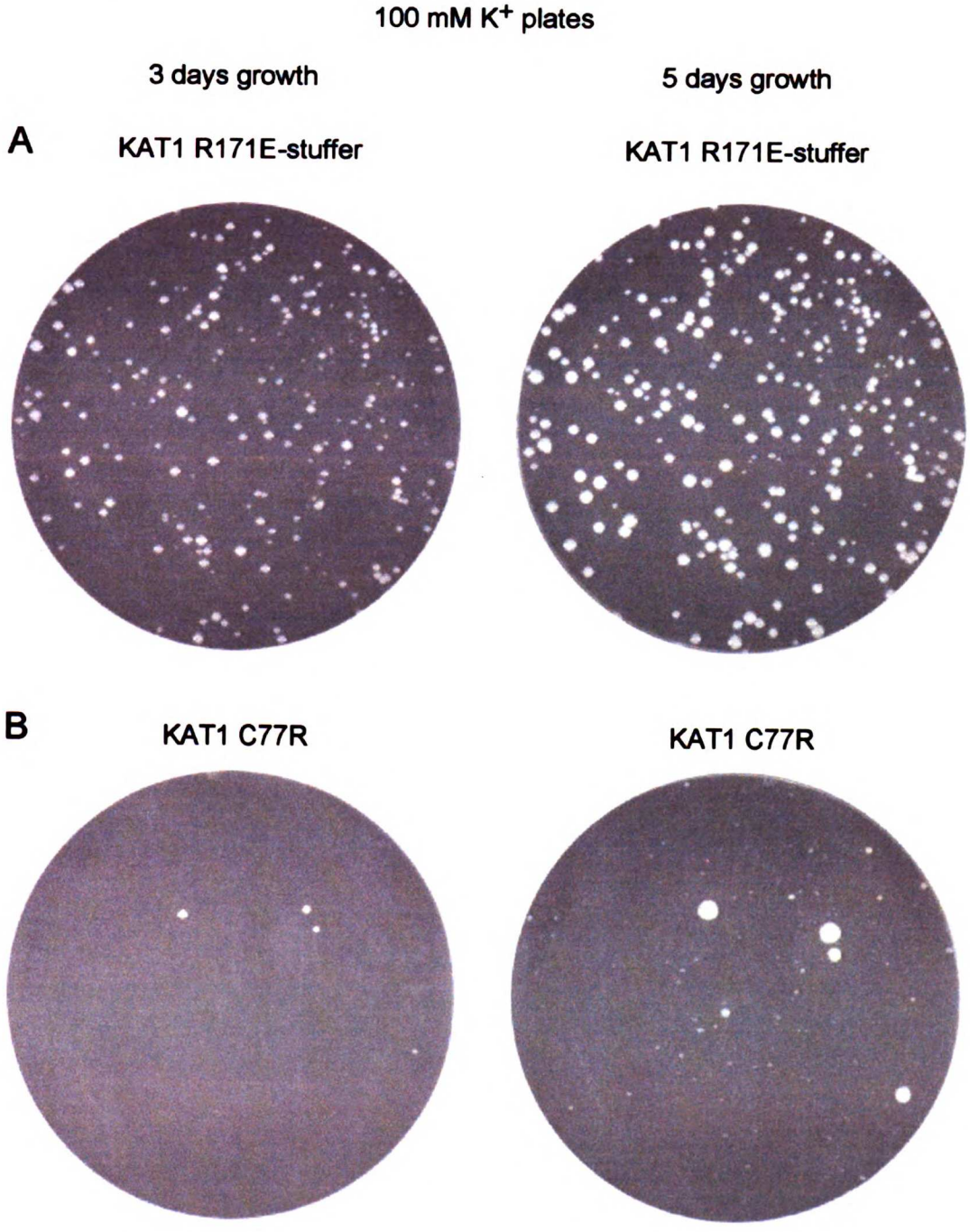

Figure 8. Potassium selectivity of KAT1-HA wildtype and the C77R mutant.

Currents recorded from (A) uninjected, (B) C-terminally tagged KAT1 wildtype, and (C) C-terminally tagged KAT1 C77R in 90K(MES) and 90Na(MES) (see Figure 6 caption for recording solutions and voltage protocol).

Figure 8. Potassium selectivity of KAT1-HA wildtype and the C77R mutant.

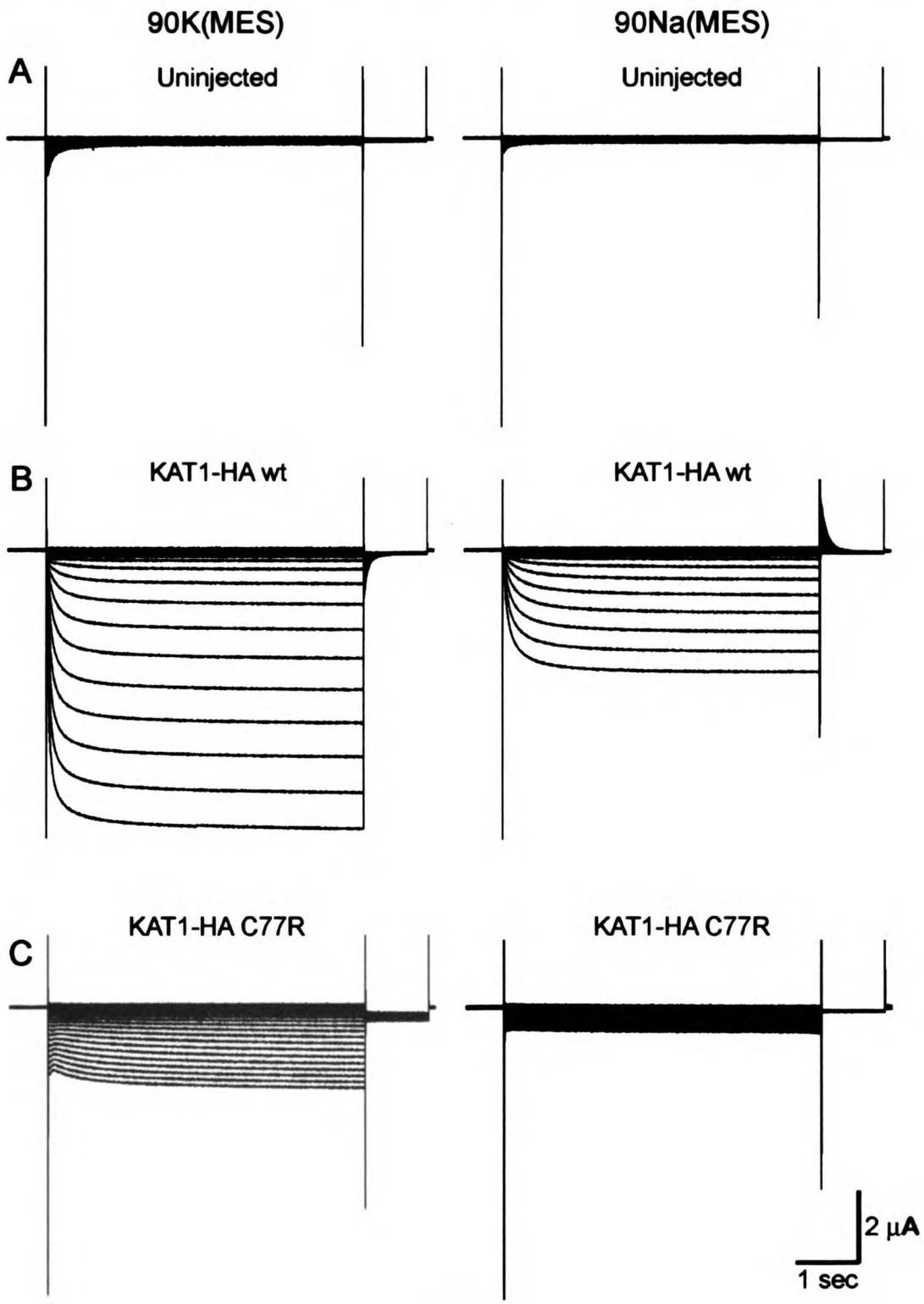

Figure 9. Current-voltage curves evaluating the selectivity for KAT1-HA and the C77R mutant.

I-V curves for uninjected, KAT1-HA, and C77R in 90K(MES) and 90Na(MES). Sample current traces and recording conditions are given in Figure 8.

Figure 9. Current-voltage curves evaluating the selectivity for KAT1-HA and the C77R mutant.

A

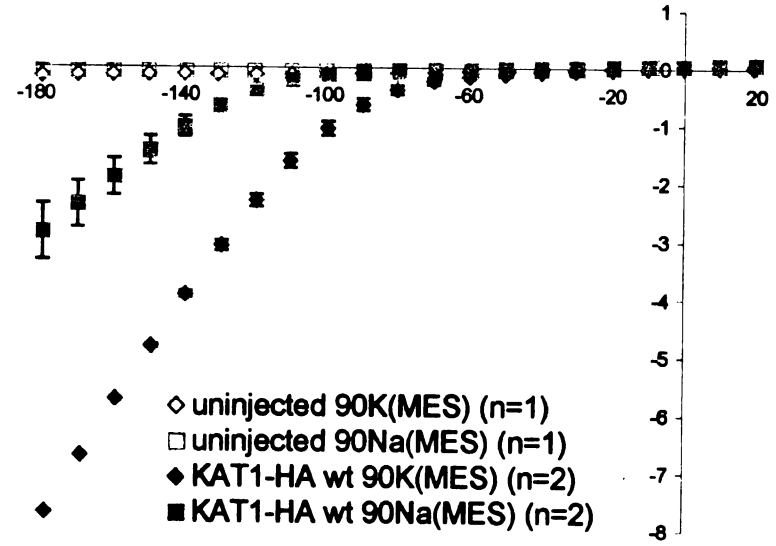

B

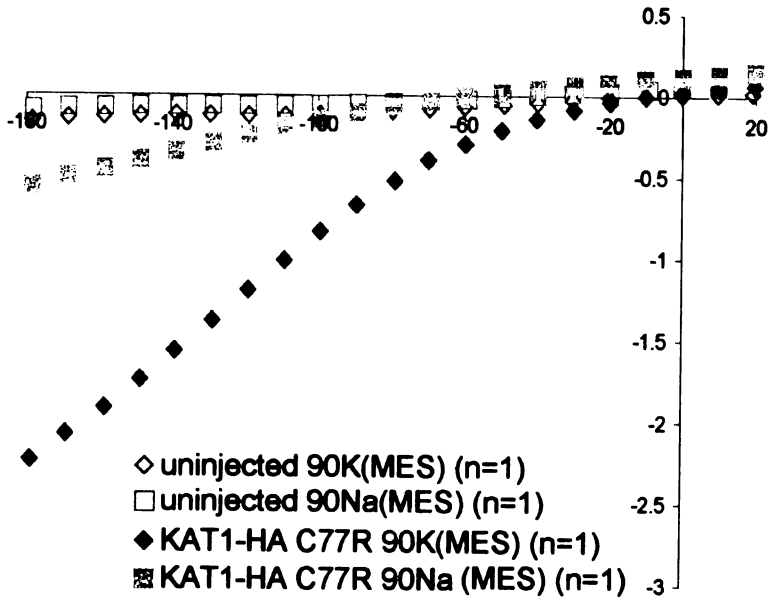

Figure 10. Two extracellular cysteines in Kir 3.2 do not necessarily form a disulfide bond.

I-V curve of Kir 3.2 wt (blue diamonds), C134S + C166S (pink squares), and C134A + C166A (green circles) when activated with Gβγ. Mutation of the two extracellular cysteines to alanine does not affect channel function while mutation to serine had some affect. SEM are shown and n=3 for each condition. 5 ng RNA of the channel construct, 2 ng of Gβ1, and 2 ng of Gγ2 were injected in *Xenopus* oocytes and recorded by TEVC after 4 days expression in 90K solution (90 mM KCl, 1 mM $MgCl_2$, 10 mM HEPES, pH 7.5). Currents were recorded at potentials from +40 mV to –150 mV in 10 mV increments from a holding potential of –30 mV for 100 ms.

Figure 10. Two extracellular cysteines in Kir3.2 do not necessarily form a disulfide bond.

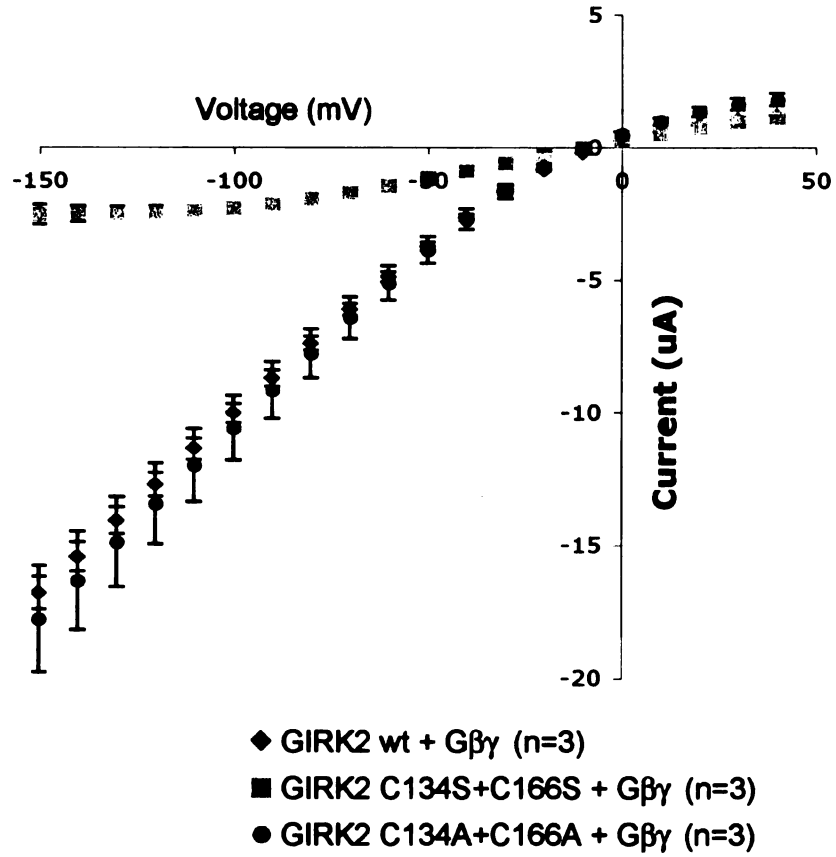

Tables

Table 1. Summary of crosslinking KAT1 wildtype and double mutants, S179C + V204C and M169C + H210C.

The double mutants gave a similar oligomer pattern compared to wildtype. A number 1 designates a KAT1-HA monomeric band was detected by Western. A number 2 designates a dimer and 4 designates a tetramer. A star next to a number means that the band was faint.

Table 1. Summary of crosslinking KAT1 wildtype and double mutants, S179C + V204C and M169C + H210C.

Description	Reducing	Non-Reducing	MTS-2-MTS	MTS-6-MTS	BMB	$BM[PEO]_3$	0.1% H_2O_2	Cu(Phen)
KAT1 wt - HA	1	1	1, 2, 4*	1, 2, 4*	1, 4*	1, 4*	1, 2	1, 2*
KAT1 S179C + V204C - HA	1	1	1, 2, 4*	1, 2, 4*	1, 4*	1, 4*	1, 2	1, 2*
KAT1 M169C + H210C - HA	1	1	1, 2, 4*	1, 2, 4*	1, 4*	1, 4*	1, 2	1, 2*

1 = monomer
2 = dimer
4 = tetramer
* means a faint band of that oligomer

Table 2. Summary of data evaluating the fast and slow growing phenotype of the KAT1 C77R mutant.

The KAT1 C77R mutant was transformed into the SGY1528 yeast strain and plated directly onto 100 mM K^+ plates or directly onto 0.4 mM K^+ plates. After 3 or 5 days of growth on 100 mM K^+ plates, six fast and slow growing colonies were streaked onto 0.4 mM K^+ plates and after 2 days of growth, only the fast growing colonies persisted on 0.4 mM K^+ plates. Direct plating onto 0.4 mM K^+ plates resulted in more colonies than those on 100 mM K^+ plates after 3 days of growth. Two fast and slow growing colonies were cultured in 100 mM K^+ media or 0.4 mM K^+ media. The fast growing colonies had additional mutations while the slow growing colonies did not. Streaking a glycerol stock of yeast transformed KAT1 C77R resulted in no colonies on 100 mM K^+ plates and some colonies on 0.4 mM K^+ plates.

Table 2. Summary of data evaluating the fast and slow growing phenotype of the KAT1 C77R mutant.

	Culture and extract		Plating			Glycerol Stock	
	100mM K+ SD -URA/-MET	0.4 mM K+ SD -URA/-MET	Directly on to 100 mM K+	Streaked from 100 mM K+ to 0.4 mM K+	Directly on to 0.4 mM K+	Directly on to 100 mM K+ plates	Directly on to 0.4 mM K+ plates
C77R fast #1	2 days; **G38E**+C77R	2 days; **G38E**+C77R	3 days, 6 colonies grew	2 days, 5 of 6 grew	3 days, 17 colonies grew	no growth after 7 days	3 days
C77R fast #2	2 days; C77R+**R177L**	2 days; C77R+**R177L**					
C77R slow #1	6 days; C77R	3 days	5 days	2 days, 0 of 6 grew	n/a		
C77R slow #2	6 days; C77R	3 days					

References

Abramson, J., Smirnova, I., Kasho, V., Verner, G., Kaback, H. R., and Iwata, S. (2003). Structure and mechanism of the lactose permease of Escherichia coli. Science *301*, 610-615.

Broomand, A., Mannikko, R., Larsson, H. P., and Elinder, F. (2003). Molecular movement of the voltage sensor in a K channel. J Gen Physiol *122*, 741-748.

Cho, H. C., Tsushima, R. G., Nguyen, T. T., Guy, H. R., and Backx, P. H. (2000). Two critical cysteine residues implicated in disulfide bond formation and proper folding of Kir2.1. Biochemistry *39*, 4649-4657.

Gandhi, C. S., Clark, E., Loots, E., Pralle, A., and Isacoff, E. Y. (2003). The orientation and molecular movement of a k(+) channel voltage-sensing domain. Neuron *40*, 515-525.

Heidenreich, E., and Wintersberger, U. (2001). Adaptive reversions of a frameshift mutation in arrested Saccharomyces cerevisiae cells by simple deletions in mononucleotide repeats. Mutat Res *473*, 101-107.

Kowdley, G. C., Ackerman, S. J., John, J. E., 3rd, Jones, L. R., and Moorman, J. R. (1994). Hyperpolarization-activated chloride currents in Xenopus oocytes. J Gen Physiol *103*, 217-230.

Kuruma, A., Hirayama, Y., and Hartzell, H. C. (2000). A hyperpolarization- and acid-activated nonselective cation current in Xenopus oocytes. Am J Physiol Cell Physiol *279*, C1401-1413.

Laine, M., Lin, M. C., Bannister, J. P., Silverman, W. R., Mock, A. F., Roux, B., and Papazian, D. M. (2003). Atomic proximity between S4 segment and pore domain in Shaker potassium channels. Neuron *39*, 467-481.

Liman, E. R., Tytgat, J., and Hess, P. (1992). Subunit stoichiometry of a mammalian K+ channel determined by construction of multimeric cDNAs. Neuron *9*, 861-871.

Loo, T. W., and Clarke, D. M. (2001). Determining the dimensions of the drug-binding domain of human P-glycoprotein using thiol cross-linking compounds as molecular rulers. J Biol Chem *276*, 36877-36880.

Mordoch, S. S., Granot, D., Lebendiker, M., and Schuldiner, S. (1999). Scanning cysteine accessibility of EmrE, an H+-coupled multidrug transporter from Escherichia coli, reveals a hydrophobic pathway for solutes. J Biol Chem *274*, 19480-19486.

Schachtman, D. P., Schroeder, J. I., Lucas, W. J., Anderson, J. A., and Gaber, R. F. (1992). Expression of an inward-rectifying potassium channel by the Arabidopsis KAT1 cDNA. Science *258*, 1654-1658.

Schulteis, C. T., Nagaya, N., and Papazian, D. M. (1996). Intersubunit interaction between amino- and carboxyl-terminal cysteine residues in tetrameric shaker K+ channels. Biochemistry *35*, 12133-12140.

Steele, D. F., and Jinks-Robertson, S. (1992). An examination of adaptive reversion in Saccharomyces cerevisiae. Genetics *132*, 9-21.

Tokimasa, T., and North, R. A. (1996). Effects of barium, lanthanum and gadolinium on endogenous chloride and potassium currents in Xenopus oocytes. J Physiol *496 (Pt 3)*, 677-686.

Tzounopoulos, T., Maylie, J., and Adelman, J. P. (1995). Induction of endogenous channels by high levels of heterologous membrane proteins in Xenopus oocytes. Biophys J *69*, 904-908.

Yi, B. A., Lin, Y. F., Jan, Y. N., and Jan, L. Y. (2001). Yeast screen for constitutively active mutant G protein-activated potassium channels. Neuron *29*, 657-667.